
Electronic Thesis and Dissertation Repository

9-24-2014 12:00 AM

Finite Element Modeling of the Proximal Humerus to Compare Stemless, Short and Standard Stem Humeral Components of Varying Material Stiffness for Shoulder Arthroplasty

Najmeh Razfar
The University of Western Ontario

Supervisor
Dr. James Johnson
The University of Western Ontario Joint Supervisor
Dr. George Athwal
The University of Western Ontario

Graduate Program in Biomedical Engineering
A thesis submitted in partial fulfillment of the requirements for the degree in Master of Engineering Science
© Najmeh Razfar 2014

Follow this and additional works at: <https://ir.lib.uwo.ca/etd>

 Part of the [Other Biomedical Engineering and Bioengineering Commons](#)

Recommended Citation

Razfar, Najmeh, "Finite Element Modeling of the Proximal Humerus to Compare Stemless, Short and Standard Stem Humeral Components of Varying Material Stiffness for Shoulder Arthroplasty" (2014). *Electronic Thesis and Dissertation Repository*. 2431.
<https://ir.lib.uwo.ca/etd/2431>

This Dissertation/Thesis is brought to you for free and open access by Scholarship@Western. It has been accepted for inclusion in Electronic Thesis and Dissertation Repository by an authorized administrator of Scholarship@Western. For more information, please contact wlsadmin@uwo.ca.

FINITE ELEMENT MODELING OF THE PROXIMAL HUMERUS TO COMPARE
STEMLESS, SHORT AND STANDARD STEM HUMERAL COMPONENTS OF
VARYING MATERIAL STIFFNESS FOR SHOULDER ARTHROPLASTY

(Thesis format: Monograph)

by

Najmeh Razfar

Graduate Program in Biomedical Engineering

A thesis submitted in partial fulfillment
of the requirements for the degree of
Master of Engineering Science

The School of Graduate and Postdoctoral Studies
The University of Western Ontario
London, Ontario, Canada

© Najmeh Razfar 2014

Abstract

In patients with debilitating pain due to osteoarthritis, total shoulder arthroplasty can restore function and provide effective pain relief. Newer implant designs vary in length and material stiffness. Unfortunately, literature on these newer implants is limited. This thesis investigates the effect of stem length and implant material stiffness on proximal humeral bone stresses. 3D bone models with implants of various stem lengths (stemless, short, and standard) and different material stiffness (CoCr, Ti and PEEK) were generated using MIMICS, Solidworks and ABAQUS for varying abduction angles (15°, 45° and 75°). Cortical and trabecular stresses were contrasted with the intact bone state. As expected, the reduction in stem length and material stiffness yielded humeral stresses that better matched the intact stress distribution in cortical bone, but opposing trends presented in trabecular bone. Future work should continue to build on these models and investigate implant fixation through the analysis of micromotion.

Keywords

Total shoulder arthroplasty, Humerus, Implant, Finite element modeling, Trabecular bone, Cortical bone, Hounsfield Unit, ABAQUS, MIMICS, SolidWorks, Arthritis, Young's modulus, Identical mesh, Shoulder, Abduction angles.

Co-Authorship Statement

This thesis would not be possible without the support and help of others. I would like to acknowledge my collaborators.

Chapter 1: Najmeh Razfar – wrote manuscript; Dr. James Johnson, Dr. George Athwal, Jacob Reeves – edited manuscript.

Chapter 2: Najmeh Razfar – wrote manuscript, methods; Dr. James Johnson, Dr. George Athwal, Dr. Ryan Willing, Jacob Reeves – edited manuscript, methods; Dan Langohr – methods.

Chapter 3: Najmeh Razfar – wrote manuscript, model development, data collection and analysis; Dr. James Johnson, Dr. George Athwal, Dr. Ryan Willing – edited manuscript; Jacob Reeves – edited manuscript, data collection and analysis; Jakub Szmit – data collection and analysis.

Chapter 4: Najmeh Razfar – wrote manuscript; Dr. James Johnson, Dr. George Athwal, Dr. Ryan Willing, Jacob Reeves – edited manuscript.

Dedication

To my mother, Sima, who continues to teach me the virtues of love and patience.

To my father, Hashem, who continues to teach me the importance of hard work.

Acknowledgments

I would like to start by acknowledging the continual guidance and support of my supervisors Dr. James Johnson and Dr. George Athwal. I cannot thank you enough for your advice and the passion that you gave me for this great project that you helped me to find. You always helped me to see the end goal of improving patient care. Dr. Johnson, thank you for accepting me into the HULC and for providing such a relaxed and productive work environment. Dr. Athwal, your encouragement and excitement was contagious and always welcome.

I will always appreciate Dr. Ryan Willing for his unlimited help and support. You taught me how to approach research, and to not give up when problems arose in simulations. I can remember many times that I could not get what I was looking for, and your words helped me to start over and find the best results by learning how to troubleshoot. Thanks Ryan, for teaching me that I can learn a new software by myself, and for making me an expert in Abaqus.

Jacob Reeves, I really do not know how I can express how much I appreciate your help and support in all the moments of my research. You were there whenever I had a question, and were always willing to listen. I cannot thank you enough for all you have done and taught me. My English improved so much with you. Thank you for teaching me to be an expert in SolidWorks, and for editing my thesis.

I am truly grateful for Dr. Mariam Afshin, who introduced me to Dr. Johnson and the HULC lab, and who gave me all of her support during the time that I was new to London. You are a great friend.

I would like to thank all of the past and present HULC Bioengineering lab members who I was fortunate enough to share the lab with. You all contributed to the great work environment that helped to increase the productivity of the lab. Special thanks to TankFM producers Dan and Andrew for their great tunes, to all my tennis and squash competitors for the stress relief, and to Jakub for his dedication to data analysis. Dan, your input was always appreciated and helpful.

To Hadi and Saeed, the best brothers in the world, and my nephew, Artin, and sister-in-law, Parisa, I am glad to have your love and humor with me no matter where I am. Your support via phone, Skype, or any other means, is a strong foundation for me to fall back on at the end of each day.

Last, but not least, this achievement would not be possible without my mom and dad's support during my long distance studies. Mom, I know that it was hard for you to be a 14-hour flight away from your only daughter, and that communication was difficult when I was working late troubleshooting my research, but you always gave me all of your love and understanding without saying a word. Dad the greatest skill that you thought me was to never give up, and when I hear that you are proud of me, it means the world to me. I love you both so much, and will never be able to repay you for the unconditional love that you give to me during my lifetime. I would not have found success in my life without you both. You let me follow my dreams.

Table of Contents

Abstract.....	ii
Co-Authorship Statement.....	iii
Dedication.....	iv
Acknowledgments.....	v
Table of Contents.....	vii
List of Tables.....	x
List of Figures.....	xi
List of Appendices.....	xv
List of Abbreviations, Symbols, and Nomenclature.....	xvi
Chapter 1.....	1
1 Introduction.....	1
1.1 Anatomy of the Shoulder Complex.....	1
1.1.1 Osseous Constructs.....	1
1.1.2 Soft Tissue Constructs.....	6
1.2 Structure and Elastic Properties of Bone.....	7
1.2.1 Structure of Bone.....	7
1.2.2 Elastic Properties of Bone.....	8
1.3 Wolff's Law and Stress Shielding.....	10
1.4 Total Shoulder Replacement.....	11
1.5 Humeral Implant Stem Design Features.....	12
1.5.1 Biomechanical Studies on the Influence of Stem Design.....	14
1.5.2 Stem Length.....	14
1.5.3 Stem Stiffness.....	15

1.6 Finite Element (FE) Studies of Shoulder Replacements.....	16
1.7 Project Scope and Objectives.....	19
1.8 Thesis Overview	20
Chapter 2.....	21
2 Methods.....	21
2.1 Data Acquisition (3-Dimension Model Development).....	21
2.2 Bone Resection	23
2.3 Implant Development.....	23
2.4 Implant Positioning and Sizing.....	28
2.5 Identical Mesh Preparation	28
2.6 Application of Material Properties.....	30
2.7 Finite Element Model Construction.....	32
2.7.1 Boundary Conditions, Abduction Angles and Muscle Modeling.....	37
2.8 Outcome Variables.....	37
2.9 Convergence Analysis	44
2.10 Summary	44
Chapter 3.....	46
3 Results.....	46
3.1 Mesh Convergence.....	46
3.2 Effect of Stem Length.....	46
3.2.1 Regional Stresses in the Proximal Humerus.....	46
3.2.2 Average Proximal Humeral Bone Stresses	62
3.3 Effect of Implant Material Stiffness	62
3.3.1 Regional Stresses in the Proximal Humerus.....	62
3.3.2 Average Proximal Humeral Bone Stresses	66

Chapter 4.....	67
4 Discussion and Conclusions.....	67
4.1 Summary.....	67
4.2 Understanding Regional Significance.....	67
4.2.1 The Effect of Variation in Stem Length	68
4.2.2 Effect of Changing Material Stiffness	70
4.3 Hypotheses Revisited.....	73
4.4 Strengths and Limitations	74
4.5 Future Directions	77
4.6 Conclusion	78
Curriculum Vitae	118

List of Tables

Table 2.1: Joint Reaction Forces for 15°, 45° and 75° of Shoulder Abduction According to Bergmann <i>et al</i> (2007).....	41
Table C.1: Patient Demographic Information.....	92
Table H.1: Computational Parameters of FE Models.....	95
Table H.1: Implant Yield Assessment	117

List of Figures

Figure 1.1: Bones and Articulations of the Shoulder.....	2
Figure 1.2: Landmarks of the Humerus	4
Figure 1.3: Bony Projections of the Scapula	5
Figure 1.4: Cortical and Trabecular Bone.....	9
Figure 1.5: Forms of Shoulder Reconstruction.....	13
Figure 1.6: Geometry Discretization.....	17
Figure 2.1: Solid Model Development - Cortical and Trabecular Bone.....	22
Figure 2.2: Trabecular and Cortical Mesh Division	24
Figure 2.3: Humeral Head Resection.....	25
Figure 2.4: Implant Division - Head and Stem Components.....	26
Figure 2.5: Implant Geometries	27
Figure 2.6: Implant-Bone Mating	29
Figure 2.7: CT Density Calibration	31
Figure 2.8: Trabecular Young's modulus Distribution	33
Figure 2.9: Breakdown of Model Variations	34
Figure 2.10: Intact and Reconstructed Models	35
Figure 2.11: Standard Model Diaphyseal Contact.....	36
Figure 2.12: Shoulder Abduction Angles	40
Figure 2.13: Humeral Endosteal Path Positions	42

Figure 2.14: Humeral Slice Positions	43
Figure 3.1: Convergence Results	47
Figure 3.2: Element-Specific Medial and Lateral Stress Paths – 15° Abduction	49
Figure 3.3: Element-Specific Medial and Lateral Stress Paths – 45° Abduction	50
Figure 3.4: Element-Specific Medial and Lateral Stress Paths – 75° Abduction	51
Figure 3.5: Element-Specific Anterior and Posterior Stress Paths – 15° Abduction	52
Figure 3.6: Element-Specific Anterior and Posterior Stress Paths – 45° Abduction	53
Figure 3.7: Element-Specific Anterior and Posterior Stress Paths – 75° Abduction	54
Figure 3.8: Average Stress in Cortical Bone Slices - 15° Abduction	55
Figure 3.9: Average Stress in Cortical Bone Slices – 45° Abduction	56
Figure 3.10: Average Stress in Cortical Bone Slices – 75° Abduction	57
Figure 3.11: Average Stress in Trabecular Bone Slices – 15° Abduction	59
Figure 3.12: Average Stress in Trabecular Bone Slices – 45° Abduction	60
Figure 3.13: Average Stress in Trabecular Bone Slices – 75° Abduction	61
Figure 3.14: Average Change in Stress in the Total Cortical Stress	63
Figure 3.15: Average Change in Stress in the Total Trabecular Bone	64
Figure D.1: Free body diagram of muscle force calculation	93
Figure F.1: DICOM files were imported into Mimics	96
Figure F.2: The initial mask for cortical bone was created using thresholding function..	96
Figure F.3: Region Growing function in Mimics generated a mask (for cortical bone) ..	97

Figure F.4: In most of the cases, due to the connected pixels between humerus and scapula, after applying region growing, the humerus could not be separated from scapula.	97
Figure F.5: In this case, connected pixels were deleted in order to separate the scapula from humerus.	98
Figure F.6: The 3D model of the cortical bone was created.	98
Figure F.7: The 3D model was wrapped.	99
Figure F.8: The 3D model of cortical was smoothed.	99
Figure F.9: Triangle reduction function was also applied for the cortical 3D model.	100
Figure F.10: 3D Bone in 3-Matics software export as an STL file, after applying triangle reduction and smooth features.	100
Figure F.11: Boundary of the trabecular bone was selected manually for each slice.	101
Figure F.12: Demonstrates the outer boundary of the cortical and trabecular bone.	101
Figure G.1: Single-Element Stress Path Results of Subject 1 - CoCr	102
Figure G.2: Single-Element Stress Path Results of Subject 2 - CoCr	103
Figure G.3: Single-Element Stress Path Results of Subject 3 - CoCr	104
Figure G.4: Single-Element Stress Path Results of Subject 4 - CoCr	105
Figure G.5: Single-Element Stress Path Results of Subject 5 - CoCr	106
Figure G.6: Single-Element Stress Path Results of Subject 1 - Ti.	107
Figure G.7: Single-Element Stress Path Results of Subject 2 - Ti.	108
Figure G.8: Single-Element Stress Path Results of Subject 3 - Ti.	109

Figure G.9: Single-Element Stress Path Results of Subject 4 - Ti.....	110
Figure G.10: Single-Element Stress Path Results of Subject 5 - Ti.....	111
Figure G.11: Single-Element Stress Path Results of Subject 1 - PEEK.....	112
Figure G.12: Single-Element Stress Path Results of Subject 2 - PEEK.....	113
Figure G.13: Single-Element Stress Path Results of Subject 3 - PEEK.....	114
Figure G.14: Single-Element Stress Path Results of Subject 4 - PEEK.....	115
Figure G.15: Single-Element Stress Path Results of Subject 5 - PEEK.....	116

List of Appendices

Appendix A: Glossary of Medical Terminology	88
Appendix B: Illustrations Permission	90
Appendix C: Patient Demographic Information	92
Appendix D: Free Body Diagram Analysis of Muscle Wrapping	93
Appendix E: Computational Parameters of FE Models.....	95
Appendix F: Mimics and 3-Matics Procedures	96
Appendix G: All Single-Element Stress Path Results	102
Appendix H: Peak Stem Stresses and Implant Yield Strengths.....	117

List of Abbreviations, Symbols, and Nomenclature

°	Degree
%	Percent
@	At
©	Copyright
®	Registered Trademark
σ_{VWA}	Volume-Weighted Average Stress
ϵ	Engineering Strain
A	Cross-Sectional Area
ANOVA	Analysis of Variance
CAD	Computer Aided Design
cm	Centimeter
CT	Computed Tomographic
d	Depth
E	Young's Modulus
F	Force
F_r	Resultant Force
F_x	<i>x</i> -axis Force
F_y	<i>y</i> -axis Force
F_z	<i>z</i> -axis Force

FE	Finite Element
FEA	Finite Element Analysis
FEM	Finite Element Modeling
GPa	Gigapascal
HU	Hounsfield Units
I	Moment of Inertia
kg	Kilogram
Lat	Lateral
m	Meter
mm	Millimetre
ms	Millisecond
M	Moment
MPa	Megapascal
M_x	x-axis moment
M_y	y-axis moment
N	Newton
Nm	Newton-meter
Ns	Newton-second
ns	Nanosecond
Pa	Pascal

r	Radius
SD	Standard Deviation

Chapter 1

1 Introduction

In the field of orthopaedic implant design, finite element analysis (FEA) tools have been gradually growing in popularity due to their ability to evaluate the performance of different implant designs. This present study employs FEA to investigate the effect of implant stem design on stresses in the proximal humerus. This chapter describes the gross anatomy of the shoulder joint, material properties of bone, total shoulder arthroplasty, and finite element modeling. The hypothesis of this work is also included in this chapter*.

1.1 Anatomy of the Shoulder Complex

The shoulder is a complex system, which consists of three joints, three bones, four articulations, and a large number of muscles, ligaments, and tendons. All together these components act to stabilize the shoulder, and allow the greatest range of motion (ROM) in all three planes (sagittal, frontal or coronal, axial or transverse) compared to all other joints in the human body (Bigliani *et al.*, 1996; Culham and Peat, 1993; Jobe *et al.*, 2009).

The shoulder complex is primarily composed of the glenohumeral joint, a ball-and-socket joint, which can be categorized into its osseous constructs (bones), muscles, and the joint capsule.

1.1.1 Osseous Constructs

In total, the shoulder is composed of four articulations: the glenohumeral joint, sternoclavicular joint, acromioclavicular joint, and scapulothoracic joint (Figure 1.1) (Jobe *et al.*, 2009). The function of all shoulder articulations is to constrain undesired movement and permit required motion (Jobe *et al.*, 2009). The glenohumeral joint, which is the major articulation of the shoulder, is found between the humeral head and the glenoid concavity of the scapula, and is the primary articulation of interest in this study.

* Due to the clinical nature of this thesis, a glossary of medical terms can be found in Appendix A.

Anterior View of the Shoulder

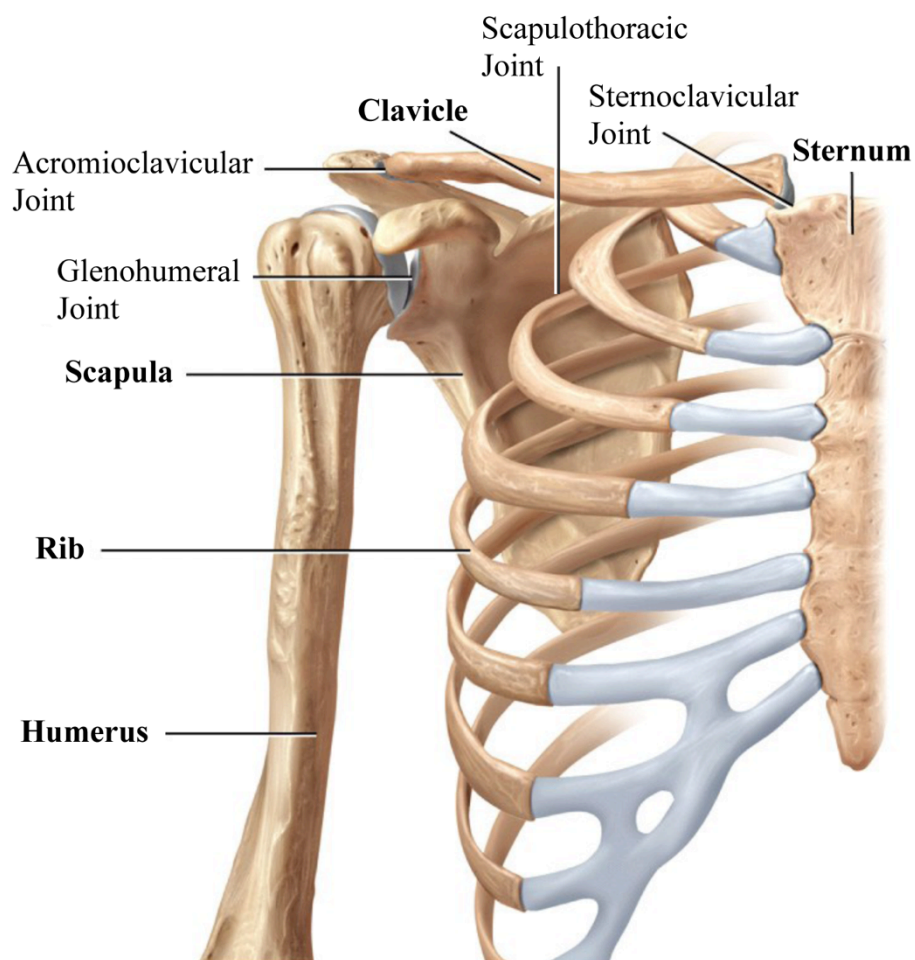


Figure 1.1: Bones and Articulations of the Shoulder

Together, the glenohumeral, acromioclavicular, scapulothoracic and sternoclavicular joints form the shoulder articulation; though the greatest range of motion is provided by the glenohumeral joint. The humerus, scapula, clavicle, sternum and ribs are the bones that create these articulations (*adapted with permission from Tortora, 2011; Appendix B*).

In addition, the shoulder complex also consists of the clavicle (more commonly known as the collarbone).

1.1.1.1 Bones

The bone of the proximal part of the upper extremity is the humerus (Figure 1.2). The humeral head, at the proximal end of humerus is oriented superior, medial and posterior relative to the humeral shaft and articulates with the glenoid. The geometry of the humeral head resembles one third of a sphere (O'Brien SJ *et al.*, 2009). Additionally, the humerus has several significant landmarks – the deltoid tuberosity, the greater tuberosity (GT), lesser tuberosity (LT), the bicipital groove (located between greater and lesser tuberosities) and the medial and lateral epicondyles (Figure 1.2).

The scapula (Figure 1.3) is a triangular bone, which forms a connection between the upper limb and the thorax, and aids in positioning the upper limb by serving as the attachment site for many muscles (Rockwood Jr *et al.*, 2009). The spine, acromion, and coracoid process are bone projections initiating from the scapula (Figure 1.3). The acromion is the origin of the middle and anterior deltoid and the trapezius muscles (O'Brien SJ *et al.*, 2009), whereas the scapular spine process serves as the insertion site for the trapezius, and the origin site of the posterior deltoid muscles. The scapula is a dynamic bone that glides over the ribcage during shoulder range of motion. Shoulder abduction range of motion results in a 2:3 ratio of glenohumeral abduction angle to gross shoulder abduction angle (Bolsterlee *et al.*, 2013; Inman and Abbott, 1944).

The deltoid tuberosity is located along the mid portion of the humeral shaft on the lateral side and is the distal insertion site of the deltoid muscle (from which it gets its name). The greater tuberosity acts as a pathway/wrapping point between the deltoid insertion (situated on the humerus) and origin (situated on the acromion). It allows the deltoid to continue acting when the arm is situated below 45° of glenohumeral abduction (Jobe *et al.*, 2009). In addition, the greater tuberosity is the attachment site of the rotator cuff muscles (supraspinatus, infraspinatus and teres minor) and the lesser tuberosity is the subscapularis muscle insertion site.

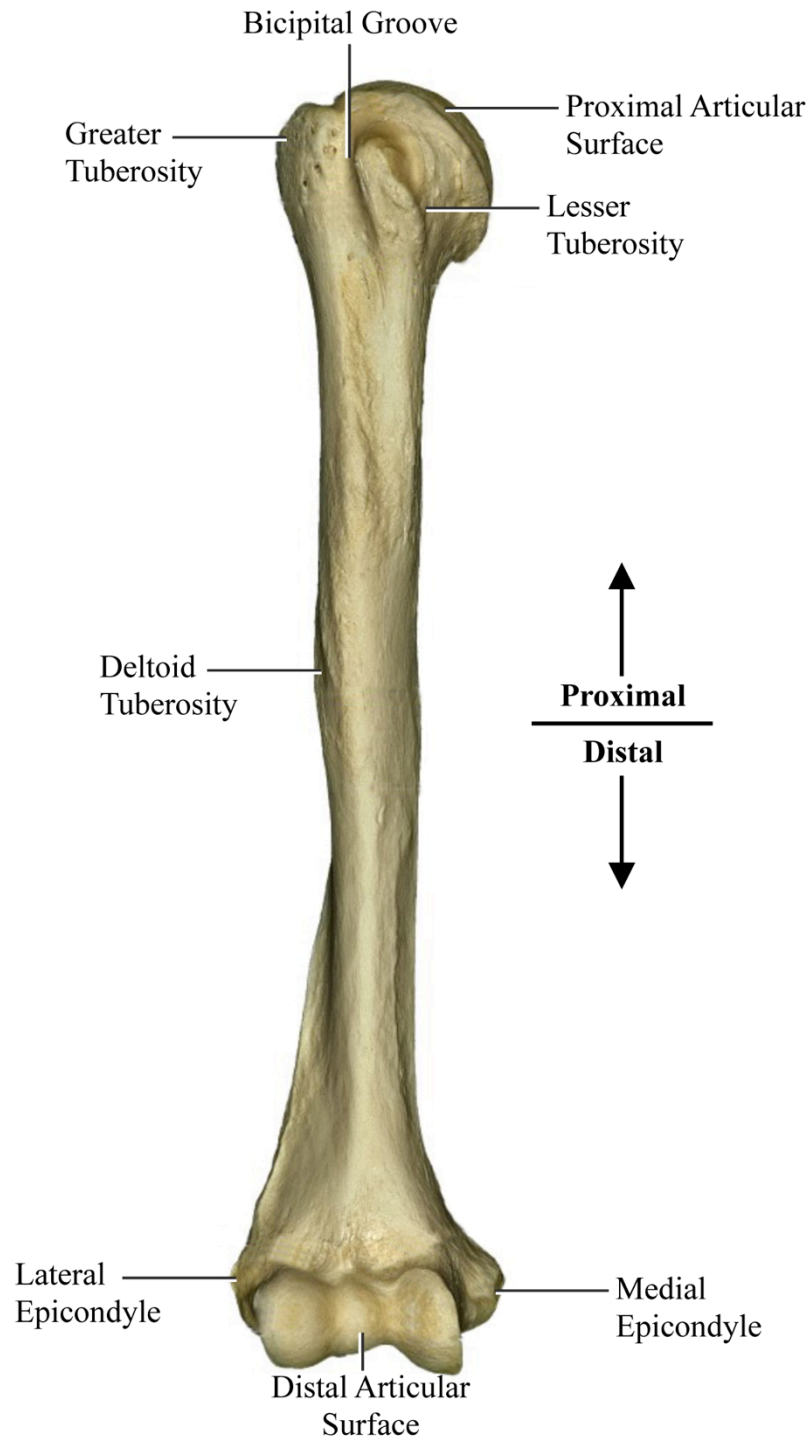


Figure 1.2: Landmarks of the Humerus

Key landmarks of the humerus include: the bicipital groove, greater tuberosity, lesser tuberosity, deltoid tuberosity, lateral epicondyle and medial epicondyle (*adapted with permission from Tortora, 2011; Appendix B*).

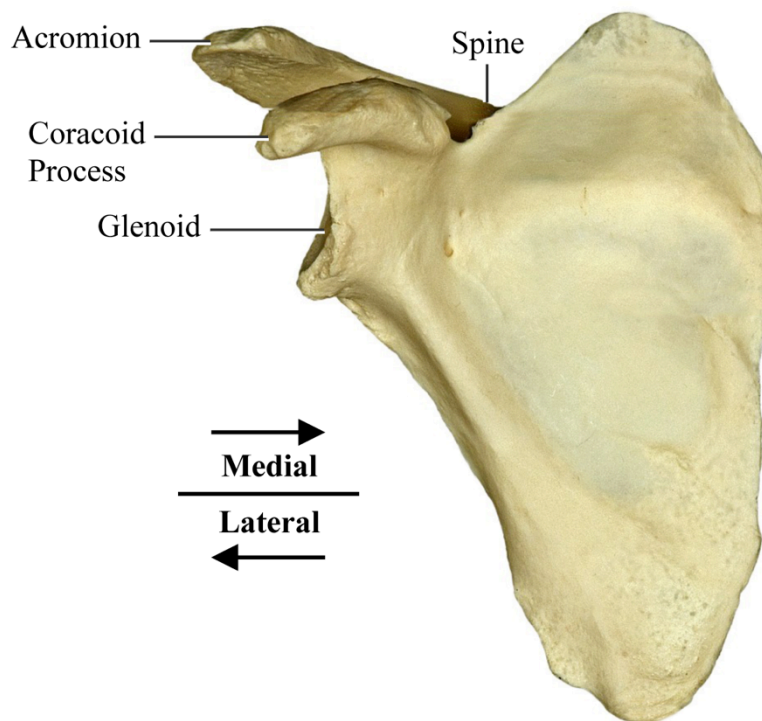


Figure 1.3: Bony Projections of the Scapula

Key bony projections of the scapula include: the acromion, coracoid process and spine (located on the posterior surface). The glenoid dish is located on the lateral side of the scapula and articulates with the humeral head (*adapted with permission from Tortora, 2011; Appendix B*).

1.1.1.2 Joints

Among the four joints of the shoulder, the glenohumeral joint, which is commonly referred to as the “shoulder joint”, is the major articulation and lies between the humeral head and the glenoid concavity of the scapula. The glenohumeral joint has the greatest range of motion in the human body (An *et al.*, 1991; Curl and Warren, 1996; Halder *et al.*, 2001; Karduna *et al.*, 1996; Lippitt and Masten, 1993) (Figure 1.1). An understanding of glenohumeral contact forces is fundamental for any research regarding the shoulder joint, including shoulder joint replacement. Over the years, several studies have investigated glenohumeral contact forces *in-vitro* (Anglin *et al.*, 2000; Conzen and Eckstein, 2000; Hopkins *et al.*, 2007) or established two or three-dimensional musculoskeletal models (Terrier *et al.*, 2010; van der Helm, 1994). However, many parameters, such as the large number of muscles (which leads to too many unknowns) result in discrepancies when calculating joint reaction forces. The innovative *in-vivo* study of Bergmann *et al.* (2007) has allowed measuring and predicting more realistic data of movements such as abduction (Bergmann *et al.*, 2007). Bergmann’s data from a telemeterized implant reported the glenohumeral contact forces for various abduction angles.

1.1.2 Soft Tissue Constructs

1.1.2.1 Joint Capsule and Ligaments

The stability of the glenohumeral joint is reinforced by the joint capsule, glenoid labrum, and various ligaments. Together, these structures directly enhance the influence of the bony anatomy, and limit forces and motions that cannot be opposed by the osseous structures, leading to improved joint stability (Burkart and Debski, 2002; Clark and Harryman, 1992; Culham and Peat, 1993; Hess, 2000; Kask *et al.*, 2010).

1.1.2.2 Muscles

A large number of muscles around the shoulder assist in stabilizing this joint while allowing movement. These muscles can be categorized into three groups – the axiohumeral muscles, the scapulohumeral muscles, and the axioscapular muscles. The axiohumeral and axioscapular muscles have their origins on the thoracic cage, however,

the insertions of axiohumeral muscles is on the humerus and correspondingly for axioscapular is on the scapula. The axiohumeral muscles are composed of the latissimus dorsi and pectoralis major muscles, while the axioscapular muscles are: the serratus anterior, the levator scapulae, the trapezius, the pectoralis minor, and the rhomboids. The function of the axioscapular group is to provide motion to the scapula. Conversely, the group of shoulder muscles that originate on the scapula and insert on the humerus are called scapulohumeral muscles, and consist of: the deltoid, teres minor, teres major, coracobrachialis, supraspinatus, subscapularis and infraspinatus.

The deltoid muscle is divided into three sections: anterior, middle and posterior. The main role of deltoid muscle is to abduct the humerus by providing approximately 50% of the moment required for elevation (Hess, 2000), with higher contributions arising from the anterior and middle sections (Jobe *et al.*, 2009). In addition, the anterior part of the deltoid assists with internal rotation and flexion of the humerus, while the posterior deltoid assists with external rotation and extension of the humerus (Ackland and Pandey, 2011).

The rotator cuff is comprised of the joint capsule, the ligaments, the muscles, and the tendons that surround the glenohumeral joint. Specifically, these muscles are the teres minor, subscapularis, supraspinatus, and infraspinatus.

1.2 Structure and Elastic Properties of Bone

1.2.1 Structure of Bone

Bone is a composite material. Two-thirds of bone is formed of mineralized inorganic matter, with the remaining one-third being organic matter. Together, the inorganic and organic phases of bone provide strength and resilience. The organic matter is comprised of collagen that can resist tensile forces and provides the viscoelastic properties to bone.

The structural components of the long bones, which constitute the appendicular (*i.e.*, arm, leg, etc.) skeleton, are divided into three sections: the diaphysis (shaft), epiphysis (end of the bone that the articulation is located), and metaphysis (between diaphysis and

epiphysis) (Figure 1.4).

Macroscopically, bone is divided into cortical or compact bone (dense bone) and cancellous bone or trabecular bone (spongy bone) (Figure 1.4). The epiphysis is composed of a cortical shell filled with cancellous bone. The diaphysis consists of a cortical shell with a hollow canal, called the medullary cavity, where the bone marrow is situated. Cancellous bone is inhomogeneous and porous throughout its volume (containing bone marrow), varying in structure to take on local anatomic roles. In osteoporosis, a common bone disease, this porosity is increased, which results in reducing bone density. Alternatively, cortical bone is dense and more uniform compared to cancellous bone.

Microscopically, cortical bone is comprised of osteons (elongated bone cells), which are parallel to the diaphysis. In contrast, highly oriented and organized individualized struts of dense tissue, known as trabeculae, form the structure of cancellous bone. These trabeculae are oriented such that they are aligned with respect to the lines of the applied stress.

The major function of bone is to carry the stress and mass of the body. It is also well established that bone remodels, or changes its structure, in response to the stresses applied to it (Huiskes *et al.*, 1987; Wolff *et al.*, 1986). This act of remodeling is an ongoing destructive and restructuring cycle carried out by bone cells known as osteoclasts and osteoblasts, which resorb and build up bone tissue, respectively (Cowin and Hegedus, 1976; Hadjidakis and Androulakis, 2006)

1.2.2 Elastic Properties of Bone

In order to quantify the elastic properties of bone, the Young's modulus or stiffness (E) is required. Since cortical bone is a more uniform structure, it has been modeled using a constant modulus of approximately 20 GPa (Rho *et al.*, 1993). Alternatively, the inhomogeneous structure of trabecular bone makes it more difficult to approximate the stiffness of each trabeculae. Accordingly, advanced medical imaging techniques are required to quantify the material properties of trabecular bone in smaller regions known

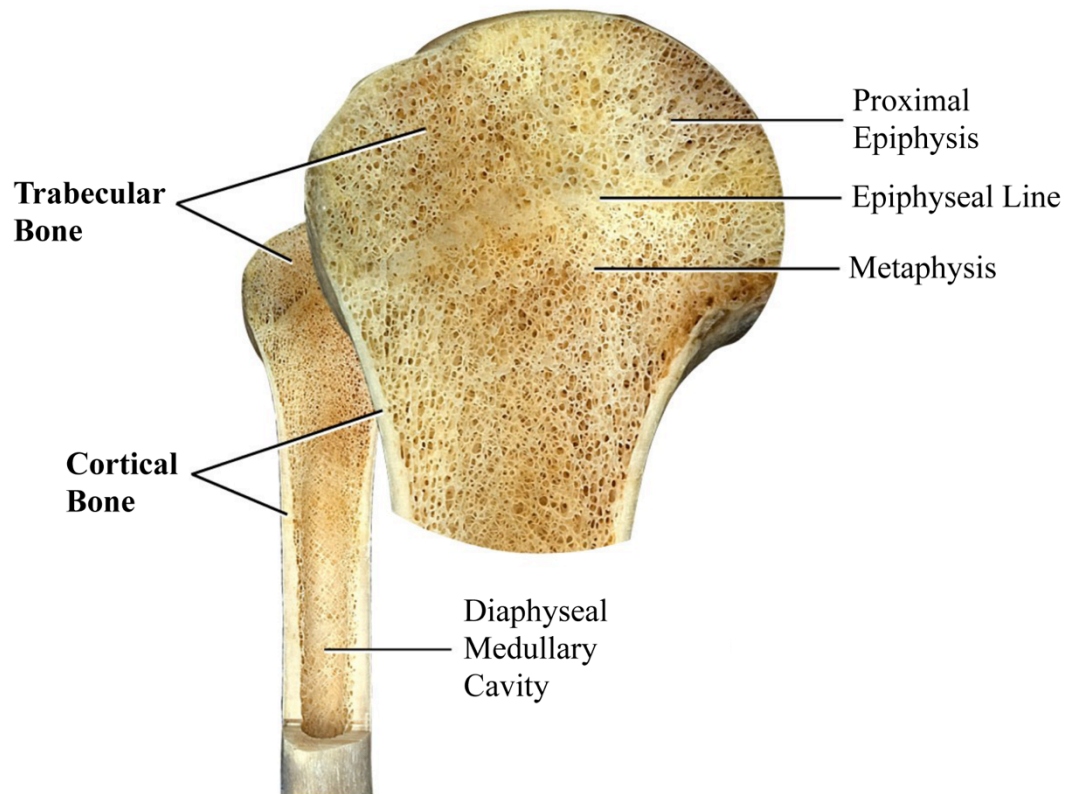


Figure 1.4: Cortical and Trabecular Bone

Bone is divided into two sections: a hard exterior shell known as cortical bone, and a porous interior structure known as trabecular bone (*adapted with permission from Tortora, 2011; Appendix B*).

as voxels. More specifically, intensity data (quantified in Hounsfield Units (HU)) can be obtained from Computed Tomographic (CT) scans of bone. Then, based on a quantitative relationship derived from bone calibration data, the apparent density (defined as wet bone mass over total volume) of a specific region of bone can be obtained (Zannoni *et al.*, 1999). From apparent density, the Young's modulus is derived. A number of density-modulus equations can be found in the literature (Austman *et al.*, 2009; Carter and Hayes, 1977; Leung *et al.*, 2009; Schileo *et al.*, 2007; Taddei *et al.*, 2006). Most of these focus on a combination of cortical and trabecular bone. However, Morgan *et al.* (2003) published a formula that specifically quantified trabecular bone at sites throughout the body (Morgan *et al.*, 2003). While this study was not specific to the humerus, its focus on trabecular bone stiffness (modulus) via a cadaver-based *in-vitro* investigation provides unique insight into metaphyseal and epiphyseal bone mechanics. Additionally, this was a study that used a large number of specimens (n=142). By assigning individual elements of a mesh with different Young's modulus values derived from CT-based HU data, the inhomogeneous and non-linear characteristics of the bone can be captured (Zannoni *et al.*, 1999).

1.3 Wolff's Law and Stress Shielding

Wolff's law is a theory originally published by Julius Wolff in 1892, which describes the behavior of bone subjected to loading. In general, Wolff's law states that bone continuously changes its architecture, strength and composition to optimally carry the loads that it is subjected to. These changes occur over time and lead to an optimized osseous structure that responds to alterations in loading. Wolff's law helps to explain the geometry of both the cortical diaphysis and trabecular epiphysis, where vastly different structures are formed due to variation in the loading environment (Carter *et al.*, 1989; Wolff *et al.*, 1986).

In a composite structure (*e.g.*, a bone-implant construct), the division of forces between the sub-components (in this case: bone and implant) is defined by the magnitude of rigidity terms (*i.e.*, bending and axial rigidity). As demonstrated in Equations 1.1 to 1.4, these rigidity terms are directly proportional to the magnitude of the stiffness (Young's modulus, E) and the geometry (Cross-Sectional Area, A ; and Moment of Inertia, I) of the

sub-components (Mow and Huiskes, 2005). Accordingly, when an implant is placed within bone, and is more rigid than the native osseous construct that it replaces, it assumes more loads, and the remaining bone is subjected to lower loads than it was originally. This phenomena is known as stress shielding, and has been documented as a cause of implant loosening, a failure mode of joint reconstruction implants (Manley *et al.*, 1983).

$$\% \text{ Axial Rigidity}_{\text{Implant}} = \frac{A_{\text{Implant}}E_{\text{Implant}}}{A_{\text{Implant}}E_{\text{Implant}} + A_{\text{Bone}}E_{\text{Bone}}} \times 100\% \quad \text{Equation 1.1}$$

$$\% \text{ Axial Rigidity}_{\text{Bone}} = \frac{A_{\text{Bone}}E_{\text{Bone}}}{A_{\text{Implant}}E_{\text{Implant}} + A_{\text{Bone}}E_{\text{Bone}}} \times 100\% \quad \text{Equation 1.2}$$

$$\% \text{ Flexural Rigidity}_{\text{Implant}} = \frac{E_{\text{Implant}}I_{\text{Implant}}}{E_{\text{Implant}}I_{\text{Implant}} + E_{\text{Bone}}I_{\text{Bone}}} \times 100\% \quad \text{Equation 1.3}$$

$$\% \text{ Flexural Rigidity}_{\text{Bone}} = \frac{E_{\text{Bone}}I_{\text{Bone}}}{E_{\text{Bone}}I_{\text{Bone}} + E_{\text{Implant}}I_{\text{Implant}}} \times 100\% \quad \text{Equation 1.4}$$

where, E is the Young's modulus, A is the cross-sectional area, and I is the moment of inertia.

1.4 Total Shoulder Replacement

The contemporary shoulder replacement for the proximal humerus was developed in 1951 by Neer. Neer used a vitallium prosthesis for the treatment of proximal humeral fractures (Mariotti *et al.*, 2014) and also published his outcomes (Mariotti *et al.*, 2014; NeerII, 1974; NeerII, 1955). Other disorders, such as osteoarthritis, rheumatoid arthritis, and traumatic arthritis, which can cause severe pain and functional limitation, may also be treated by shoulder replacement (Mariotti *et al.*, 2014; Walch *et al.*, 2010; Wiater and Fabing, 2009). Even though degenerative osteoarthritis (OA) affects the weight-bearing joints (*e.g.*, hip and knee), it is still a problem for the glenohumeral joint, the prevalence of which increases with age. Shoulder replacement restores normal kinematic and biomechanics of the shoulder and continues to relieve pain, which leads to increased quality of life (Massimini *et al.*, 2010). Currently, to replace the shoulder, there are a variety of techniques available, including total shoulder replacement (TSA), reverse

shoulder replacement (RTSA), hemi-arthroplasty and partial surface reconstruction (Figure 1.5).

It has been estimated that 11,000 shoulder replacement procedures are undertaken in North America each year (Jain *et al.*, 2006; Litchfield *et al.*, 2011; Masten III, 1996). In general, the shoulder replacement prosthesis consists of three components: the humeral head, the stem of the implant, and the glenoid component. Stem length is one important variable in implant design, and will be one focus of this work. While different manufacturers have developed novel implant systems with various stem lengths, all companies maintain an implant with a standard stem length. In order to reduce the potential for stress-shielding and also the invasiveness of the implant, newer implant designs, such as short stem models and stemless models, have been introduced; however, there is little literature available that investigates the effect of these newer stem lengths on the surrounding bone. Some of the implant manufacturers who have recently released short and stemless models are Tornier, Zimmer, Arthrex, and Biomet. Since 2004, approximately 10,000 stemless shoulder prostheses have been implanted worldwide (Ambacher, 2013).

Two methods can be used in order to fix the humeral component: cement fixation and press-fit (or cementless) fixation. Cement fixation has been used for many years. However, recently press fitting is most popular in North America since manufacturers have increased implant sizes, which has led to better matches with the varying geometries of the humeral head and glenoid (Litchfield *et al.*, 2011; Norris and Iannotti, 2002). In addition to variations in implant sizes, implants are offered with different surface finishes, such as, plasma spray, grit blasted, trabecular metal, or polished smooth.

1.5 Humeral Implant Stem Design Features

One aspect of shoulder implant design that many researchers and surgeons are interested in is stem design; particularly due to its implications with stress shielding and bone remodeling. Two aspects of interest in the design of implant stems are: the length and material stiffness of the stem.

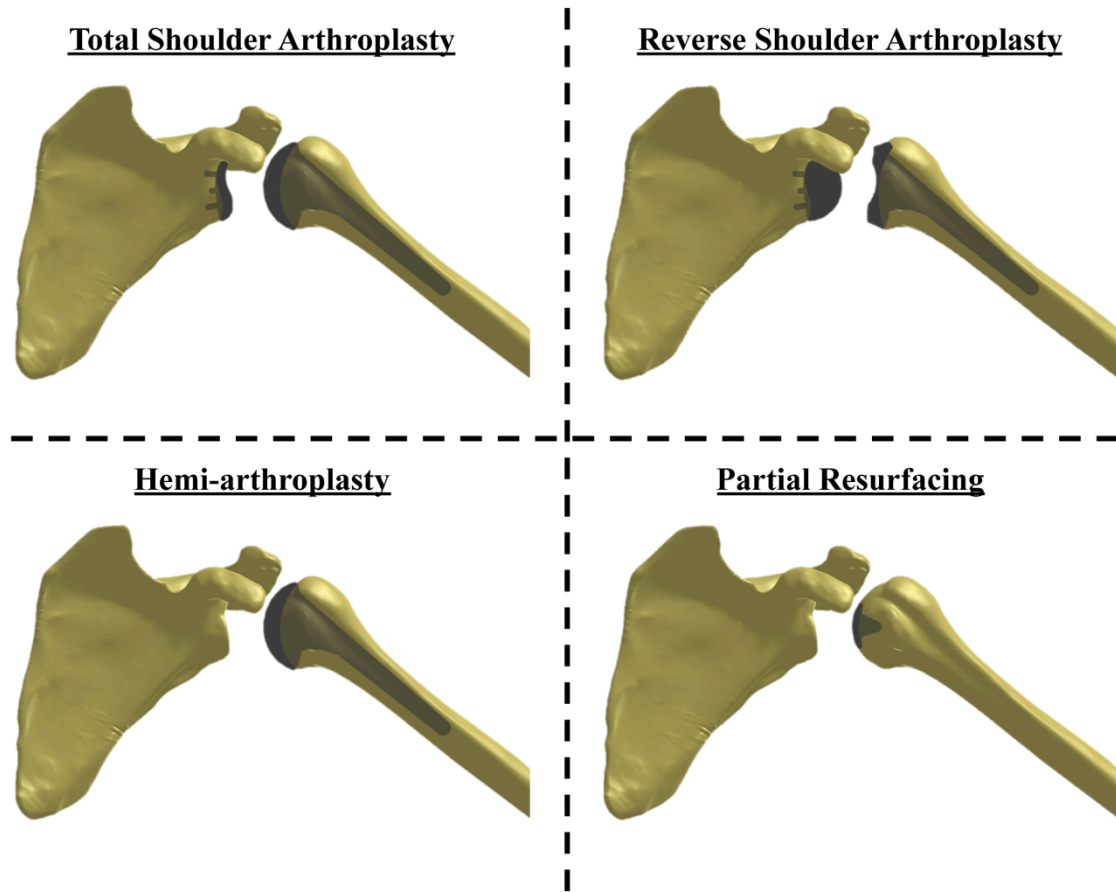


Figure 1.5: Forms of Shoulder Reconstruction

The 4 main forms of shoulder reconstruction involving the proximal humerus are: total shoulder arthroplasty, reverse shoulder arthroplasty, hemi-arthroplasty and partial resurfacing.

1.5.1 Biomechanical Studies on the Influence of Stem Design

In-vitro (cadaveric tests), and *in-silico* (computer/computational) methods are the two techniques most commonly used to investigate shoulder biomechanics, kinematics and implant design.

1.5.2 Stem Length

Stem length is a factor that is important in the design of shoulder prostheses. Recently, newer implants have arbitrarily decreased the stem length, assuming that it is reducing stress shielding and facilitates future revision surgery because of the preserved bone stock (Santori *et al.*, 2006). Unfortunately, few investigations have been conducted to determine the effect of implant stem length on proximal humeral bone stresses or strains; however, these aspects have been investigated for implants at other joints (Austman *et al.*, 2011; Huiskes and Chao, 1983; Reimeringer *et al.*, 2013; van Rietbergen and Huiskes, 2001).

An *in-vitro* study by Austman *et al.* (2007) for distal ulna arthroplasty has suggested that an optimal stem length would mimic the strains of native bone better than alternative lengths, and would decrease the influences of stress shielding (Austman *et al.*, 2007). Additionally, a study by Munting *et al.*'s (1997) show that stemless implants can significantly maintain proximal bone mineral density (BMD) in the femur, especially for patients who had low BMD values before surgery (Munting *et al.*, 1997).

Some studies have focused on load transfer in the proximal femur to evaluate the influence of stem length on hip implants (Barrack, 2000; Cook *et al.*, 1980). Sakaei *et al.* (1999) compared 125 mm and 100 mm stem lengths of hip implants and found that the canal filling of the femur at the distal end was better when a shorter stem prosthesis was used (Sakai *et al.*, 1999). From a clinical perspective, Sluimer *et al.* (2006) compared the performance of two stem lengths (standard design and 25 mm shorter than the standard design) after two years, better proximal fixation was accomplished in the shorter stem, compared to the standard stem. However, this study also indicated that, with a shorter stem, the frequency of pain is increased (Sluimer *et al.*, 2006). A FEA study by Reimeringer *et al.* (2013) evaluated the effect of stem length on initial stability for

uncemented femoral implants. It was found that the average micro-motion increased with decreasing stem length.

1.5.3 Stem Stiffness

The effect of stem material stiffness is another parameter that has a substantial role in load transfer along the bone. Currently, one essential aspect that may lead to stress shielding is differences in the stiffness (*i.e.*, Young's modulus or elastic modulus) between the implant material and surrounding bone (Bureau *et al.*, 2006). Any implants placed in the body must be constructed of biocompatible materials. Some common biocompatible materials used in the design of orthopaedic implants include: Cobalt Chrome ($E = 210.0$ GPa, $\nu = 0.3$), Titanium ($E = 105.0$ GPa, $\nu = 0.3$) and Poly Ether Ether Keytone (PEEK) ($E = 3.5$ GPa, $\nu = 0.36$) (Kurtz and Devine, 2007; Lee and Welsch, 1990).

For cemented hip replacements, some studies have evaluated the influence of altering implant material properties (Huiskes *et al.*, 1992; Jergesen and Karlen, 2002; Manley *et al.*, 1983; Rohlmann *et al.*, 1987). Cook *et al.* (1980) indicated that the stress profile of the femur is affected considerably by changes in the stiffness of an implant. A study by Huiskes *et al.* (1992) shows that flexible stems decrease bone resorption and stress shielding, and increase proximal interface stresses. Moreover, Rohmann *et al.* (1987) showed that, by increasing the stiffness of a cemented femoral stem, the stresses at the cement decrease, which allows the cement to last longer. The finite element analysis in animal models by Simon *et al.* (2003) indicated that the stress and pressure distribution of the less stiff implant was more homogeneous, leading to deformations of the implant that were similar to the adjacent trabecular bone (Simon *et al.*, 2003). However, a study by Au *et al.* (2004) determined that the loading conditions and patterns generated in total knee arthroplasty due to altered surface geometry of bone and implant, are as important and sometimes more important than the altered stiffness between the implant and surrounding bone (Au *et al.*, 2007). Austman *et al.* (2011) used a finite element study to compare the bone stresses before and after implantation of two different distal ulna implants of titanium and cobalt chrome (Austman *et al.*, 2011). Their study indicated that

the changes in bone stress between the native model and implanted model are lower in the less stiff titanium prostheses as oppose to the stiffer cobalt chrome prostheses. Consequently, it is expected that decreasing implant material stiffness may reduce stress shielding following shoulder replacement; however, an investigation specific to shoulder implants is required. It is also noted that other aspects of implant design (*i.e.*, implants geometry) may have an equivalent or more dominant effect on joint replacement performance.

1.6 Finite Element (FE) Studies of Shoulder Replacements

The development of computer models and computational techniques is a popular method used to simulate the anatomy, movement, and forces of joints. Finite element (FE) modeling is one category of the *in-silico* approach. In the field of orthopaedics and biomechanical analysis, FE methods can be used to simplify complex bone and implant geometries to investigate the stress-strain relationships experienced *in-vivo*. In addition, FE analysis provides a non-invasive manner of investigation that allows the probing of the internal structures, in small finite volumes. It is difficult to obtain these non-invasive measurements by *in-vitro* analysis (*i.e.*, cadaver testing and strain gauging). Accordingly, FE methods are an alternative to more costly (*i.e.*, time and money) *in-vitro* investigations.

By dividing a solid continuum into a finite number of small elements, connected together at nodes, a finite element mesh is produced (Figure 1.6). This method allows the investigation of the global performance of the total system based on the local behavior of each element. As a result of this technique, displacements at each node can be obtained using equations that are a function of the loads, boundary conditions, and the stiffness of the elements connecting the node. In addition, loading conditions, materials and geometry can be readily varied to expedite the investigation of variations in these parameters (*i.e.* implant geometry, material properties, etc.).

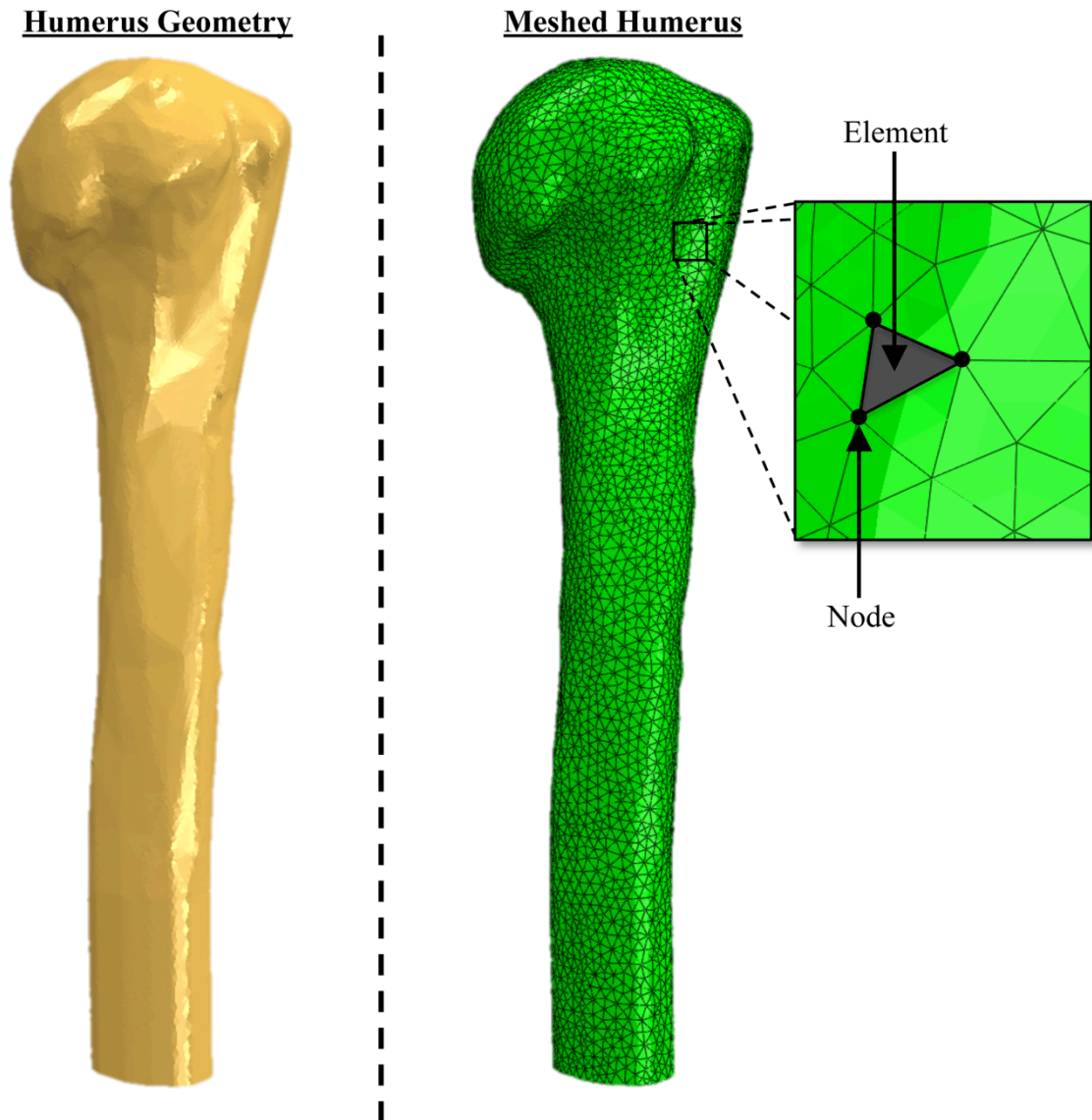


Figure 1.6: Geometry Discretization

In order to form a finite element mesh, the continuous geometry of the proximal humerus must be discretized into a finite number of elements, each of which is composed of several nodes.

As opposed to *in-vitro* experimental testing, where obtaining stresses and strains is only possible at isolated positions (*e.g.*, using load cells and strain gauges), with FE methods stresses and strains throughout the bone can be determined non-invasively.

One important factor in the accuracy of FE modeling is mesh resolution. In order to adequately characterize the physical system, an appropriate mesh size should be selected. However, as mentioned before, the number of equations within a model is related to the number of elements, and therefore increasing the element numbers will require higher computational resources and time. Consequently, the selected mesh size should be small enough, such that further reductions in mesh size will not substantially affect model accuracy, but not so small as to become computationally expensive (in terms of time). The process by which element size variation is investigated is known as convergence analysis.

Generation of the finite element mesh (discretization) is the first step in the finite element analysis. Following this, the load, boundary conditions, element properties, and material properties are indicated. Then, the displacements at each of the nodes are calculated and processed by the software (for this investigation, the software package used is ABAQUS v6.12-EF1 (Dassault Systèmes Simulia Corp., Providence, RI, USA). The final step is interpreting stresses, strains and other resulting data. FE software has advanced to allow biomechanical researchers in orthopaedic implant design to explore numerous design factor combinations, such as different implant designs, various bone geometries, several load scenarios (*i.e.* muscle force, joint reaction force, etc.), and numerous material properties (Huiskes and Chao, 1983; Prendergast, 1997).

FE surfaces or volumetric mesh can be based on a tetrahedral or hexahedral element, which can be linear (first-order) or quadratic (second-order). Curved boundaries can be modeled more closely by using quadratic mesh as opposed to linear. Previous studies have indicated that second-order tetrahedral meshes generate more accurate results (Cifuentes and Kalbag, 1992; Ramos and Simoes, 2006)

1.7 Project Scope and Objectives

In an attempt to better recreate the intact state of bone, implant manufacturers have begun designing proximal humerus implants with shorter, less invasive stems. While the principles of load sharing (*i.e.*, construct rigidity) suggest that a more natural stress distribution can be achieved through the implementation of implants with shorter and less-stiff stems (Mow and Huiskes, 2005), further investigation specific to the proximal humerus is required. Accordingly, the **overall purpose** of this work is to develop a patient specific, novel, parametric, finite element model capable of directly comparing stresses between the intact and reconstructed proximal humerus. To accomplish this, **three specific objectives**, and corresponding hypotheses, have been developed:

Objective 1: To develop a three-dimensional model of the proximal humerus from patient-specific CT scans, which will allow for direct comparison between intact and reconstructed bones.

To facilitate parametric *in silico* testing of the proximal humerus, a finite element model must first be constructed and tested for convergence (Panagiotopoulou *et al.*, 2012). A generic implant must also be developed to permit reconstruction of the proximal humerus. To allow a direct comparison of outcome measures between the intact and reconstructed states, novel methods need to be developed to create identical bone meshes for both models.

In order to appropriately represent an *in-vivo* joint reconstruction, the model must be capable of simulating the reconstruction of the proximal humerus with varying implant geometries, positions and material properties. Additionally, the model should allow for variation in boundary conditions to simulate change in the humeral abduction angle.

Hypothesis 1: It is hypothesized that a model of the proximal humerus will be developed and will generate total average stress results that converge with less than 10% variation when the number of elements in the model is increased by 50%.

Objective 2: To use the newly constructed model to investigate the effects of changing implant stem length on the distribution of stresses in the proximal humerus.

A comparison will be made between three proximal humerus implants of varying stem length (stemless, short, and standard). Average Von Mises stresses in the cortical and trabecular bone will quantify the overall change in stress state for the reconstructed bones. Furthermore, single and average elemental stresses in predefined bone slices will indicate regional stress variations that arise due to changes in stem length.

Hypothesis 2: It is hypothesized that shorter, less invasive implants will better mimic the intact stress state of the proximal humerus quantified by significantly lower stress changes when shorter stems are used.

Objective 3: To determine the effect of changing implant stiffness (Young's modulus) on the distribution of stress in the proximal humerus.

An additional investigation will confirm the versatility of the model by comparing implants of varying stiffness. Overall and slice-specific stresses will compare implant performance with reference to the intact bone state.

Hypothesis 3: It is hypothesized that less-stiff implants will better mimic the intact stress state of the proximal humerus quantified by significantly higher stress changes when stiffer stems are used.

1.8 Thesis Overview

Chapter 2 focuses on the methods used to develop the 3D bone models from CT scans and the finite element methods that are used for simulation of the proximal humerus. This chapter also describes the way the results were collected, and how statistical significance was assessed. Chapter 3 presents the results of how different stem lengths and material stiffness's affect bone stresses in the proximal humerus. Finally, in Chapter 4 the findings are discussed, and concluded. The focus of this chapter is the significance of the results. Suggestions are made for the future directions for this work.

Chapter 2

2 Methods

Overview: In the field of orthopaedic implant design, finite element (FE) analysis tools are often used to evaluate the performance of different designs due to their non-invasive nature and ability to predict stresses in considerable detail. This chapter describes the complete process taken to develop and analyze patient-based, identical material and mesh (*i.e.*, same element node locations for intact and reconstructed models) FE models of the proximal humerus. To the author's knowledge, these methods constitute the first attempt at developing a parametric model of the reconstructed proximal humerus that utilizes identical meshes between conditions to permit element-to-element comparisons.

2.1 Data Acquisition (3-Dimension Model Development)

Pre-operative CT scans were acquired from five subjects (three females and two males, mean \pm standard deviation age = 69.8 ± 5.7) who underwent total shoulder arthroplasty (Appendix C). CT images, originally in DICOM format, were processed using MIMICS software (Materialise, Leuven, Belgium), where the proximal humerus was thresholded to form a three-dimensional (3D) solid model of the bone (Figure 2.1). To permit separation of the cortical bone, a mask was applied based on a lower threshold of 226 Hounsfield Units (HU) (Willing *et al.*, 2013). In the event that the humerus and glenoid overlapped, these constructs were separated manually. Moreover, manual slice-by-slice segmentation was used to create a trabecular bone mask. These masks were then converted into separate 3D models of the cortical and trabecular bones. Once an appropriate cortical-trabecular boundary was obtained, surface geometries were exported in STL format to permit solid model development with SolidWorks software (Dassault Systèmes, S. A. (Vélizy, France)). Please see Appendix D for greater detail on the methods used in Mimics.

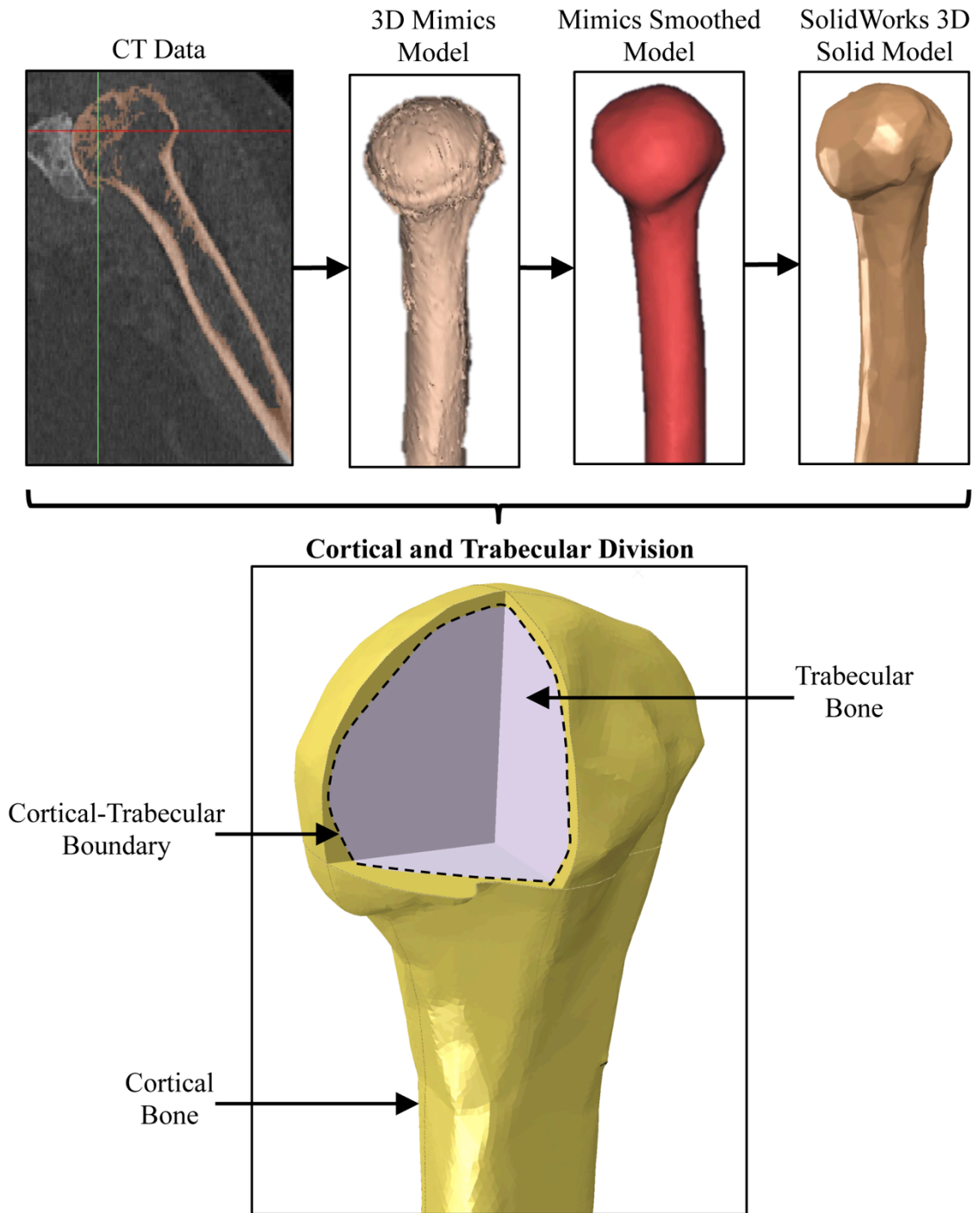


Figure 2.1: Solid Model Development - Cortical and Trabecular Bone

To create a 3D solid model of the proximal humerus, CT image data was converted into 3D cortical and trabecular surfaces that were smoothed and exported into SolidWorks.

2.2 Bone Resection

To prepare the proximal humerus for *in-silico* total shoulder arthroplasty, the 3D cortical and trabecular geometries were further divided into head and body components (Figure 2.2). The head component represented the section of bone that would be resected during surgery. Under the supervision of an orthopaedic surgeon, a cut-plane was created in SolidWorks CAD to divide the bone (Figure 2.3). The trabecular length was chosen by an orthopaedic surgeon according to the presence of bone determined from CT images.

2.3 Implant Development

After reviewing the proximal humerus implants currently available in North America, SolidWorks CAD software was used to develop three generic implants. In general, humeral implants are separated into two sections: the head component and the stem component (Figure 2.4). All developed implants shared an identical head component, and differed only in terms of the stem component. The three stems developed were classified as: standard (~100 mm), short (~50 mm) and stemless (~25 mm) stem designs, and spanned the lengths of component stems used clinically (Figure 2.5).

Two sections define the standard stem: a cylindrical polished diaphyseal region and an expanded grit blasted metaphyseal region. The short stem design removes the diaphyseal section, but maintains an identical metaphyseal design to allow for the direct comparison of these implants. Furthermore, the stemless implant was designed with an extremely short cross-shaped metaphyseal taper that transfers loads to the subchondral bone.

In order to account for geometric variations (*e.g.*, humeral head diameter, diaphyseal canal diameter, etc.) a sub-population of standard, short and stemless implants was developed. This sub-population of implants varied in terms of head diameter and stem diameter. Appropriate head geometry was maintained using an aspect ratio of 1.00:0.76 between the head radius and depth, respectively (derived from measurements of clinically used implants) (Figure 2.4).

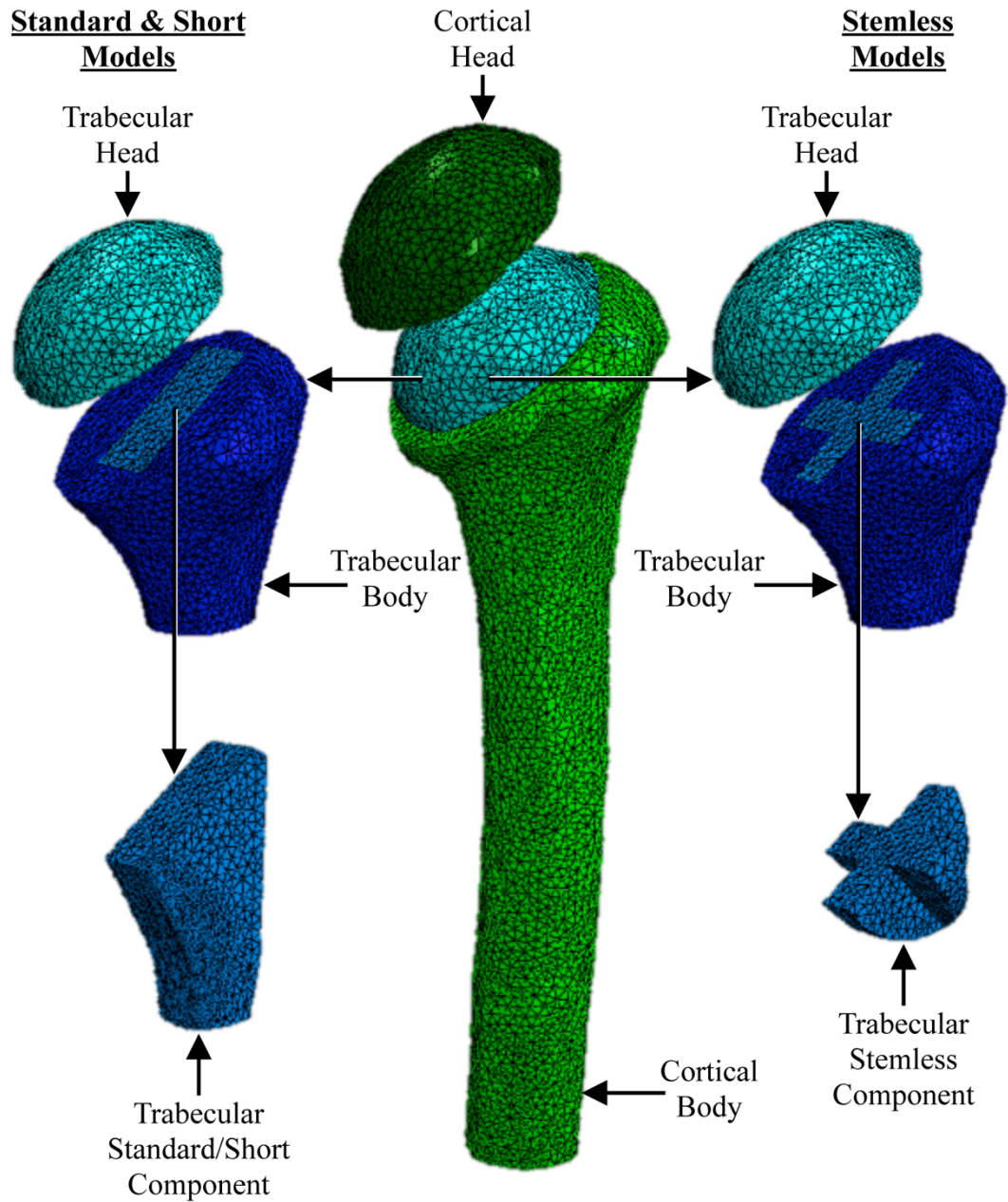


Figure 2.2: Trabecular and Cortical Mesh Division

In order to permit the development of an identical mesh between models, boundaries were assigned within cortical and trabecular bone according to the resection cut plane and the proximal portions of the standard/short and stemless implants.

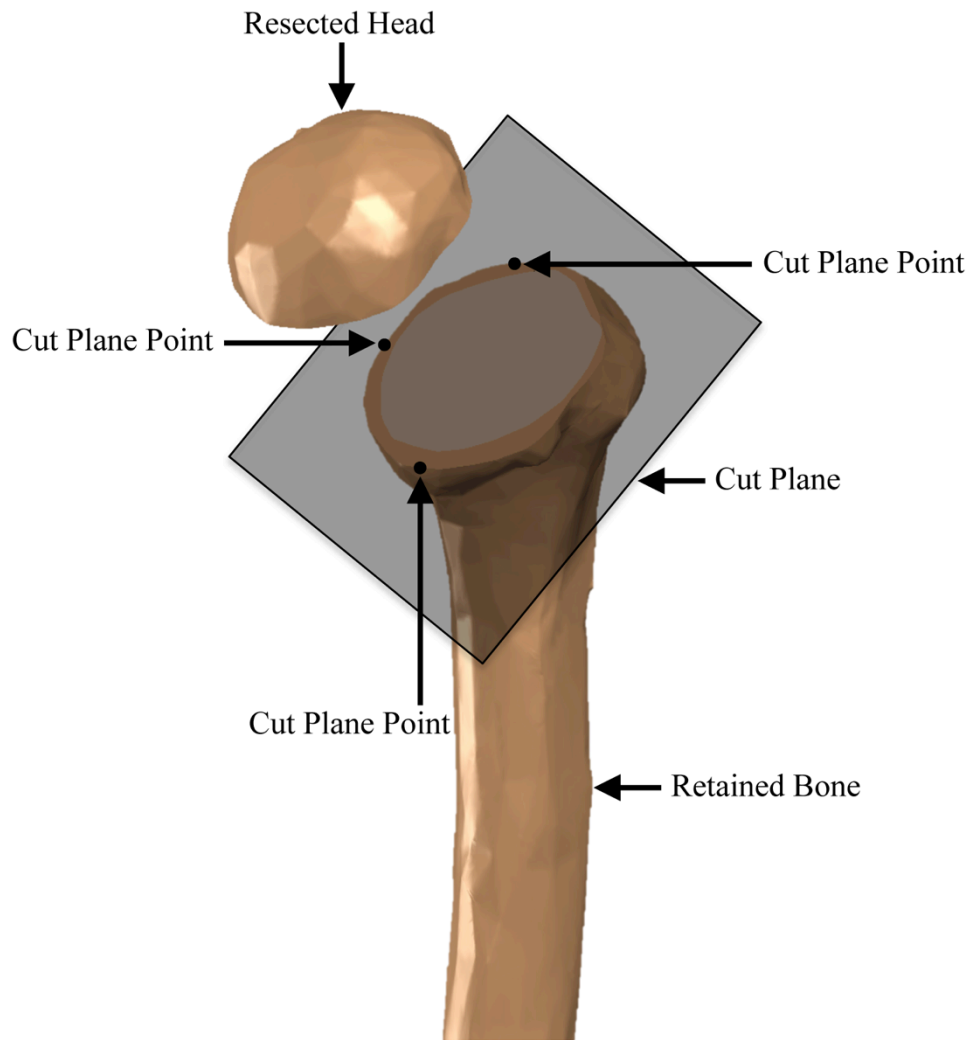


Figure 2.3: Humeral Head Resection

A detailed depiction of the plane chosen for the humeral head resection. This cut plane is defined by three points on the surface of the bone, and was confirmed by an orthopaedic surgeon prior to resection.

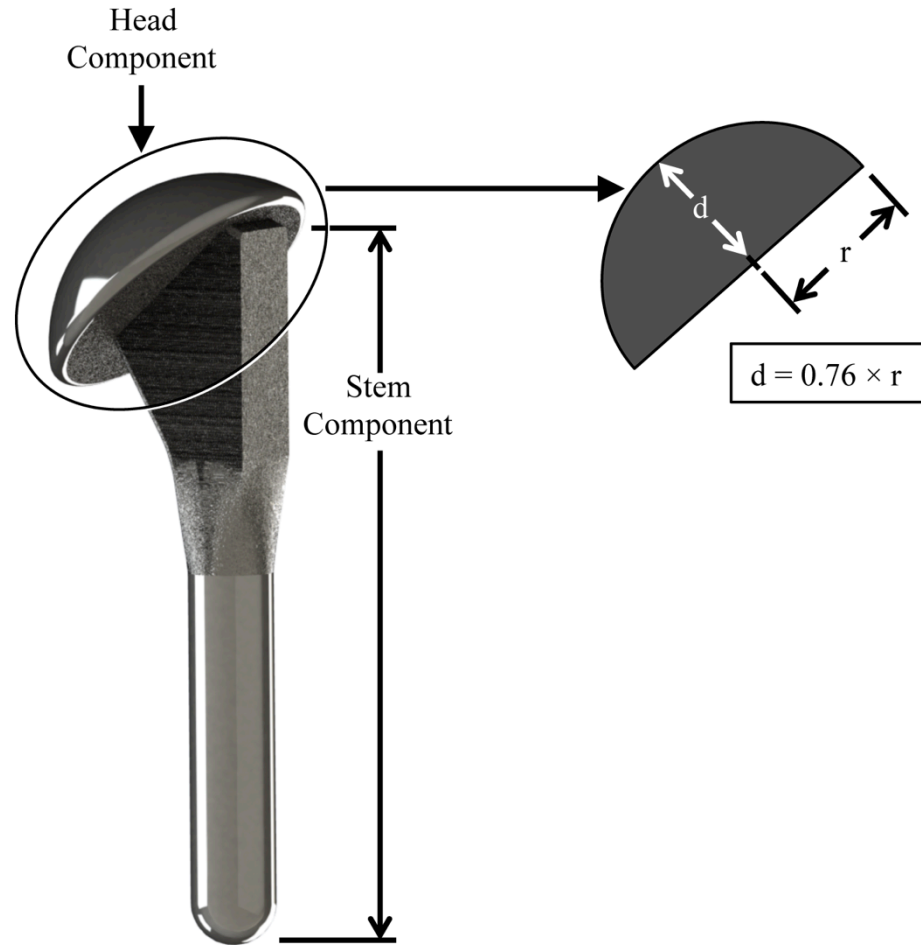


Figure 2.4: Implant Division - Head and Stem Components

Articular orthopaedic implants can be thought of as being divided into two components: the head and stem. To maintain the proper curvature for the head component, a fixed ratio between the radius (r) and depth (d) based on the measurement of clinically available implant heads was used when scaling to fit each subject.

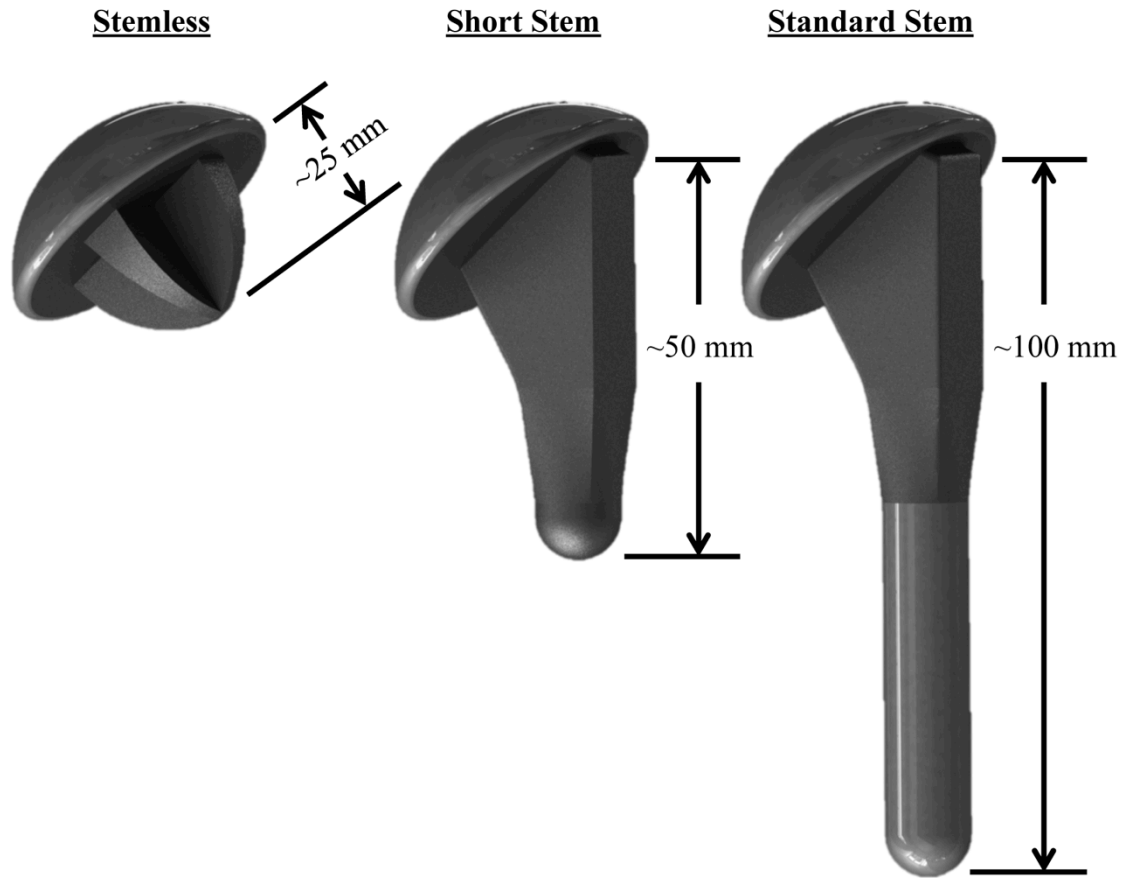


Figure 2.5: Implant Geometries

Generic stemless, short and standard stem shoulder implant designs used for our computational models.

2.4 Implant Positioning and Sizing

To recreate surgical placement *in-silico*, mates (reference geometries) were used in SolidWorks CAD software. Bone reference geometries of a diaphyseal canal axis, a bone cut surface and a circle fitted to the cut surface were created to define the bone geometry and to allow for implant positioning relative to these anatomical/surgical constructs. In addition, implant reference geometries of a stem axis, an implant head undersurface, and an implant head circular edge were also created (Figure 2.6).

To ensure that the standard implants were properly centered in the diaphyseal canal, bone and implants axes were made collinear. The implants were also positioned such that the undersides of the prostheses' heads were coincident with the bone cut surface. The implant heads were made concentric with the circle fitted on the cut surface. Following this, the short-stemmed implant was mated to the same position as the standard stem using three proximal surfaces shared between these two designs. The stemless implant was aligned with the bone cut surface such that it was centered in the cut surface of the humeral head. Together, these mates restricted the location of the implant within the proximal humerus and resulted in repeatable implant positioning (Figure 2.6).

Following implant positioning, the appropriate implant stem and head diameters were selected from the sub-population of standard, short and stemless implants. Implant size was increased in increments of 1 mm until diaphyseal contact was detected, indicating a moderate cementless that is consistent with current surgical techniques.

2.5 Identical Mesh Preparation

After implant positioning and sizing, all stem designs, as well as trabecular and cortical bone models, were transferred from SolidWorks to ABAQUS v6.12 (Dassault Systèmes simulia Corp., Providence, RI, USA) in STEP AP214 format. All geometries were then merged in a way that the geometrical lines of the implants were maintained, allowing the creation of identical meshes in overlapping regions regardless of stem size. At this point, the bone was meshed using appropriately sized quadratic tetrahedral elements (see

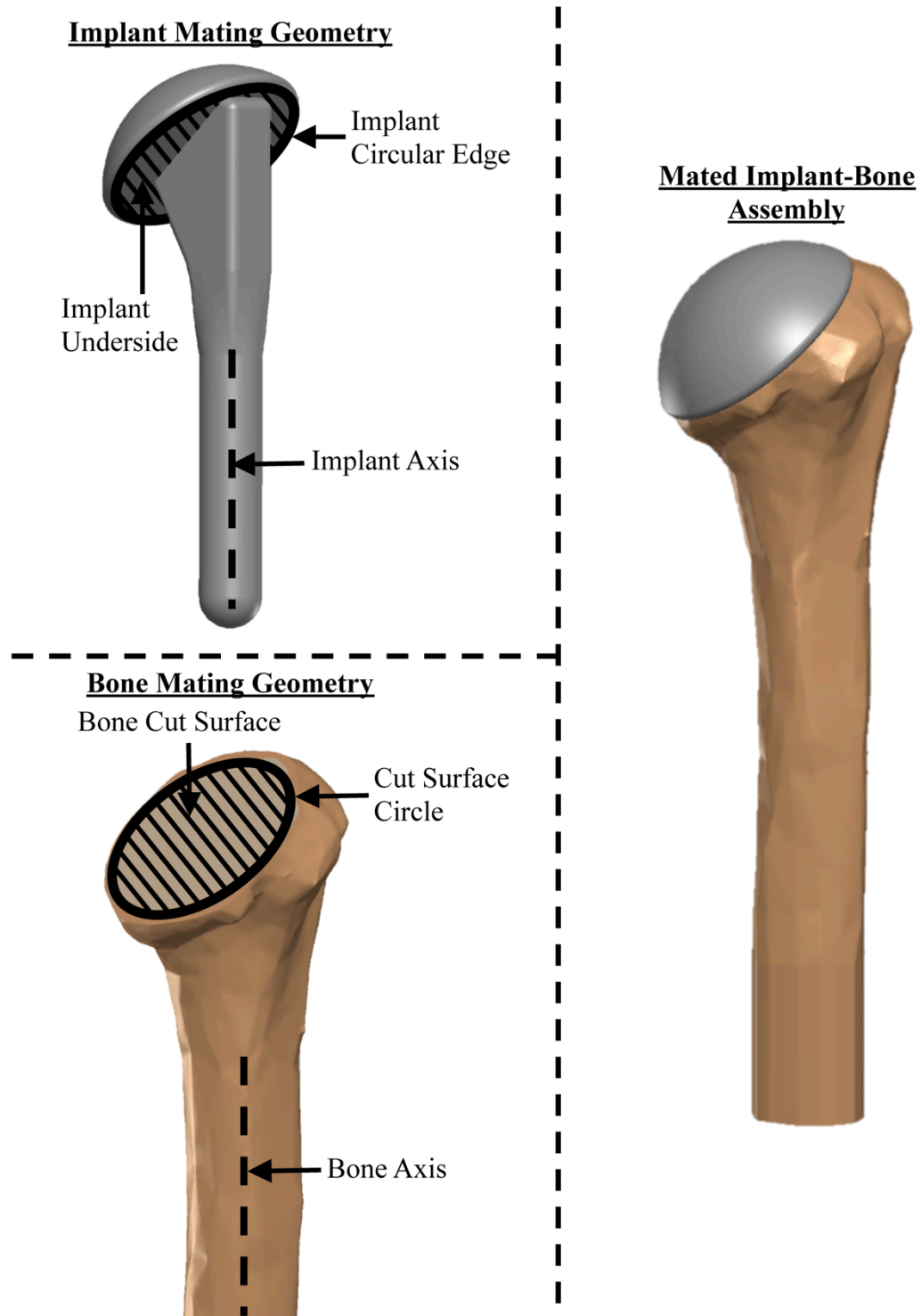


Figure 2.6: Implant-Bone Mating

Visual depiction of the mating surfaces, edges and axes on both the implant and bone.

convergence analysis, Section 2.9). A mesh refinement (element edge length = 0.25 mm) was applied to all sharp edges where implant-trabecular contact would be made.

2.6 Application of Material Properties

As discussed in Chapter 1 (Section 1.2.1), trabecular bone is an inhomogeneous structure with non-uniform mechanical properties, while cortical bone is far more uniform and can be approximated by Young's modulus and Poisson's ratio of 20 GPa and 0.3, respectively. In order to create a trabecular bone mesh that mimics the mechanical properties of *in-vivo* bone, element-specific Young's moduli need to be applied. To date, several studies have developed equations to relate CT scan data to bone stiffness (Austman *et al.*, 2009; Carter and Hayes, 1977; Leung *et al.*, 2009; Schileo *et al.*, 2007; Taddei *et al.*, 2006). The equation chosen for this investigation, which was reported by Morgan, *et al* (2003), is specific to trabecular bone (Equation 2.1).

$$E = 8920\rho_{app}^{1.83} \quad \text{Equation 2.1}$$

where, E is Young's modulus, and ρ_{app} is the apparent density of bone.

In order to apply Equation 2.1, the apparent density of the bone must first be known. Apparent density can be calculated from the Hounsfield (HU) data from a CT scan using MIMICS software. To calibrate HU to density, a linear relationship is applied based on two substances of known densities within the CT scan (Les *et al.*, 1994; Taddei *et al.*, 2006). The two known substances used were: SB3 cortical bone (Gammex, Middleton WI; density = 1.82 g/cm³) and water (density = 1.00 g/cm³). Unfortunately, these substances were not present in the pre-operative clinical patient CT scans from which the bone models were derived; however, the CT scan settings were known. Consequently, a calibration scan was taken with the known CT settings, and led to the linear calibration relationship shown in Figure 2.7. Since the density of any single voxel could contain both bone and water, to avoid overestimating the stiffness of fluid-filled regions within bone when calculating the Young's modulus, it was assumed that a voxel with the HU of water would contain no bone. Accordingly, the resulting bone density in a voxel with a HU of zero (water) would be 0 g/cm³.

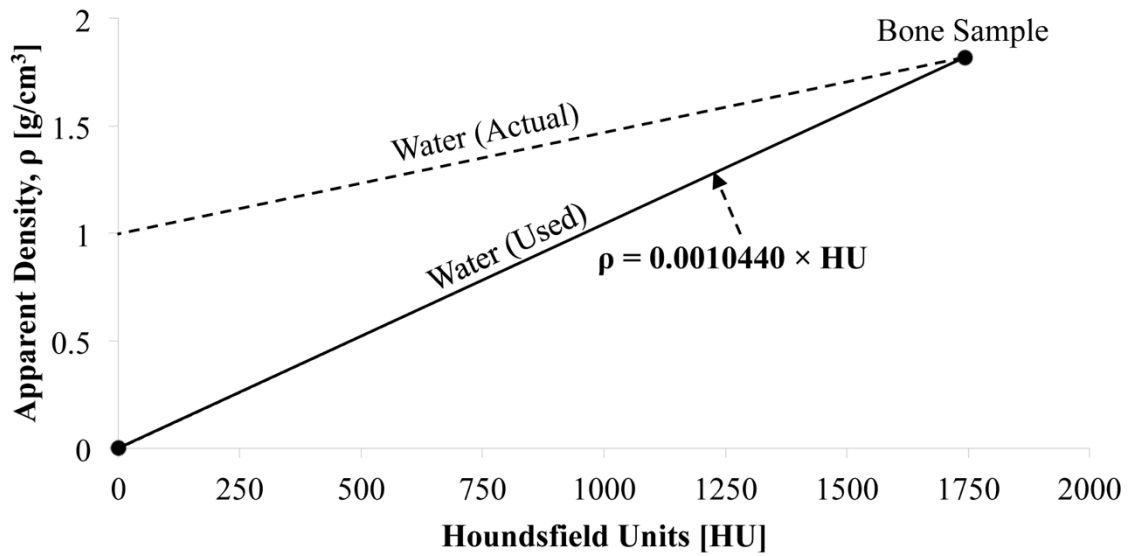


Figure 2.7: CT Density Calibration

To calibrate a CT scan Hounsfield Unit (HU) data into density (ρ), an artificial bone sample and water with known densities were scanned to provide 2 points that allow for the development of a linear ρ -HU calibration relationship.

Accordingly, the mesh files for the trabecular bone of each subject were imported into MIMICS, where element-specific Young's moduli and a Poisson's ratio of 0.3 were assigned based on the calibration relationship established in Equation 2.1. This process led to the creation of proximal humerus FE models that better mimic the behavior of *in-vivo* bone (Figure 2.8).

2.7 Finite Element Model Construction

With the bone and implant developed, all components were then combined using ABAQUS to create 30 finite element models ([3 stem lengths \times 3 different materials + 1 intact model] \times 3 different degrees of abduction) for each subject, for a total of 150 models (5 subjects \times 30 models). The breakdown of model variations is given in Figure 2.9. The four principal models were an intact proximal humerus model, and three reconstructed models with standard, short and stemless prostheses (Figure 2.10). All implant parts were meshed using appropriately sized quadratic, tetrahedral elements (see convergence analysis, Section 2.9; Appendix E), and cobalt-chrome material properties were assigned ($E = 210$ GPa, $\nu = 0.3$). Each component was then assembled into its respective model (*e.g.*, Intact model: complete cortical bone + complete trabecular bone; Standard model: cut cortical bone + cut trabecular bone + standard implant, etc.).

Implant-bone contact was defined as frictional. For all prostheses, proximal contact was modeled using a coefficient of friction of 0.63 to simulate wet bone on grit-blasted implant surfaces (Grant *et al.*, 2007). Additionally, distal contact between the standard stem and endosteal cortical bone was assigned a coefficient of friction of 0.40 to represent smooth/polished metal on wet bone (Kuiper and Huiskes, 1996) (Figure 2.11).

To investigate the effect of varying implant material stiffness, two additional models were created for the reconstructions, each with a different material applied: Titanium ($E = 105.0$ GPa, $\nu = 0.3$) and Poly Ether Ether Keytone (PEEK) ($E = 3.5$ GPa, $\nu = 0.36$) (Kurtz and Devine, 2007; Lee and Welsch, 1990). These materials were chosen to investigate how the proximal humerus would respond to a 50% reduction in material stiffness (Ti), as well as a low stiffness biocompatible material (PEEK).

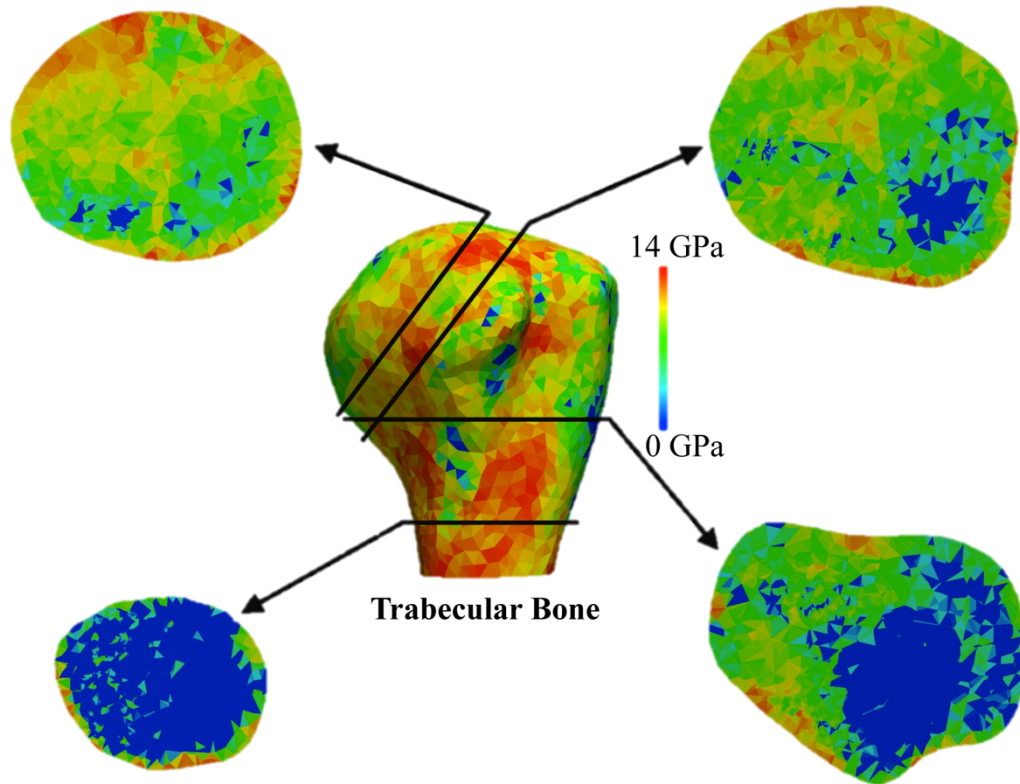


Figure 2.8: Trabecular Young's modulus Distribution

To account for the inhomogeneous nature of the trabecular bone stiffness, the Young's modulus was assigned based on regional bone density data. Accordingly, the models created had variable stiffness that better represented true trabecular bone.

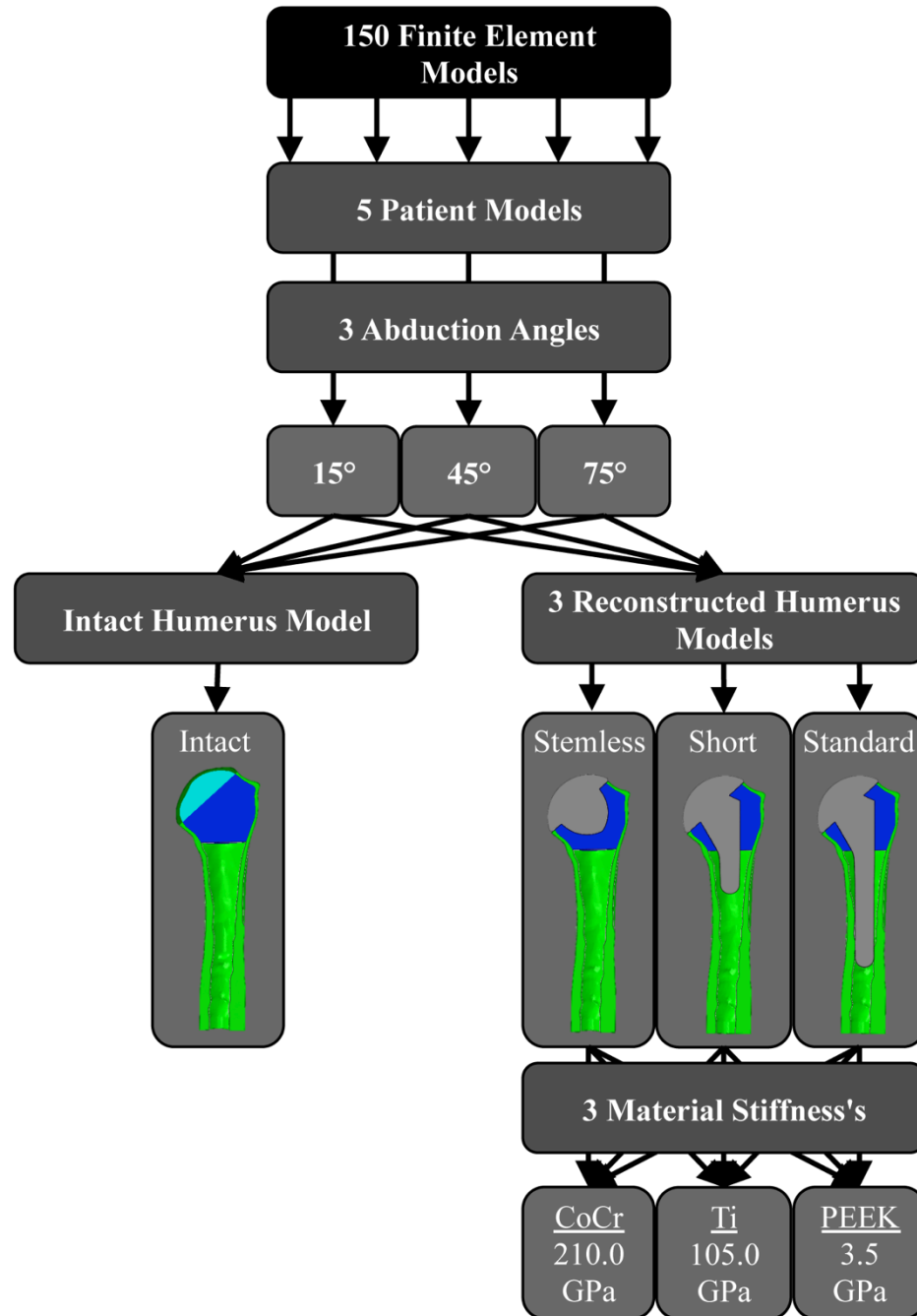


Figure 2.9: Breakdown of Model Variations

To investigate variation in both stem length and material stiffness, a total of 150 finite element models were developed from the CT scans of 5 patients. In total, 3 abduction angles were considered for the intact and reconstructed proximal humerus. Reconstructions consisted of standard, short and stemless implants, each constructed with CoCr, Ti and PEEK.

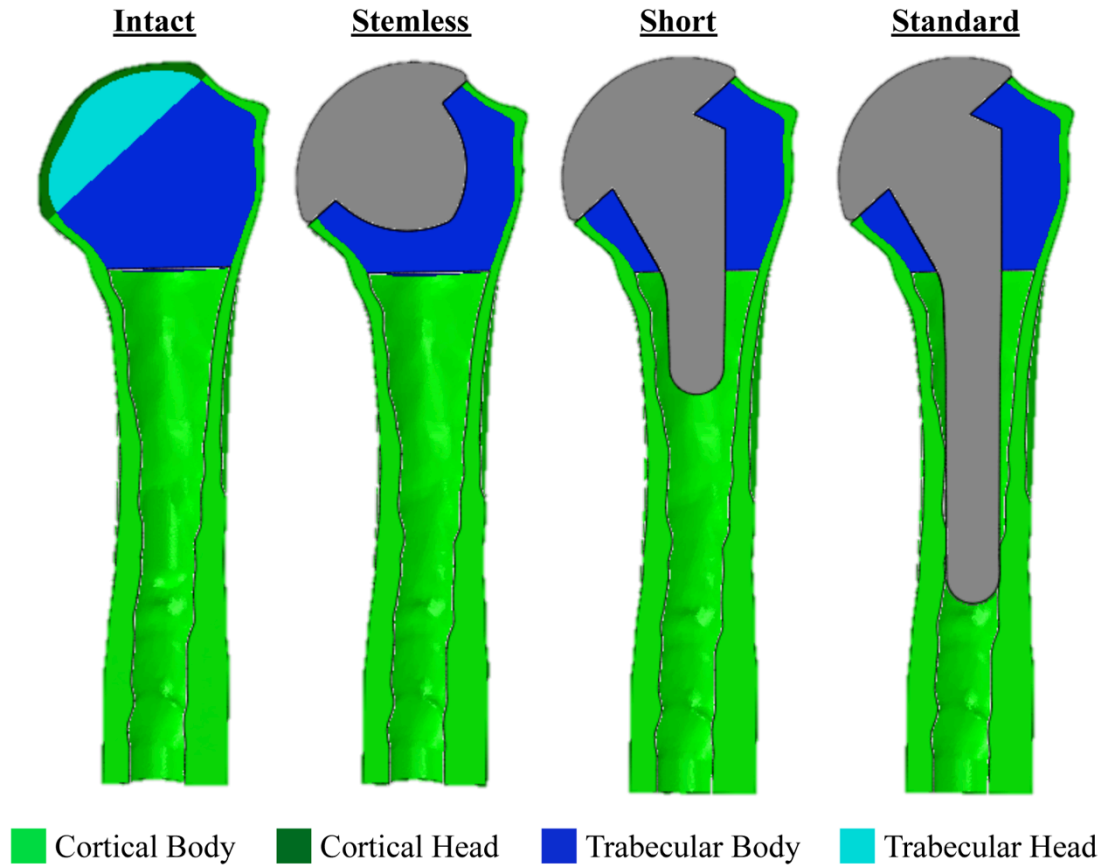


Figure 2.10: Intact and Reconstructed Models

To properly compare the effect of stem length on bone stresses in the proximal humerus, three reconstructed models with standard short and stemless implants were created and compared to the intact bone model.

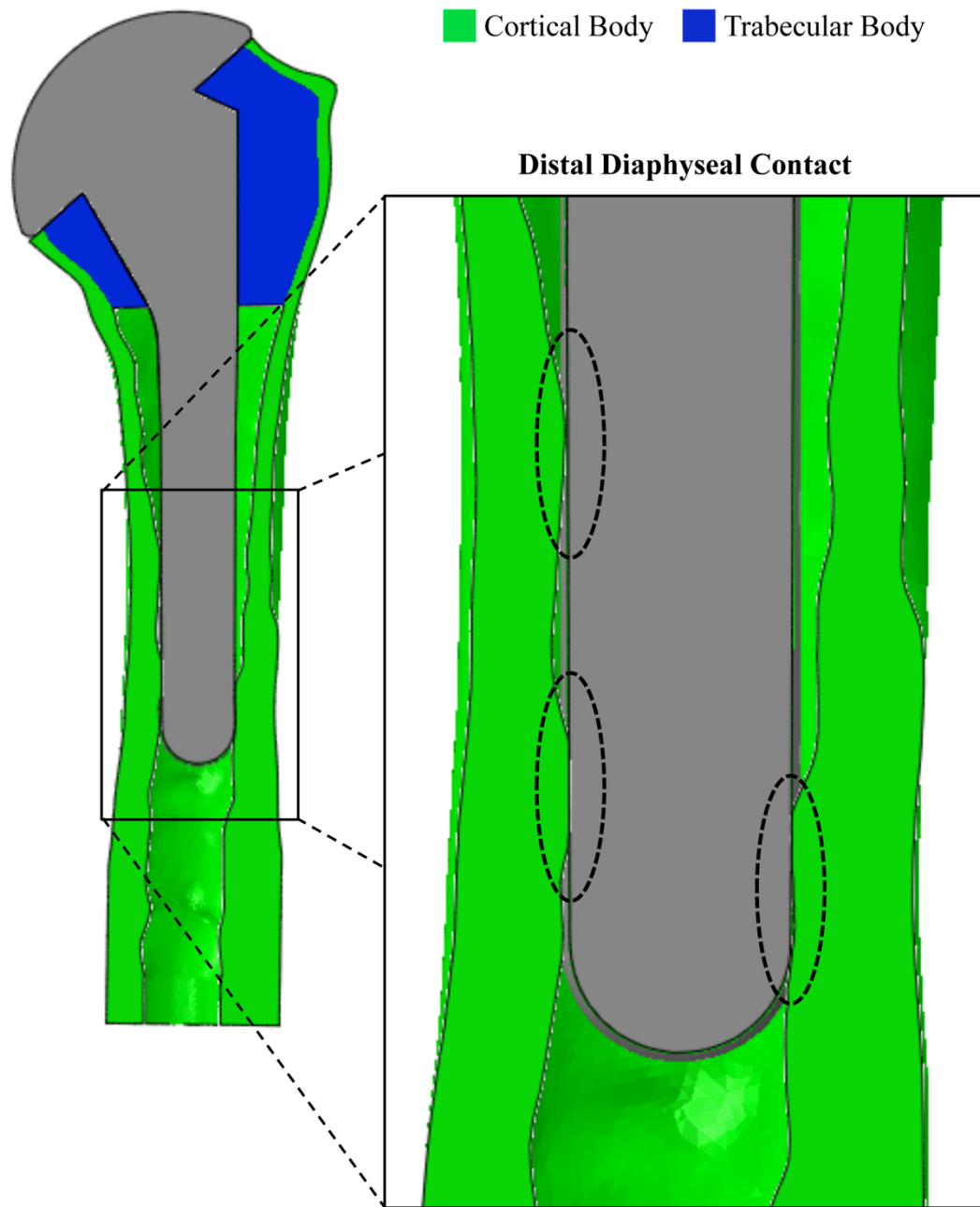


Figure 2.11: Standard Model Diaphyseal Contact

Distal frictional contact was simulated in the standard implant models, where the distal end of the stem came into contact with the endosteal bone surface. Stem diameter was chosen to create contact in the diaphysis and represents how this implant would be positioned clinically.

2.7.1 Boundary Conditions, Abduction Angles and Muscle Modeling

To restrict each model in space, the distal end of the humerus was rigidly fixed. To simulate the joint reaction force acting on the humerus, a point load was directed from the surface of the articulation towards the center of the humeral head according to *in-vivo* implant data (Bergmann *et al.*, 2007).

The action of shoulder abduction is a common motion of the arm. Three models representing typical abduction angles (15°, 45° and 75°) were developed for each material model (Figure 2.12). Changes in shoulder abduction were modeled by varying the magnitude and direction of the joint reaction force (Table 2.1). Force magnitude and direction were derived from *in-vivo* studies, where the force components (reported as percent of body weight) relative to a humeral coordinate system were recorded for varying abduction angles. A muscle force of 80 N was maintained as a constant for all subjects, assuming a 50th percentile male body weight of 88.3 kg (Bergmann *et al.*, 2007; McDowell *et al.*, 2008).

In lower angles of shoulder abduction, the deltoid muscle ‘wraps’ over the greater tuberosity of the proximal humerus. Accordingly, for the 15° model, muscle ‘wrapping’ was modeled with an outrigger running between the scapular muscle origin and the humeral insertion point. Tension was applied as a force of 80N based on a force-balance analysis of the system (Appendix F).

2.8 Outcome Variables

Due to changes in the structure of the proximal humerus following joint arthroplasty (*i.e.*, implanting a prosthesis), bone remodeling can occur. This phenomenon is known as stress shielding. Wolff’s Law suggests that changes in bone remodeling can be directly linked to the stress state of the bone (Wolff *et al.*, 1986). Unfortunately, bone remodeling following arthroplasty can lead to weakening of the bone structure and ultimately implant loosening and possibly failure (Manley *et al.*, 1983). Accordingly, to quantify changes in the proximal humerus following total shoulder arthroplasty, bone stresses were investigated for both the intact and reconstructed models. Specifically, the single element

endosteal stresses along the medial, lateral, anterior, and posterior aspects of the implants in bone, average stress in site-specific bone slices, and overall average elemental stress changes were found for both the cortical and trabecular bones. The creation of an identical mesh allows for the direct comparison of elemental stresses for all stem conditions within each subject.

To further map how bone stresses change along the implant as a function of the distance from the humeral head, single element endosteal stresses were found for the medial, lateral, anterior and posterior sides of the humerus for 17 slices in total (Figure 2.13). A subset of three slices were chosen to allow statistical comparison between stem conditions and across all subjects. These three slices corresponded to slices that crossed the tip of stemless, short, and standard implants. Again, due to the development of a novel identical mesh, the exact same element was chosen from the intact and reconstructed models for each slice.

To quantify change in the stress between intact and reconstructed models, the six components of stress (3 normal and 3 shear) were found for each element in both the intact and reconstructed models. Then, the change in stress for these six components was found for each element by subtracting the intact stress values from the reconstructed stress values. Following this, the Von Mises of the change in stress was calculated using Equation 2.2 for each element (Budynas R.G, 2011).

Von Mises Equation:

$$\sigma_{VM} = \sqrt{0.5 \times ((\sigma_{11} - \sigma_{22})^2 + (\sigma_{22} - \sigma_{33})^2 + (\sigma_{11} - \sigma_{33})^2 + 6 \times (\sigma_{12}^2 + \sigma_{23}^2 + \sigma_{31}^2))}$$

(Equation. 2.2)

where σ_{VM} represents the Von Mises stress and σ_{11} , σ_{22} , σ_{33} are the changes in normal stresses in x, y and z directions, respectively, while σ_{12} , σ_{23} , σ_{31} represent the change in the shear stresses.

To avoid any one element from having too profound of an effect on the global stress state of the bone, a volume-weighted average was then calculated for the change in stress of the bone (σ_{VWA}) (Equation. 2.3). To permit comparison of this stress term across multiple

subjects, the σ_{VWA} change in stress values were represented as percent-changes with reference to the intact model's σ_{VWA} . The overall σ_{VWA} changes were calculated for cortical and trabecular bone separately.

Volume-Weighted Average Stress Equation:

$$\sigma_{VWA} = \frac{\sum(\sigma_{VM} \times Volume \ of \ the \ element)}{\sum(Element \ Volume)} \quad (\text{Equation. 2.3})$$

where σ_{VWA} is the Von Mises of the change in stress for each element (Equation. 2.2).

To provide further insight into regional changes in the bone stress state, σ_{VWA} was also calculated for transverse slices of the humerus at predefined distances from the humeral head. In total, nine slices of cortical bone, and three slices of trabecular bone were chosen (Figure 2.14). These stress values were then averaged for intact, standard, short and stemless models across all specimens.

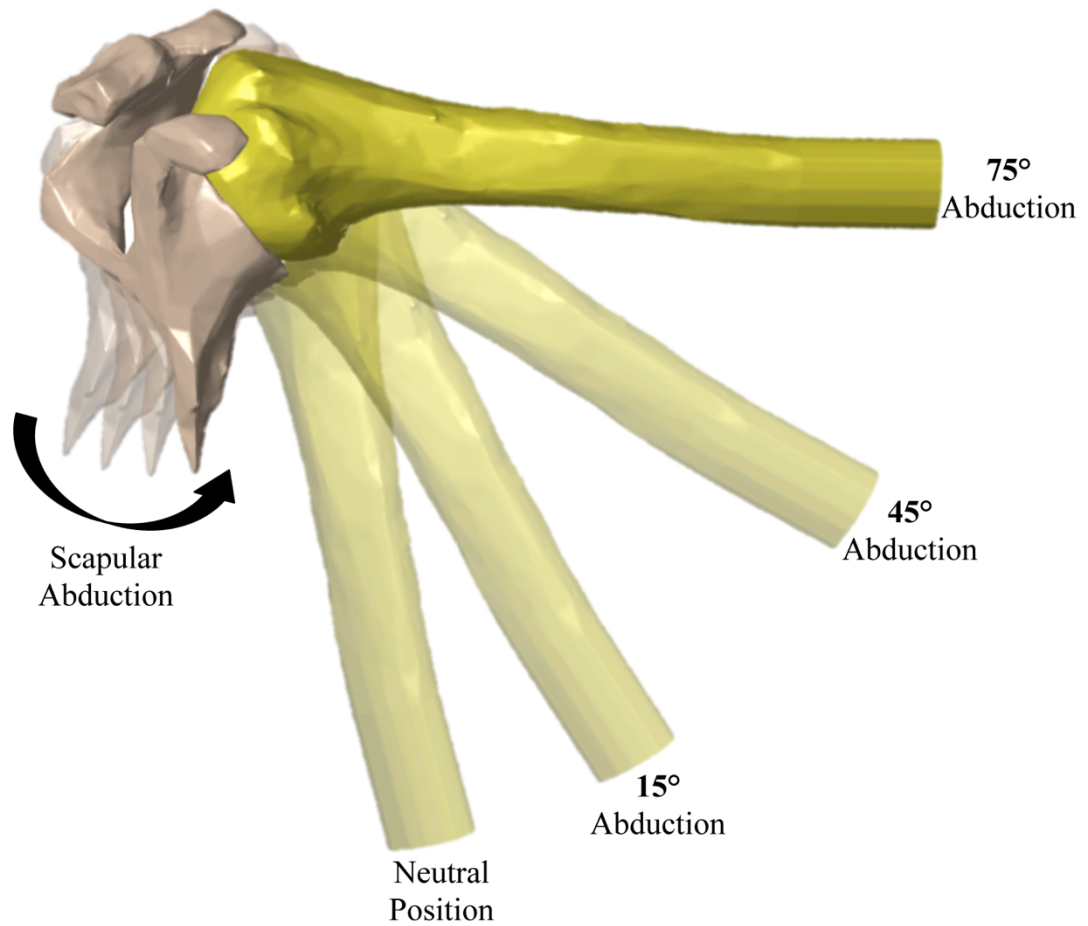


Figure 2.12: Shoulder Abduction Angles

To account to changes in shoulder loads throughout the completion of many daily activities, 3 abduction angles were chosen for investigation: 15°, 45° and 75°.

Table 2.1: Joint Reaction Forces for 15°, 45° and 75° of Shoulder Abduction According to Bergmann *et al* (2007)

Abduction Angle	Joint Reaction Force Components [N]*			
	Superior-Inferior	Anterior-Posterior	Medial-Lateral	Resultant
15°	20	-7	5	190
45°	44	-21	16	440
75°	74	-34	25	740

* Data converted to Newtons assuming 88.3 kg body-weight.

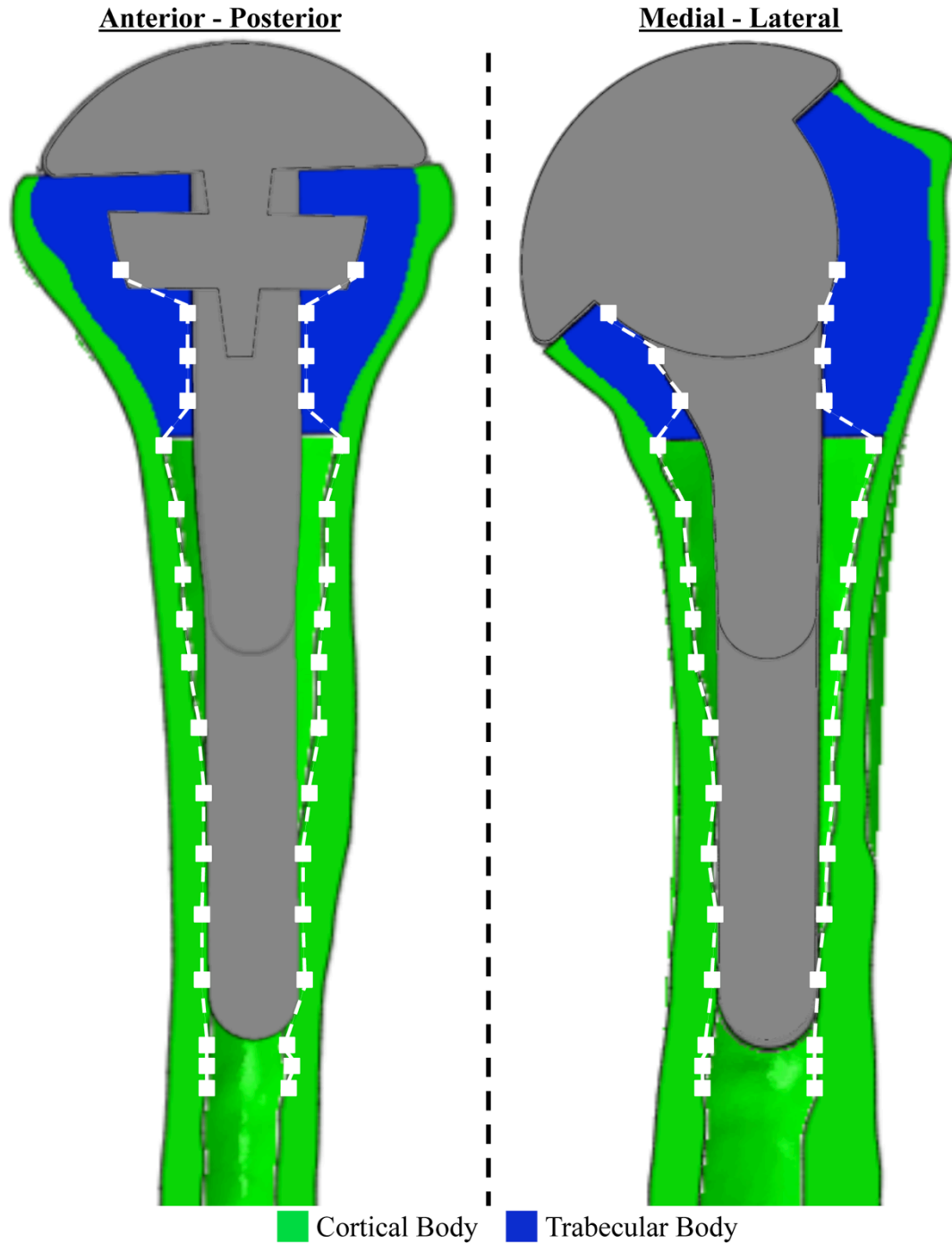


Figure 2.13: Humeral Endosteal Path Positions

Endosteal path points (shown in white) were chosen to lie on the intersection of pre-determined slices (perpendicular to the humeral axis) with anterior-posterior and medial-lateral planes.

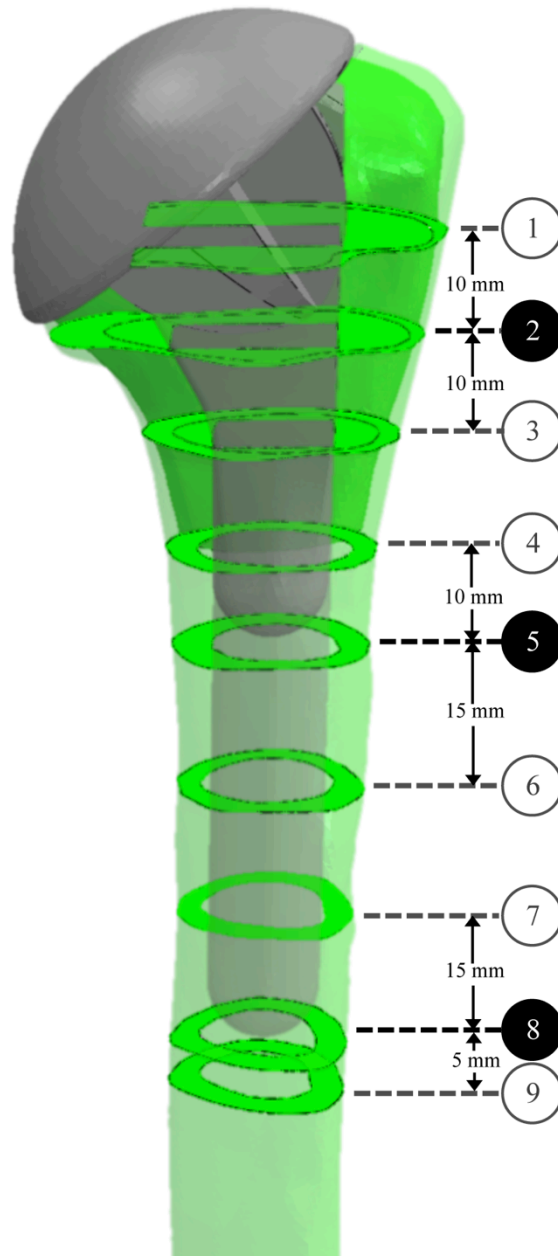


Figure 2.14: Humeral Slice Positions

To quantify regional stresses in the intact and reconstructed models, cortical and trabecular slices were chosen at predefined slices spaced along the humerus. Reference slices 2, 5 and 8 were chosen to coincide with the tip of each implant.

To test the effect of varying stem length and material stiffness on each of the above outcomes, a three-way repeated measures ANOVA (with Bonferroni post-hoc test) was conducted using SPSS software (IBM, New York, USA); where the three independent variables were: stem length, implant material stiffness and abduction angle. Alpha was set at 0.05 for all statistical tests.

2.9 Convergence Analysis

When a model represents a continuous geometry with a finite number of sections as in finite element analysis (FEA), steps must be taken to ensure that the model accurately represents the mechanical properties of the continuous structure (Panagiotopoulou *et al.*, 2012). This process is known as a convergence analysis. To select the appropriate mesh size, a convergence analysis was conducted using models from a single subject, in 45° of abduction with cobalt chrome implants. Convergence was investigated using the volume-weighted average stress (σ_{VWA}) of the cortical and trabecular bone, and the number of elements present in each model. The number of elements in the model was increased by approximately 50% with each iteration. Once the variation in σ_{VWA} between mesh refinements was less than 10%, the optimal mesh size was chosen for that model; however in order to create an identical mesh across models, the lowest global mesh size was chosen. The results indicated that all models had successfully converged when a global element size of 2 mm was used (Chapter 3, Section 3.1).

2.10 Summary

To investigate how changes in implant length and material stiffness affect the bone stresses of the proximal humerus, 150 finite element models were developed. These models consist of an intact state and three reconstructed states (*i.e.*, standard, short and stemless), each of which was constructed with three separate biocompatible materials (*i.e.*, CoCr, Ti and PEEK). Three outcome measures (*i.e.*, single-element stress paths, average bone slice stresses and overall average cortical and trabecular stresses) were chosen to provide insight into how stresses change (overall and regionally) within the proximal humerus after joint reconstruction. Following convergence analysis and the

successful completion of all models, results were collected and are presented and discussed in the following chapters.

Chapter 3

3 Results

3.1 Mesh Convergence

Using the CT scan data of a single specimen, a total of 20 FE models were successfully developed for the purpose of quantifying mesh convergence (4 models: intact, standard, short and stemless; 5 mesh sizes (corresponding to 50% increases in number of elements): 4.70 mm, 3.51 mm, 2.75 mm, 2.00 mm and 1.45 mm). The resulting volume weighted average stresses in cortical and trabecular bone demonstrated convergence at a mesh size greater than or equal to 2.00 mm for all models (Figure 3.1). The chosen mesh sizes corresponded to percent-differences less than 10%. The short model converged at the largest mesh size (Cortical: 3.51 mm, 5.3% difference; Trabecular: 3.51 mm, 2.2% difference), followed by intact (Cortical: 2.75 mm, 0.3% difference; Trabecular: 2.75 mm, 4.1% difference), standard (Cortical: 4.7 mm, 1.0% difference; Trabecular: 2 mm, 3.5% difference) and stemless (Cortical: 2 mm, 9.0% difference; Trabecular: 2 mm, 0.7% difference) models.

3.2 Effect of Stem Length

The effect of stem length was investigated through the quantification of single-element Von Mises stresses at 17 predefined endosteal points for each of the anterior, posterior, medial and lateral sides of the bone, as well as the average Von Mises stress in 9 predefined slices along the long axis of the proximal humerus. In addition, a volume weighted average of the change in stress between the intact and reconstructed model was measured to provide a single value indicating how stresses changed in the cortical and trabecular bone for each implant stem length.

3.2.1 Regional Stresses in the Proximal Humerus

3.2.1.1 Single-Element Path Results

Due to inter-specimen trabecular length variation, of the 17 available endosteal points, three points corresponding to the slices through the tip of each prosthesis were chosen for

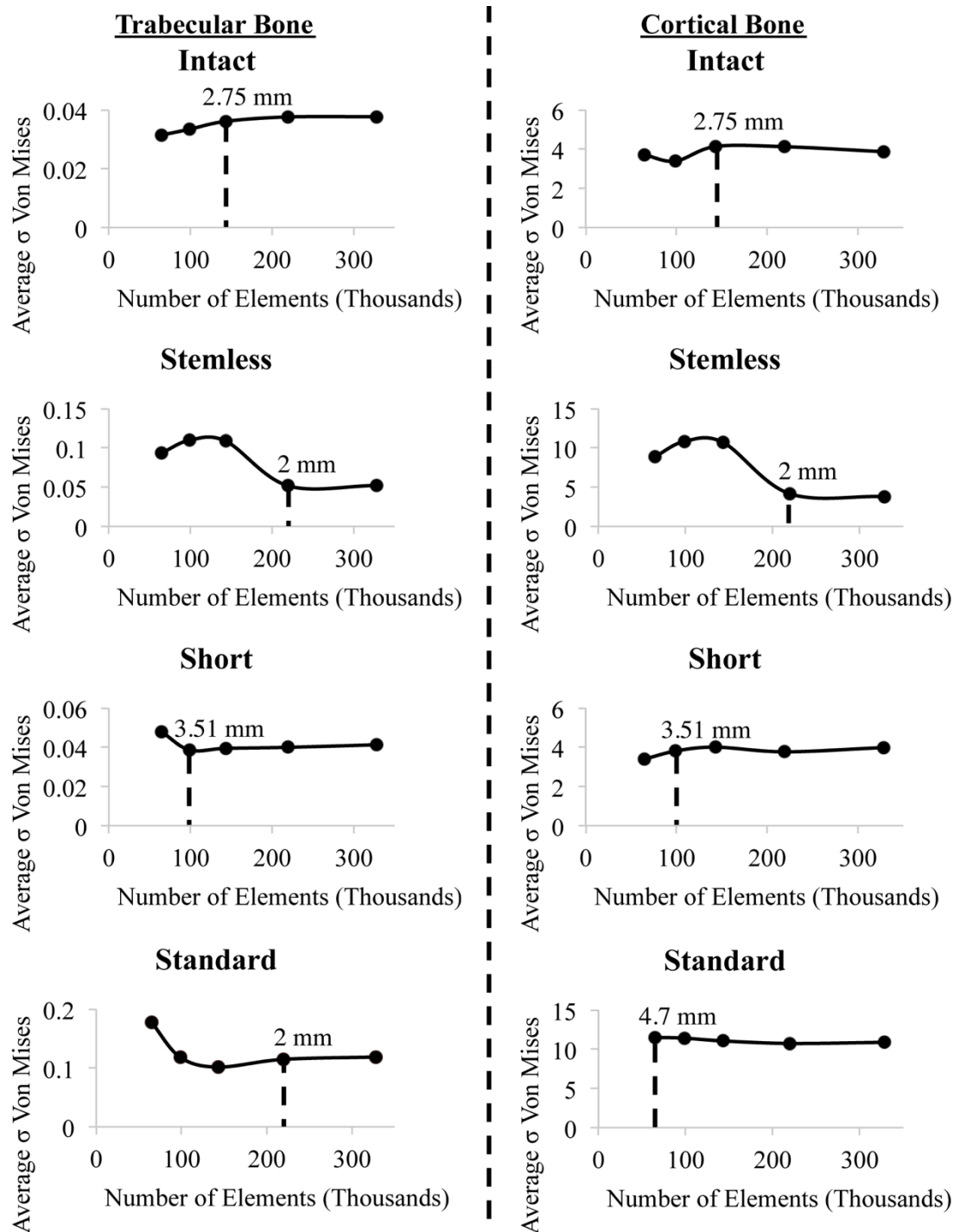


Figure 3.1: Convergence Results

Mesh sizes at which convergence of the intact, standard, short and stemless models occurred are represented by dashed lines. Investigated mesh sizes were chosen corresponding to increases of 50% in the total number of elements in the intact model.

statistical comparison between models (points 3, 9 & 15) (Figures 3.2 - 3.7). Significant differences were only found in the most distal point (point 15) and arose from a material-by-length-by-abduction angle interaction. Specifically, use of the standard implant resulted in significantly different bone stresses than the intact model for all combinations of material and abduction angle ($p = 0.037$), except for PEEK reconstructions in 15° and 45° . Additionally, the bone stress in short and stemless prostheses models were only found to significantly diverge from the intact state in the higher abduction angles of 45° and 75° (for all materials and sides of the bone) ($p = 0.037$). The CoCr and Ti constructions of the standard length stem were found to produce significantly different bone stress results compared to the short (CoCr: $\sim 10\%$ change, Ti: $\sim 9\%$ change) and stemless (CoCr: $\sim 11\%$ change, Ti: $\sim 10\%$ change) designs in both 15° and 75° of abduction ($p = 0.037$).

3.2.1.2 Bone Slice Stress Results

Considering the average stress in cortical bone slices, it was found that only the two most proximal slices (slices 1 & 2) and the most distal slice (slice 9) presented with significant differences (Figures 3.8 - 3.10). Within the first slice, the average stresses were significantly affected by a stem length main effect, such that the stemless implant seems to cause significantly higher cortical bone stresses than both the short ($\sim 17 \pm 18\%$ change) and standard stem designs ($\sim 34 \pm 20\%$ change) ($p < 0.045$), though all were still typically less than the bone stresses produced in the intact model except stemless 45° and 75° of abduction. Additionally, a material-by-length interaction lead to significant reductions in cortical bone stresses when the standard and short prostheses were used compared to the intact and stemless models when all were constructed with CoCr ($p = 0.005$). The standard implants also lead to significantly less bone stress than the intact ($\sim 40 \pm 19\%$ less), stemless ($\sim 40 \pm 21\%$ less) and short ($\sim 23 \pm 25\%$ less) models when constructed with Ti ($p = 0.005$). Furthermore, a length-by-abduction angle interaction yielded significant reductions in bone stress for standard implants contrasted with intact and stemless models for all abduction angles, and for short stems compared to the intact state for 15° of abduction ($p = 0.017$).

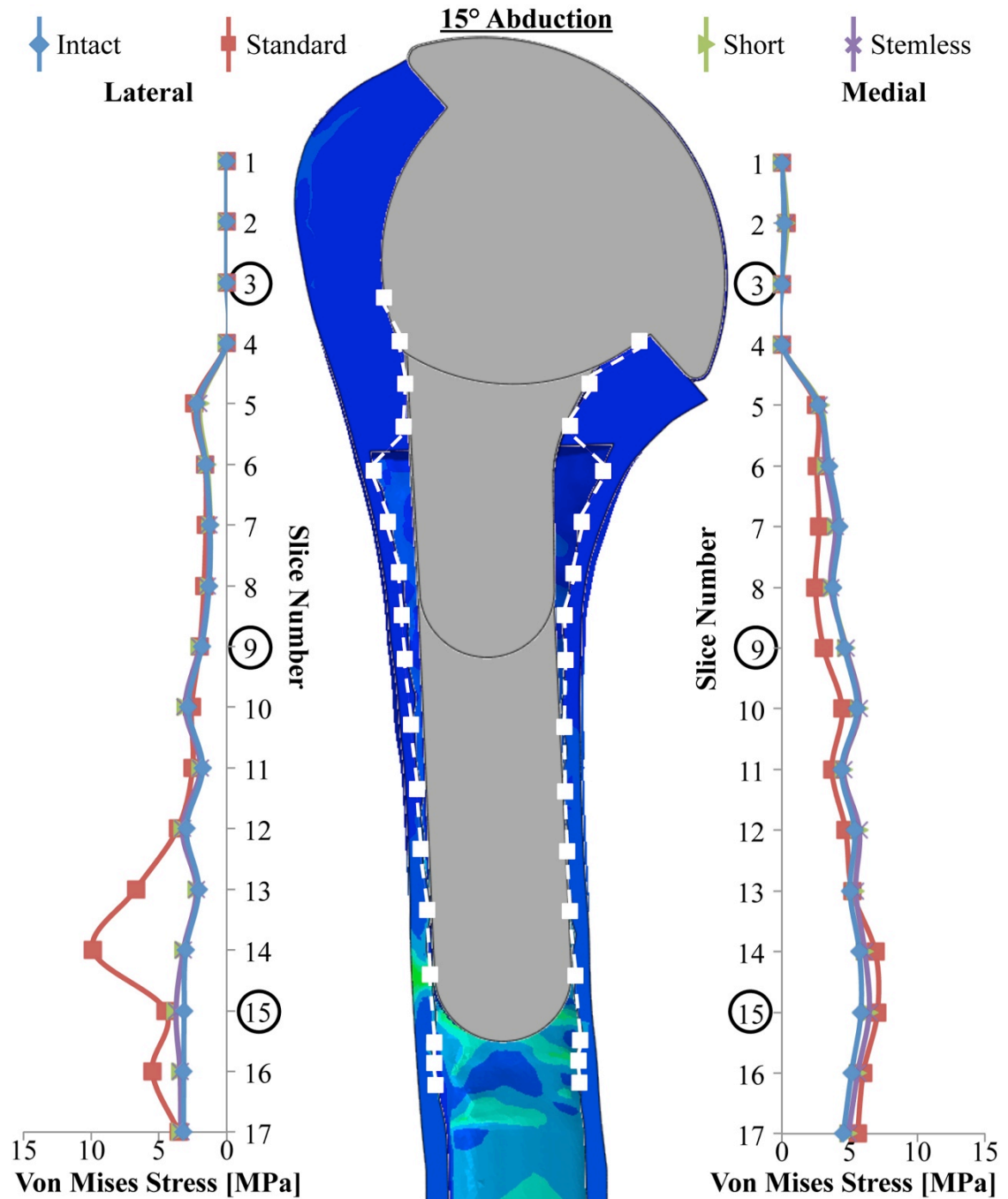


Figure 3.2: Element-Specific Medial and Lateral Stress Paths – 15° Abduction

Single element stress values are present at 17 points on both the medial and lateral endosteal bone surface of a representative patient with CoCr implants. Circled points are those which correspond to the tip of each implant type (standard, short and stemless) and which were assessed for statistically significant differences (Results for all subjects can be found in Appendix G).

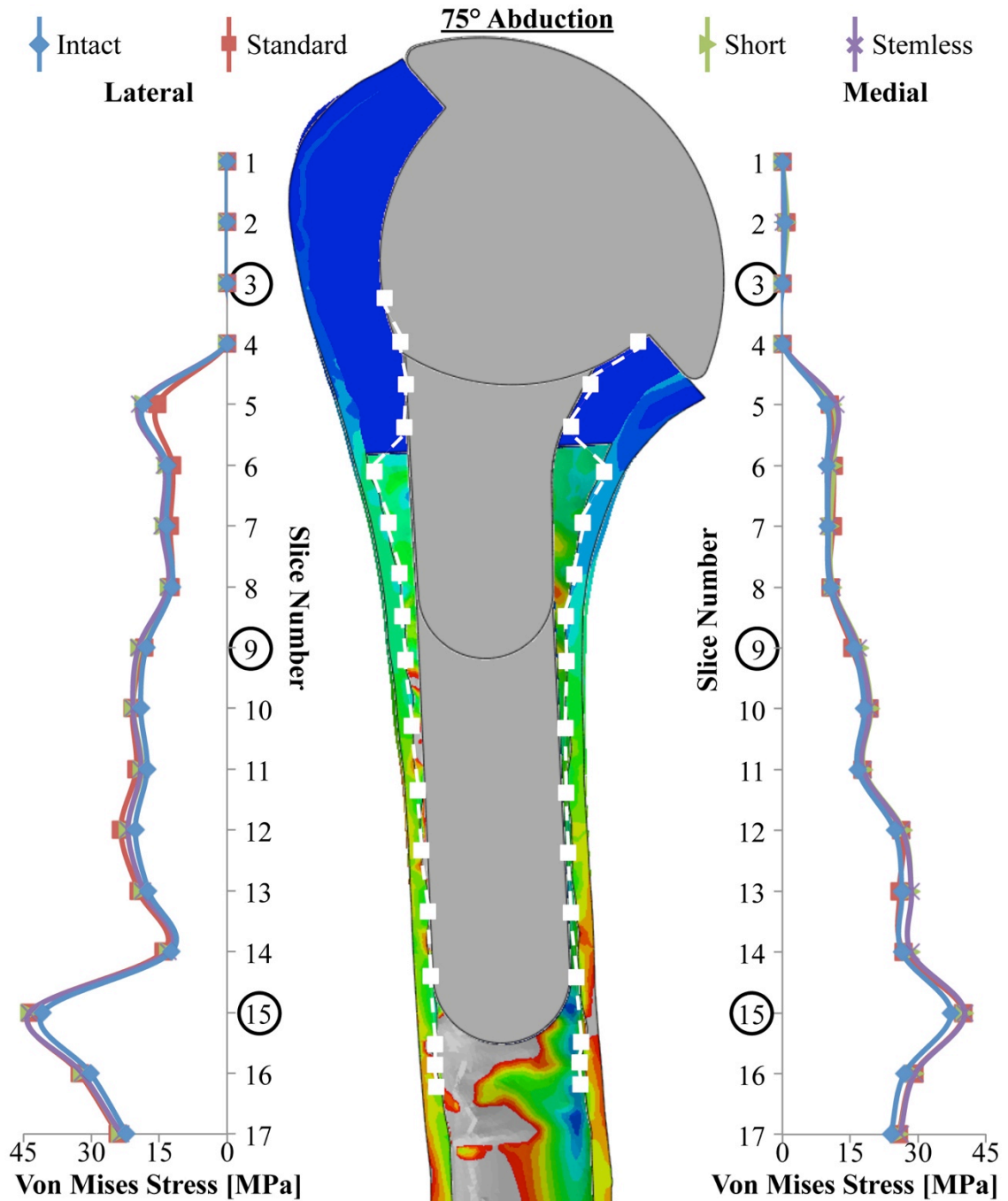


Figure 3.4: Element-Specific Medial and Lateral Stress Paths – 75° Abduction

Single element stress values are present at 17 points on both the medial and lateral endosteal bone surface of a representative patient with CoCr implants. Circled points are those which correspond to the tip of each implant type (standard, short and stemless) and which were assessed for statistically significant differences (Results for all subjects can be found in Appendix G).

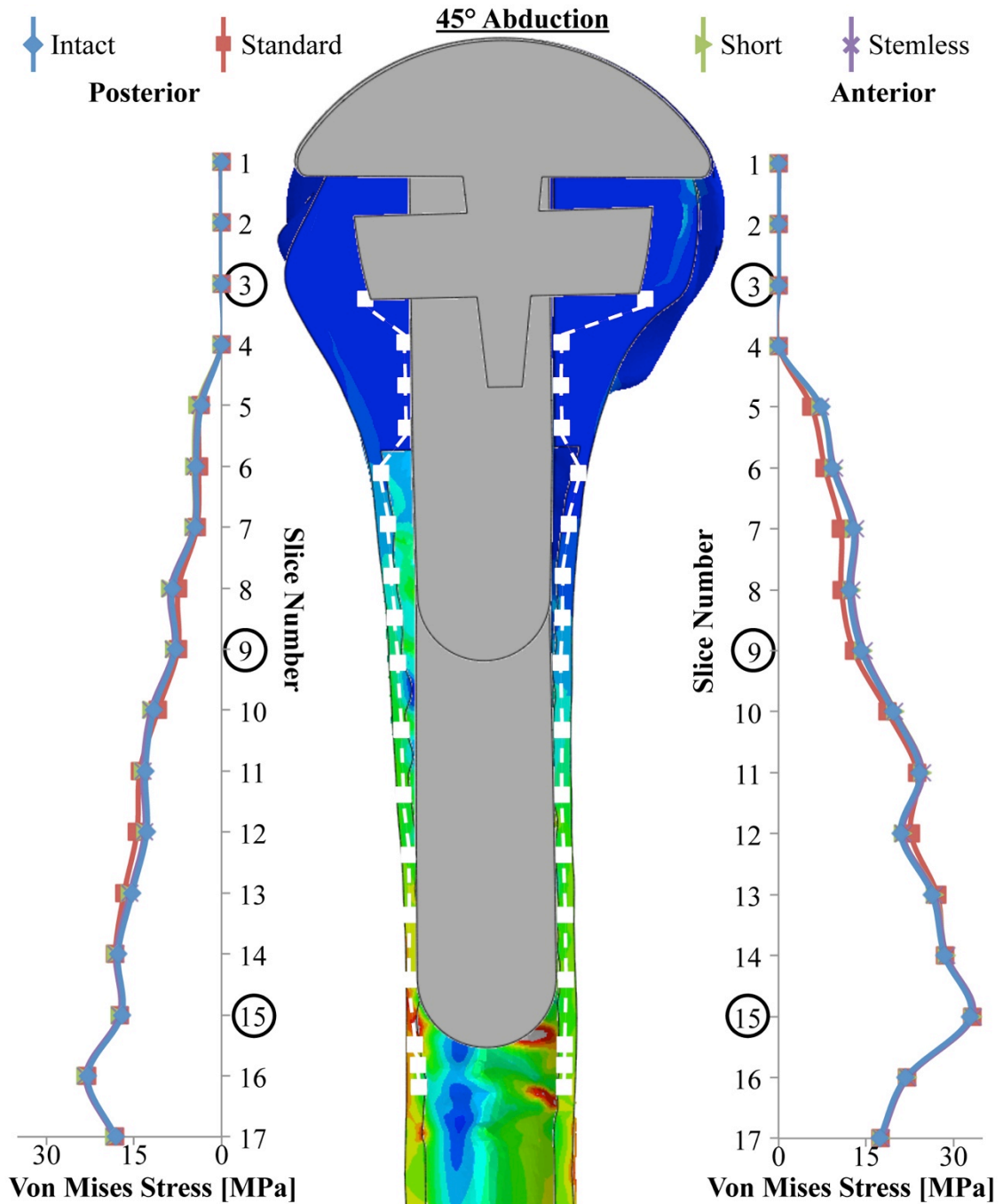


Figure 3.6: Element-Specific Anterior and Posterior Stress Paths – 45° Abduction

Single element stress values are present at 17 points on both the anterior and posterior endosteal bone surface of a representative patient with CoCr implants. Circled points are those which correspond to the tip of each implant type (standard, short and stemless) and which were assessed for statistically significant differences (Results for all subjects can be found in Appendix G).

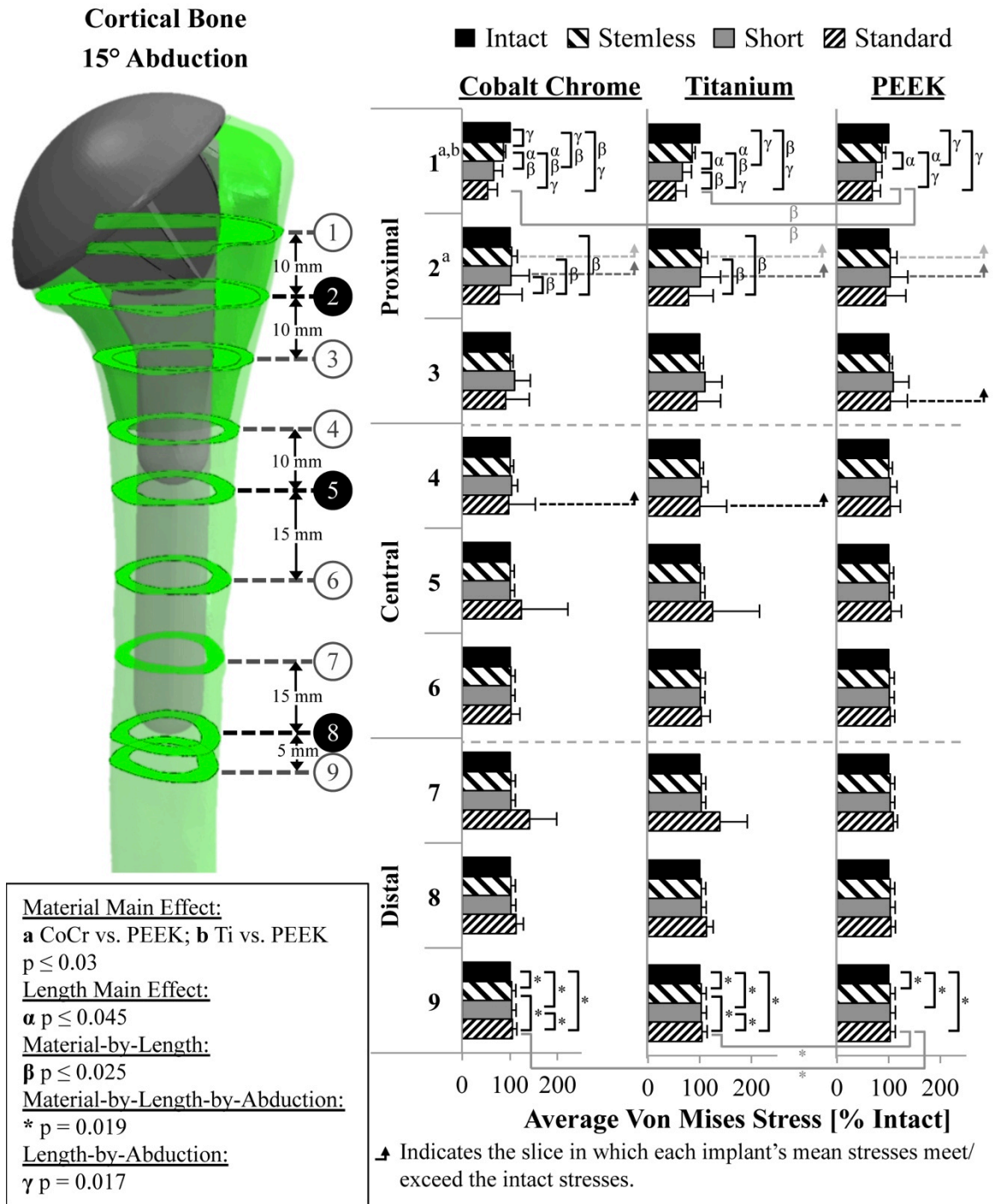


Figure 3.8: Average Stress in Cortical Bone Slices - 15° Abduction

Mean (+SD) average stress in cortical bone slices are given for all stem length variations, where the resulting stress is presented as a percentage of the intact bone stress in each slice.

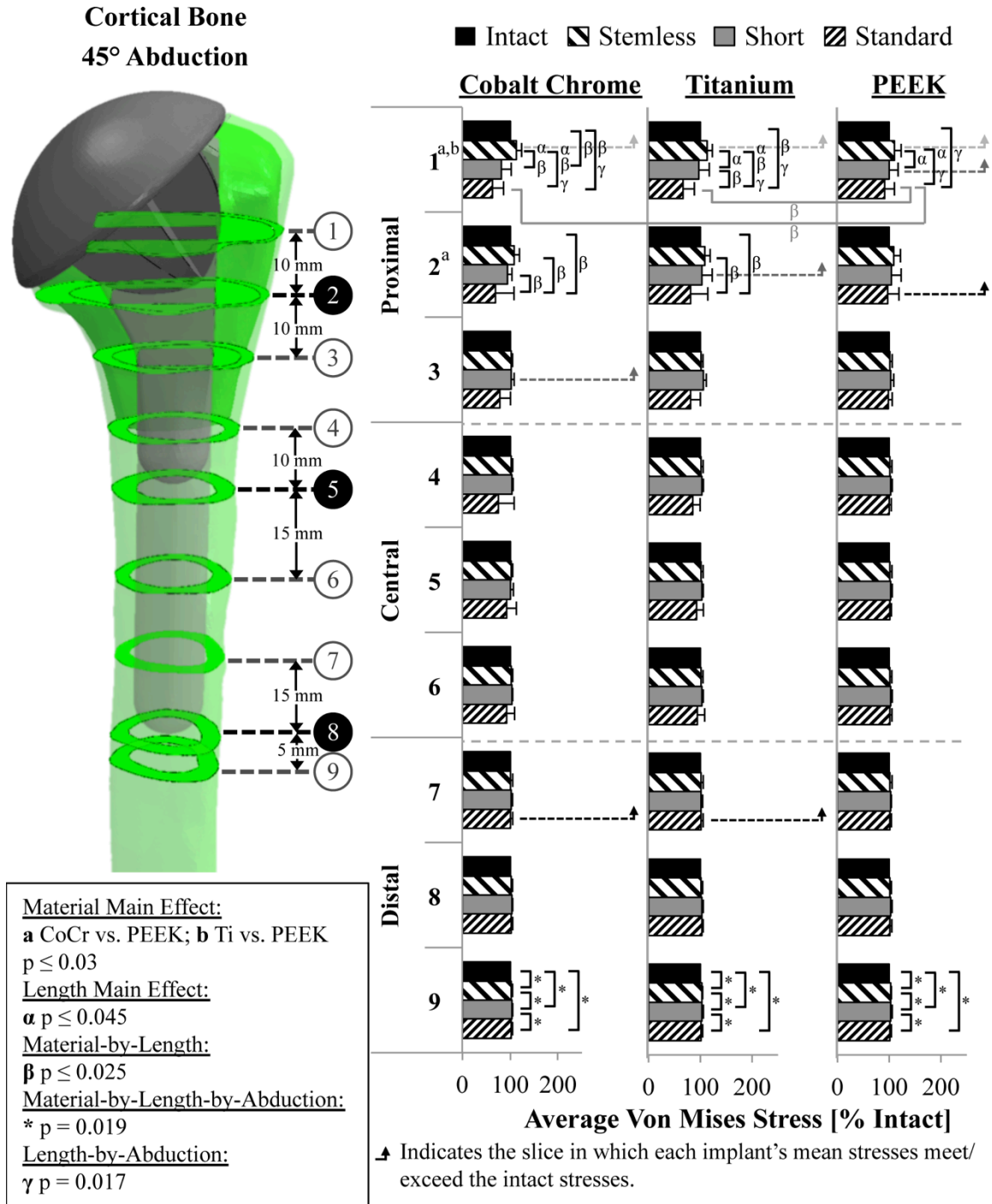
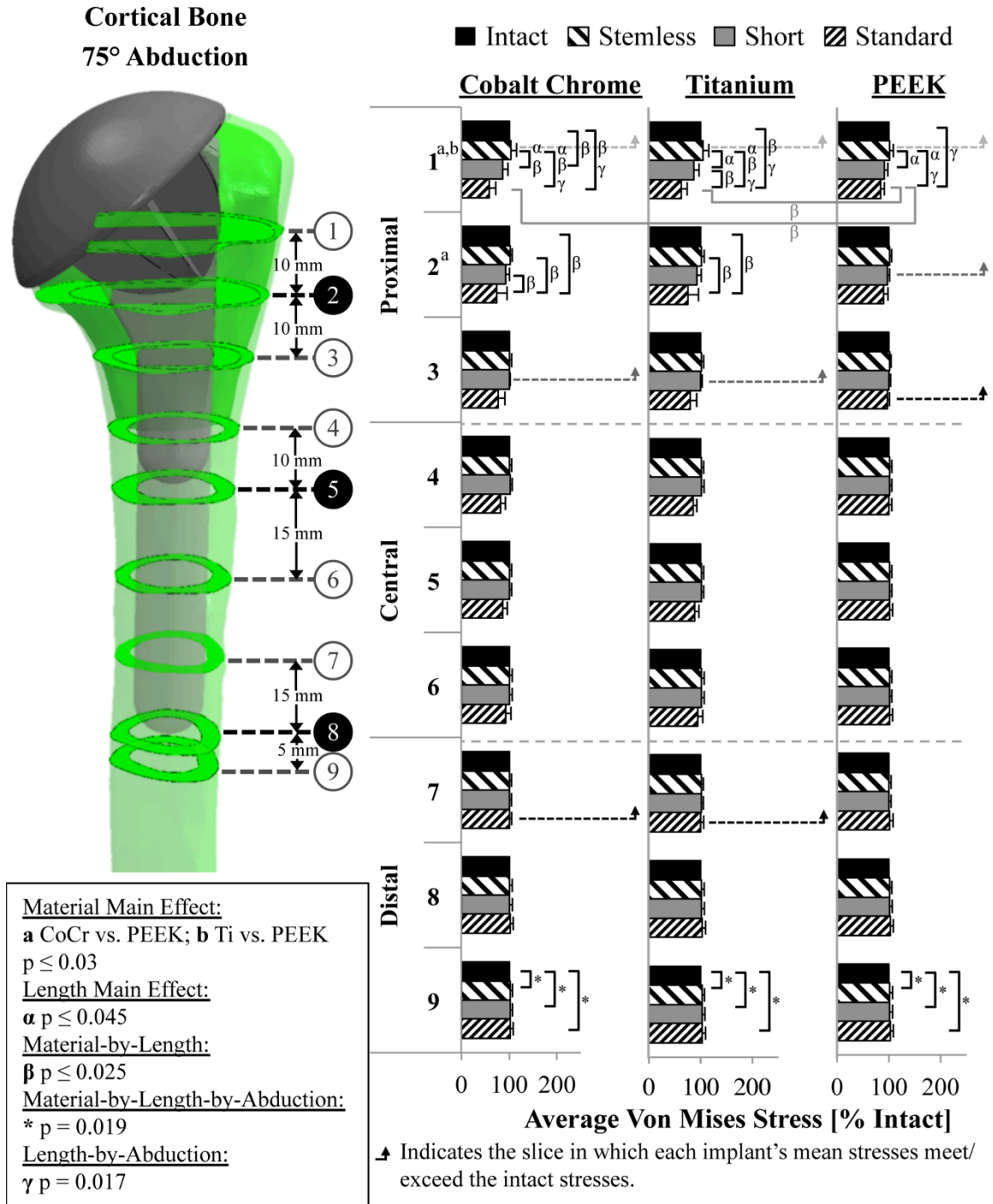


Figure 3.9: Average Stress in Cortical Bone Slices – 45° Abduction

Mean (+SD) average stress in cortical bone slices are given for all stem length variations, where the resulting stress is presented as a percentage of the intact bone stress in each slice.

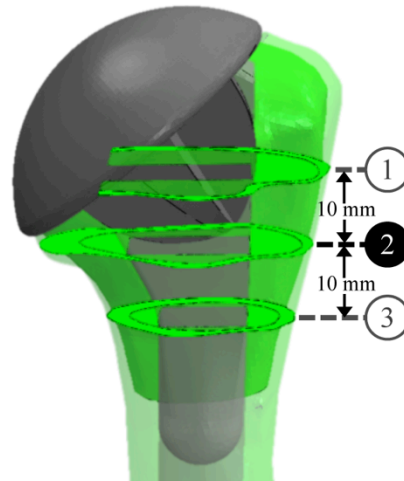


In the second slice, a material-by-length interaction indicated that significant reductions in cortical bone stresses persisted for the standard length prostheses constructed with CoCr compared to the intact ($\sim 26 \pm 36\%$ less), stemless ($\sim 31 \pm 37\%$ less) and short ($\sim 23 \pm 42\%$ less) models ($p = 0.025$). Similar reductions in stress were also significantly different between the standard and intact, and standard and stemless models when Ti was used as the implant material ($p = 0.025$), though the standard and short models no longer differed significantly.

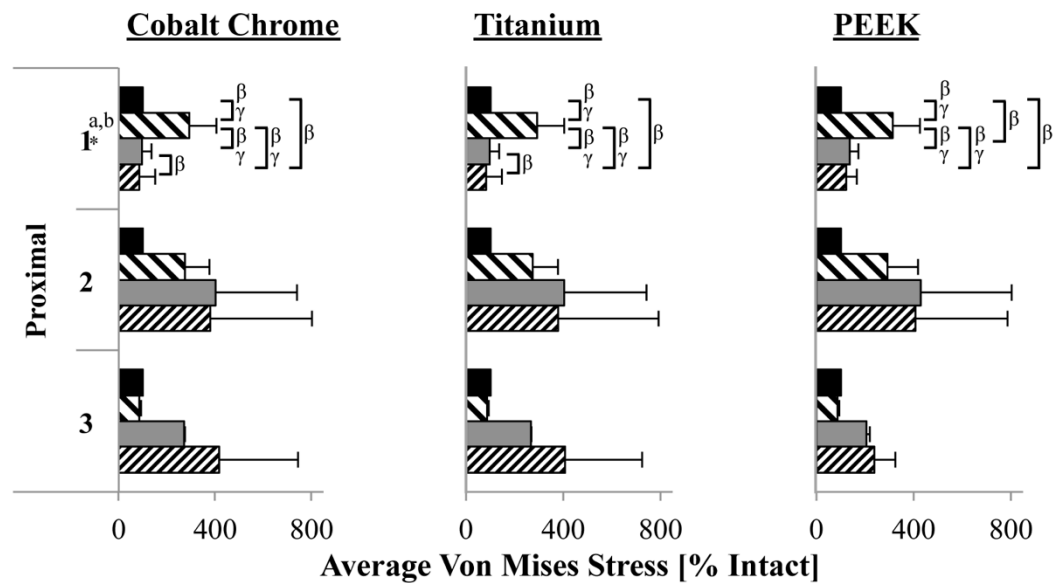
Surprisingly, in the 9th and most distal slice, a material-by-length-by-abduction angle interaction suggested that cortical bone stresses of the intact models were significantly different than all reconstructions regardless of the material used and the abduction angle ($p = 0.019$). Additionally, within 15° of abduction, significant differences were again found between standard and short, and standard and stemless prostheses constructed of CoCr and Ti. Moreover, regardless of material, bone stress in the short stem model presented as significantly different from the standard and stemless prostheses models in 45° of abduction ($p = 0.019$).

Due to inter-specimen trabecular bone length variations, regional average stresses in slices were obtained in five specimens for the two most proximal trabecular slices, but in only two specimens for the third slice. Statistically significant differences between stem types only presented in the first trabecular bone slice (Figures 3.11 - 3.13). Within this slice, a length main effect demonstrated that the average stress was significantly less for the standard length stem compared to both the short ($\sim 17 \pm 53\%$ less) and stemless ($\sim 148 \pm 100\%$ less) prostheses ($p < 0.038$). Additionally, standard model bone stresses were also significantly different than the intact state ($\sim 14 \pm 40\%$ change) for all materials tested due to a material-by-length interaction ($p \leq 0.001$). Furthermore, material-by-length and length-by-abduction angle interactions demonstrated that regardless of implant material stiffness and abduction angle, the stemless implant significantly elevated trabecular stresses compared to intact, short and standard models ($p \leq 0.001$). Moreover, a material-by-length interaction illustrated that the short stemmed implant bone stresses were significantly higher than the standard implant when constructed of either CoCr or Ti, but significantly higher than the intact state when constructed of PEEK ($p \leq 0.001$).

**Trabecular Bone
15° Abduction**



■ Intact ▨ Stemless ■ Short ▩ Standard

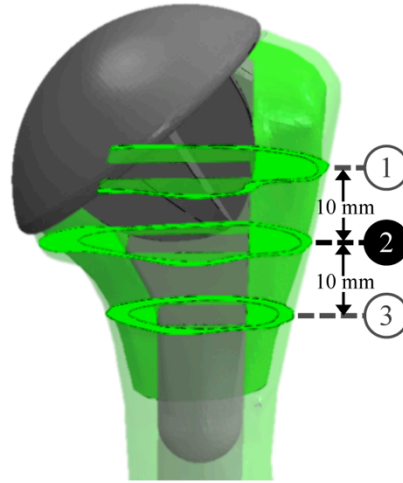


- a** Material Main Effect: $p = 0.001$ (PEEK vs. CoCr, and PEEK vs. Ti)
b Length Main Effect: $p \leq 0.038$ (Standard vs. Stemless, and Standard vs. Short)
 β Material-by-Length: $p < 0.001$
 γ Length-by-Abduction Angle: $p = 0.043$
 $*$ Material-by-Abduction Angle: $p = 0.029$ (PEEK vs. CoCr, and PEEK vs. Ti)

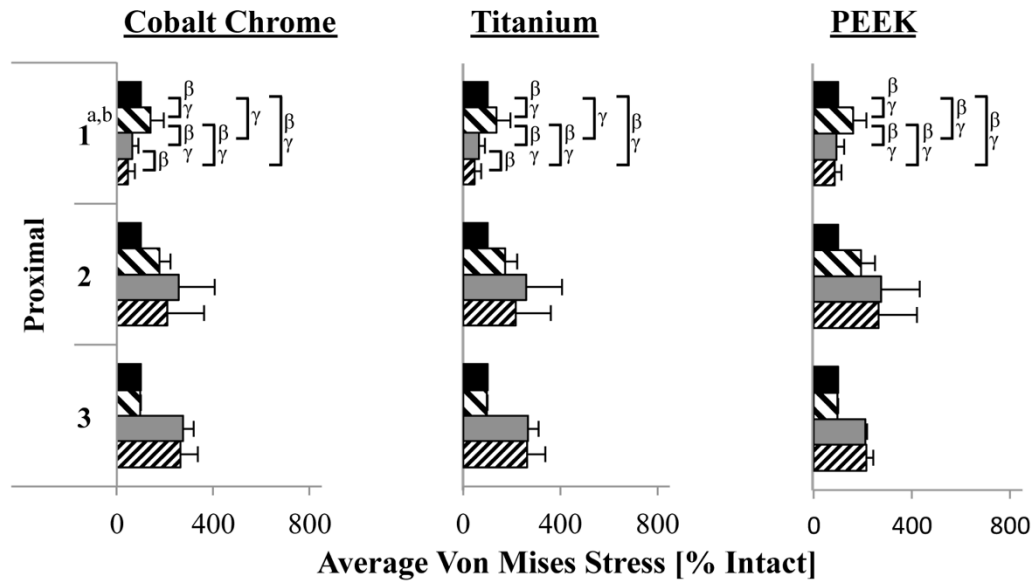
Figure 3.11: Average Stress in Trabecular Bone Slices – 15° Abduction

Mean (+SD) average stress in trabecular bone slices are given for all stem length variations, where the resulting stress is presented as a percentage of the intact bone stress in each slice.

**Trabecular Bone
45° Abduction**



■ Intact ▨ Stemless ■ Short ▩ Standard

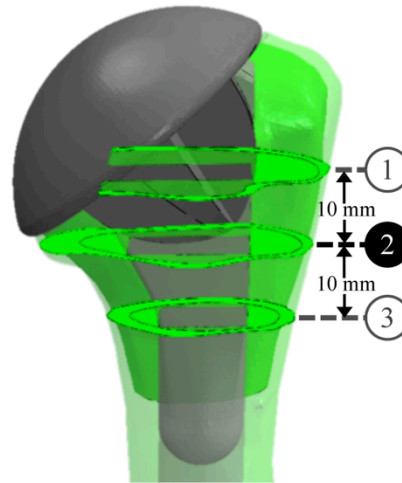


a Material Main Effect: $p = 0.001$ (PEEK vs. CoCr, and PEEK vs. Ti)
b Length Main Effect: $p \leq 0.038$ (Standard vs. Stemless, and Standard vs. Short)
 β Material-by-Length: $p < 0.001$
 γ Length-by-Abduction Angle: $p = 0.043$

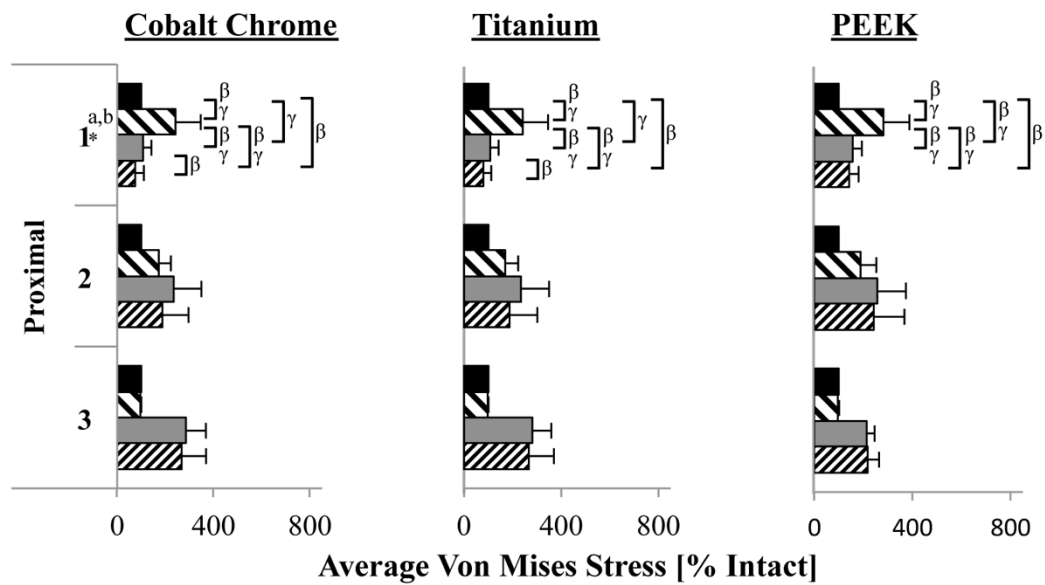
Figure 3.12: Average Stress in Trabecular Bone Slices – 45° Abduction

Mean (+SD) average stress in trabecular bone slices are given for all stem length variations, where the resulting stress is presented as a percentage of the intact bone stress in each slice.

**Trabecular Bone
75° Abduction**



■ Intact ▨ Stemless ■ Short ▩ Standard



a Material Main Effect: $p = 0.001$ (PEEK vs. CoCr, and PEEK vs. Ti)

b Length Main Effect: $p \leq 0.038$ (Standard vs. Stemless, and Standard vs. Short)

β Material-by-Length: $p < 0.001$

γ Length-by-Abduction Angle: $p = 0.043$

* Material-by-Abduction Angle: $p = 0.029$ (PEEK vs. CoCr, and PEEK vs. Ti)

Figure 3.13: Average Stress in Trabecular Bone Slices – 75° Abduction

Mean (+SD) average stress in trabecular bone slices are given for all stem length variations, where the resulting stress is presented as a percentage of the intact bone stress in each slice.

As a result of a length-by-abduction angle interaction, the intact trabecular stresses in the first slice varied significantly from the standard implant for 45° of abduction, and the short implant for both 45° and 75° ($p = 0.043$).

3.2.2 Average Proximal Humeral Bone Stresses

Within cortical bone a stem length main effect resulted in significantly greater divergence from the intact state for the standard model, compared to the short and stemless prostheses ($p \leq 0.042$) (Figure 3.14). A material-by-length interaction revealed that this significant increase was limited to CoCr and Ti prostheses ($p = 0.008$). Across all materials and abduction angles, the average change in cortical bone stresses (relative to the intact state) for standard, short and stemless models were $\sim 30 \pm 12\%$, $\sim 17 \pm 10\%$ and $\sim 16 \pm 8\%$, respectively. Stem length was not determined to significantly affect the total volume weighted average change in stress for trabecular bone; however a trend presented where the largest change from the intact stresses occurred with standard prostheses (Figure 3.15).

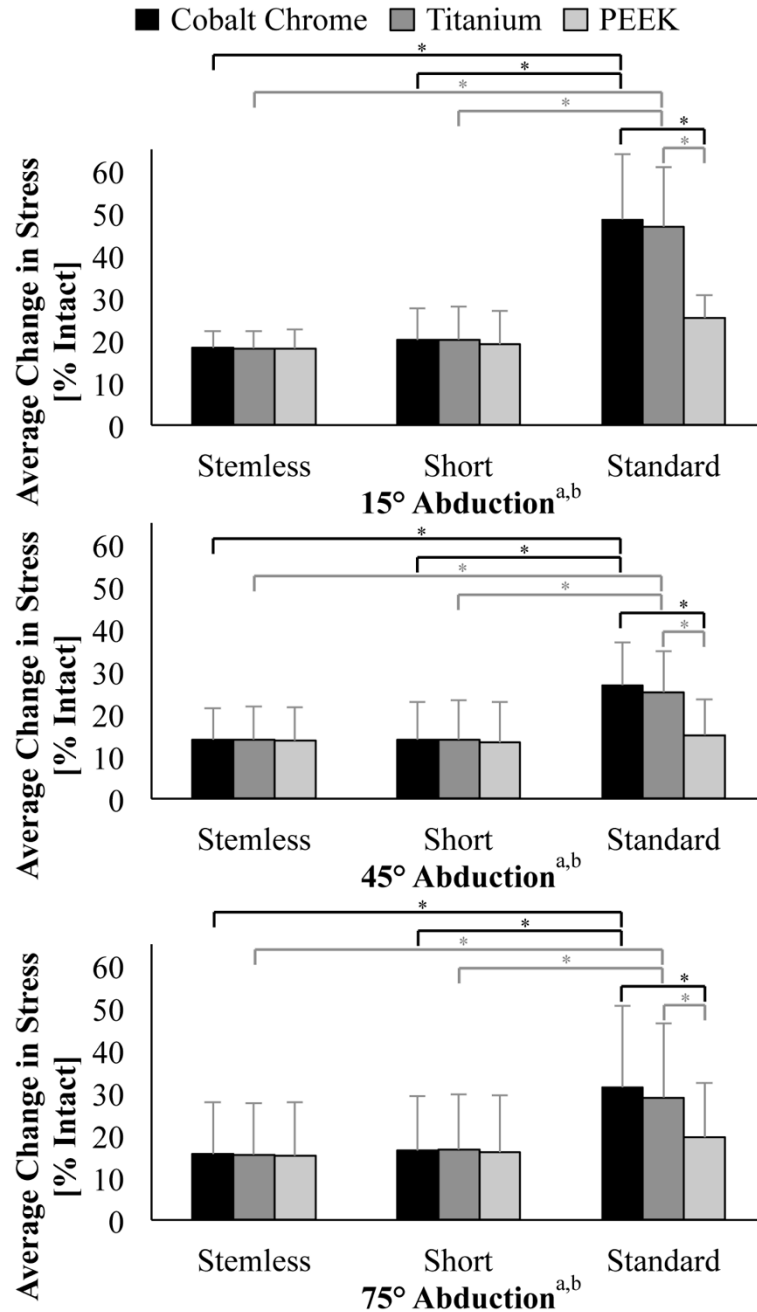
3.3 Effect of Implant Material Stiffness

To quantify the effect of changing implant material stiffness, the same single-element stresses, average stresses in predefined slices, and average total cortical and trabecular bone stresses were investigated.

3.3.1 Regional Stresses in the Proximal Humerus

3.3.1.1 Single-Element Path Results

In the three points of endosteal stresses corresponding to the tips of each implant, significant differences were again only found in the most distal point (point 15) (Figures 3.2 - 3.7). A material-by-length-by-abduction angle interaction suggested that standard implants in 15° of abduction caused significantly different stresses (closer to intact) when constructed with PEEK compared to CoCr ($\sim 12\%$ change) and Ti ($\sim 11\%$ change) ($p = 0.037$). Additionally, it was noted that, when PEEK was used as the implant material, standard length stems did not produce stresses that were significantly different from short and stemless reconstructions.



* Material-by-Length ($p = 0.008$)

a Material Main Effect (PEEK vs. CoCr $p = 0.026$; PEEK vs. Ti $p = 0.022$)

b Length Main Effect (Standard vs. Short $p = 0.042$; Standard vs. Stemless $p = 0.034$)

Figure 3.14: Average Change in Stress in the Total Cortical Stress

Mean (+SD) average change in stress in the cortical bone is given for all stem length variations, where the resulting stress is given as a percentage increase over the intact bone stress of the entire cortical bone.

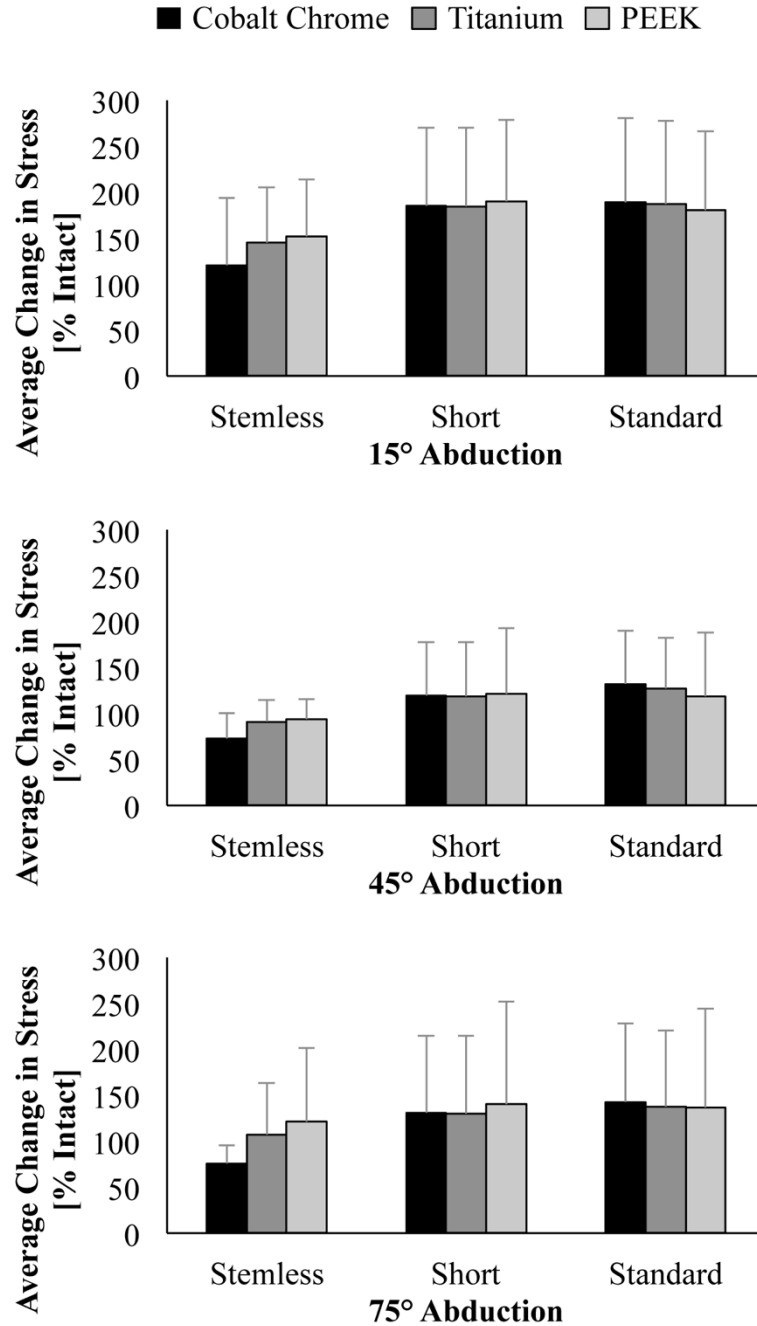


Figure 3.15: Average Change in Stress in the Total Trabecular Bone

Mean (+SD) average change in stress in the trabecular bone is given for all stem length variations, where the resulting stress is given as a percentage increase over the intact bone stress of the entire trabecular bone.

3.3.1.2 Bone Slice Stress Results

Investigation of varying implant material stiffness was conducted within cortical bone slices, where statistical significant differences were again only found in the two most proximal slices (slices 1 & 2) and the distal most slice (slices 9) (Figures 3.8 - 3.10). Overall, a material main effect in the first slice, lead to significant changes in bone stresses for models constructed with PEEK compared to both CoCr ($p \leq 0.03$) and Ti ($p \leq 0.009$). More specifically, a material-by-length interaction suggested that standard stems were particularly affected by material stiffness changes, where an increase in bone stresses with PEEK prostheses was found ($\sim 23 \pm 24\%$ higher than CoCr, and $\sim 21 \pm 23\%$ higher than Ti) ($p = 0.005$). Additionally, within the second slice, PEEK was again found to cause significantly different results compared to CoCr ($p = 0.041$) due to a material main effect, though not Ti. Finally, within the most distal slice (slice 9), to the surprise of the author, a material-by-length-by-abduction angle interaction suggested significant differences between the average cortical stresses of prostheses constructed with PEEK compared to CoCr and Ti for standard stems in 15° of abduction ($p = 0.019$).

Interestingly, unlike CoCr and Ti, implant models constructed using PEEK did not present with significant bone stress differences between standard and short, standard and stemless, and short and stemless models in the two most proximal cortical bone slices.

Statistical investigation of bone stresses in the three proximal trabecular bone slices yielded significance in only the most proximal slice (slice 1) (Figures 3.11 - 3.13). Overall, due to a main effect of material, prostheses constructed with PEEK were found to have significant changes in average stresses compared to models developed with CoCr and Ti ($p = 0.001$). Principally, a material-by-abduction angle interaction demonstrated that all PEEK prostheses had significantly higher stresses compared to CoCr and Ti models for angles of 15° (CoCr: $\sim 34 \pm 98\%$ higher, Ti: $\sim 34 \pm 97\%$ higher) and 75° of abduction (CoCr: $\sim 52 \pm 84\%$ higher, Ti: $\sim 51 \pm 84\%$ higher) ($p = 0.029$). Similar trends presented for 45° of abduction, though they were not significantly different (Figure 3.12).

3.3.2 Average Proximal Humeral Bone Stresses

For cortical bone, a material main effect demonstrated that PEEK resulted in significantly less stress changes than CoCr and Ti prostheses ($p \leq 0.026$) (Figure 3.15). A material-by-length interaction more specifically suggested that the reduction in stress changes were only significantly different for standard length PEEK prostheses compared to CoCr ($\sim 16 \pm 18\%$ reduction) and Ti ($\sim 14 \pm 16\%$ reduction) ($P=0.008$). Again, the average proximal humeral trabecular bone stresses did not present with any significant differences in terms of material stiffness; however a trend presented where the largest stress changes from the intact stress state occurred with PEEK for the stemless model (Figure 3.14).

In addition, peak stem stresses were never found to exceed the yield strength of the implant material (see Appendix H). Overall, these results demonstrated that significant differences can be found in average and regional bone stresses due to varying implant stem length and material stiffness. Proposed causes of the observed differences and trends are discussed in the following chapter, which concludes with a summary of the importance of the findings.

Chapter 4

4 Discussion and Conclusions

4.1 Summary

Total shoulder arthroplasty implant design is one important aspect that may have a strong influence on the survivability of prosthesis. Stem length and material stiffness are two principles of implant design that are being considered as important for affecting outcomes. However, to the knowledge of the author, no study has focused on the use of multiple subjects for the comparison of stemless to short and standard humeral implant models from the perspective of proximal humeral bone stresses. Accordingly, three methods including the single-element, slices, and average bone stress changes were chosen to precisely investigate the effect of stem length and implant material stiffness, on stress in cortical and trabecular bone. These outcomes were studied in three reconstructed proximal humerus models (*i.e.*, standard, short, stemless) and were compared to an intact bone model. In this chapter, understanding of the significant differences that presented in the results, and the future direction of this work are discussed.

4.2 Understanding Regional Significance

The use of multiple specimens ($n = 5$) in this study allowed statistical significance to be assessed. As mentioned in Chapter 3, results indicated that statistically significant differences presented in the most proximal region for the slice results (*i.e.*, slices 1 & 2), and in the distal region of the humerus model for both single-element and slice results (*i.e.*, point 15 and slice 9) (Figures 3.2 - 3.13). Proximal significant differences arose due to load transfer between the implants and bone. In the intact model of the proximal humerus, the joint reaction force is applied directly to the subchondral bone, and is principally carried around the softer trabecular bone by the hard cortical shell. Alternatively, in the reconstructed humerus models, the load is applied to the implants, which in turn progressively transfer load to the trabecular bone before it is diffused into the cortical shell more distally. This is clearly a different scenario than in the intact model (and in-part may cause proximal stress shielding). Distally, changes between standard

compared to other stem lengths (*i.e.*, stemless and short), and PEEK compared to other materials (*i.e.*, cobalt-chrome and titanium) are thought to arise because the stresses (and corresponding stress changes) borne by the cortical bone are higher due to increases in the bending component of stress. Moreover, distal contact in the standard length implant models led to load sharing patterns over a greater length, compared to other stem designs. These patterns in turn caused higher single-element stresses in the distal endosteal bone, and more inter-specimen variability.

4.2.1 The Effect of Variation in Stem Length

Stress shielding, where a reconstructed bone is subjected to less stress than prior to reconstruction (*i.e.*, the intact model), is exhibited in the proximal region of cortical bone. In particular, statistically significant reductions in stress were found for both the short and standard implant models in the two most proximal slices of cortical bone. This stress shielding was more evident in the proximal region of standard models, where distal endosteal contact allowed the implants to carry load over a longer distance within the bone, delaying cortical load transfer to more distal regions. Contrasting this, the stemless model, which has no mechanism for central or distal load transfer, is seen to elevate bone stresses over its length proximally (in order to transfer the loads from the implant to bone in this region alone) relative to the other reconstructed models. The presence of stress shielding is further supported by observations of proximal stress reductions made within the slice cortical bone results. Specifically, within the slice results (Figures 3.8 – 3.13), the location at which the mean stresses in the reconstructed models reach the intact stresses is seen to be consistently more distal with increasing stem length. Moreover, the single-element results (Figures 3.2 – 3.7) consistently show reductions in proximal endosteal stresses.

Furthermore, changes in cortical bone stresses were also detected between the standard and short, and standard and stemless implants using the average change in stress measure (Figure 3.14). Though this measure was of an absolute value, and thus positive and negative changes in bone stress were additive, trends in the regional results suggest that at least some of the changes noted are likely proximal reductions in stress, while others are likely distal increases in stress arising due to endosteal contact. Interestingly, while

the regional results highlight some statistically significant increases in the proximal trabecular bone stresses for different implants (*i.e.*, greater increases in stress in slice 1 with the stemless implant), the average change in stress in the total trabecular bone (Figure 3.14) suggests that the stresses of the trabecular bone is equally changed (*i.e.*, combination of increases and decreases) regardless of which implant is used. According to Wolff's Law, which dictates that bone remodels in-part in response to mechanical stimulation, it is suggested that any change in bone stress, be it an increase or decrease, acts to remove the bone from its natural (*i.e.*, intact) state (Mow and Huiskes, 2005; Wolff *et al.*, 1986). For the purpose of this investigation, it is proposed that any changes in bone stress are consequences of joint reconstruction and accordingly should be minimized, as stress changes could lead to a cascade effect where stress shielding is amplified. Considering this, according to the average change in stress results, all other things being equal (*i.e.*, implant fixation), all stem designs are expected to have equally negative consequences for the proximal trabecular bone; however, the standard length implant would have the most pronounced effect on cortical bone remodeling.

The arthroplasty literature agrees well with the present results, suggesting that decreasing stem length at other joints (*e.g.*, hip, wrist and knee joints) can lead to a bone state that better agrees with the intact state (Arno *et al.*, 2012; Austman *et al.*, 2011; Bieger *et al.*, 2012; Munting *et al.*, 1997; Reimeringer *et al.*, 2013). Specifically, Reimeringer *et al.* (2012) indicated that decreases in stem length might lead to reduced stress shielding of the proximal femur. Additionally, Austman *et al.* (2011) demonstrated that shorter stem lengths aided in returning bone strains to their intact levels along the length of distal ulnar implants. Furthermore, investigating bone mineral density (BMD), Munting *et al.* (1997) have shown that stemless implants considerably preserved BMD of the proximal femur following *in-vivo* implantation.

A previous study by Arno *et al.* (2012) investigated the strain distribution of femoral bone with three different stem length implants: stemless, ultra-short and short, and compared them to the intact strain distribution. Their results also agree with the present study, and indicated that the best match to the intact femur was the stemless design;

however, they expressed concern about the stability of the stemless implant. Bieger *et al.* (2012) also found that the short stem prosthesis resulted in less stress shielding.

Stress shielding can be a long term problem of shoulder arthroplasty resulting in bone becoming thinner over time, and has been noted in several *in-vivo* investigations (Huiskes *et al.*, 1992; Stewart and Kelly, 1997; Torchia *et al.*, 1997). Nagels *et al.* (2003) investigated standard stem implantation for signs of stress shielding by measuring cortex thickness at 4 regions along the stem length (70 radiographs; average follow up of 5.3 years). The results indicated that 9% had a significant reduction in cortex thickness surrounding the humeral stem. They also indicated that the stress shielding has a relationship with the stem diameter, where larger diameters resulted in greater incidence of stress shielding (Nagels *et al.*, 2003).

Huguet *et al.* (2009) investigated the results of stemless shoulder implants after a minimum three years follow up. They reported no implant migration or radiolucencies, suggesting that stemless implants maintain fixation at least during the first three year post-operatively. However, they cautioned that long-term follow up is still needed to confirm these results (Huguet *et al.*, 2010). Adequate stemless fixation was further supported by Ballas and Begin (2013), who found no implant loosening with stemless reverse shoulder implants, after a mean post-operative time of 58 months (Ballas and Béguin, 2013). Berth, *et al.* (2013) have also estimated that mean operative time and blood loss are significantly lower when stemless shoulder implants are used compared to standard length implants (Berth and Pap, 2013).

4.2.2 Effect of Changing Material Stiffness

In addition to examining the effect of implant stem length, implant material stiffness was also investigated. Both regional and average stress changes were found to vary as a function of implant stiffness, where decreases in stiffness lead to less deviation from the intact state for cortical bone stresses. More specifically, when comparing CoCr ($E = 210$ GPa), Ti ($E = 105$ GPa) and PEEK ($E = 3.5$ GPa) reconstructions in terms of average bone stresses in the two most proximal cortical slices, it was found that the stiffer CoCr and Ti implants exhibited significantly larger stress reductions than the flexible PEEK

models, for all angles of abduction (Figures 3.8 - 3.10). These changes were found to be most pronounced with the standard length implant, as was highlighted by a material-by-length interaction in slice 1. Accordingly, it is suggested that stress shielding in the proximal humerus is partially reduced by decreasing implant material stiffness. This is further supported by considering where the reconstructed models reached the intact stress levels. For instance, the standard stem stresses remained below intact-levels 1 to 5 slices longer (*i.e.*, more distally) when constructed with CoCr or Ti as compared to PEEK.

In contrast to this, the trabecular bone stresses in the most proximal slice significantly increased as the material stiffness decreased (PEEK vs. CoCr, and PEEK vs. Ti) (Figures 3.11 – 3.13). This was demonstrated by material main effects, as well as a material-by-abduction angle interaction. These stress increases are perhaps a result of the trabecular bone carrying more loads due to reduced prosthesis rigidity with decreasing material stiffness (*i.e.*, changes in the rigidity of the bone-implant assembly).

The total average changes in bone stresses also support the results seen in cortical slices. In particular, regardless of abduction angle, the standard length models caused significantly larger changes in stress than short and stemless models only when constructed of CoCr and Ti, but interestingly not PEEK (Figure 3.15). Additionally, standard prosthesis bone stress changes were significantly lower when constructed with PEEK as opposed to CoCr or Ti.

For some time, material stiffness has been thought to greatly influence the stress profiles in surrounding bone (Cook *et al.*, 1980). Though not explicitly investigated in the proximal humerus, present results that show a reduction in cortical bone stresses with decreasing material stiffness agree well with previous work at other joints (Austman *et al.*, 2007; Mow and Huiskes, 2005). Some studies on cemented proximal femoral implants have shown that stiffer stems increase stress shielding (Mow and Huiskes, 2005; Yan *et al.*, 2011). Moreover, other investigations have focused on cemented Ti femoral stems compare to CoCr, and have indicated that the less stiff Ti stems decrease proximal bone loss (Yan *et al.*, 2011). A study by Austman *et al* (2007) focusing on ulnar

reconstructions again suggested that Ti stems performed better compare to CoCr stems in terms of load transfer, returning the bone to a state more representative of the intact bone.

Furthermore, Huiskes *et al.* (1992) investigated stress shielding and bone resorption relationships in total hip arthroplasty, and determined that the rigidity of the implant is an important aspect affecting these phenomena (Huiskes *et al.*, 1992). Additionally, an animal study by Sumner *et al.* (1998) agreed with the results of the present study, showing that the stress shielding was higher (~26%) for stiffer stem compared to the low stiffness stem (~7.5%) (Sumner *et al.*, 1998).

Huiskes and Mo suggest that, when considering stress transfer, a bone-implant structure can be thought of as a simple composite bar, where each section has a different material stiffness and cross-sectional area. In accordance, the stress distribution (*i.e.*, load sharing equilibrium) in a bone-implant structure depends on each material's elastic modulus and cross-sectional area (*i.e.*, the section with the larger product of Young's modulus and cross-sectional area carrying more load, and subsequently more stress, see Equation 4.1) (Mow and Huiskes, 2005). Basically, the stress distribution is not continuous over the interface between the bone and implant when the Young's moduli of bone and implant are different, and the greater the difference the more discontinuous the load sharing is along the bone-implant assembly. Consequently, Huskies and Mo propose that bone stresses are higher when a flexible implant is used. This theory compliments the findings of the present investigation, where bone stresses were higher when the softer implant material was used (*i.e.*, PEEK). Accordingly, reductions in implant stiffness cause the bone to carry more of the applied load when PEEK is used, which better mimics the intact state in the stress shielded cortical bone, but overstresses the implant's direct contact with trabecular bone due to elevated shear stresses transferring greater loads to the bone.

$$F_{Bone} = \frac{Area_{Bone}E_{Bone}}{(Area_{Implant}E_{Implant} + Area_{Bone}E_{Bone})} \times F_{Total} \quad \text{Equation 4.1}$$

where, E indicates the Youngs' modulus and $F_{Total} = F_{Bone} + F_{Implant}$.

In a related investigation, Engh and Bobyn (1988) examined bone resorption between larger stems (≥ 13.5 mm in diameter) and smaller (stems ≤ 12.0 mm in diameter). Their results indicated that larger diameter stems (*i.e.*, higher axial and flexural rigidity) resulted in bone resorption that was five times more pronounced. They also demonstrated that there was a strong relationship between the observed bone resorption and stress shielding (Engh and Bobyn, 1988).

Huskies and Mo also suggest that there are three sections along an implant stem, in which load is shared differently. In the proximal region, more load is carried by the implant, but is gradually transferred to the bone until the middle region, where the above load sharing equilibrium (Equation 4.1) is met. Following this section, there is a distal region that ends with the stem tip, in which the remaining load is gradually transferred to the bone again. Huskies and Mo state that lengthening the stem only acts to increase the length of the middle section, with the proximal and distal sections remaining fixed lengths. Accordingly, it is only when the stem length is shortened to be less than the sum of the proximal and distal regions that interface stresses must begin to change to transfer the load to the bone faster (Mow and Huiskes, 2005).

4.3 Hypotheses Revisited

Hypothesis 1: It is hypothesized that a model of the proximal humerus will be developed and will generate total average stress results that converge with less than 10% variation when the number of elements in the model is increased by 50%.

The results indicated that all reconstructed models and the intact model converged at mesh sizes greater than or equal to 2 mm, which corresponded to total average stress variations of 9% or less. Accordingly, hypothesis 1 is accepted, as all models converged, permitting the investigation of multiple specimens and conditions within an appropriate timeline.

Hypothesis 2: It was hypothesized that shorter, less invasive implants would better mimic the intact stress state of the proximal humerus quantified by significantly lower stress changes when shorter stems were used.

Though some significant increases in trabecular stresses were found with decreases in stem length (due to reductions in implant-bone contact area), significant differences suggesting that the shorter less invasive implants do better mimic the intact stress state of the proximal humerus were found in cortical bone. In particular, significant reductions in cortical stress slices are most pronounced with the standard implants, and least pronounced when stemless implants are used. As such, hypothesis 2 is accepted for cortical bone and rejected for trabecular bone.

Hypothesis 3: It was hypothesized that less-stiff implants would better mimic the intact stress state of the proximal humerus quantified by significantly higher stress changes when stiffer stems were used.

Despite some increases in trabecular stresses, cortical stresses were found to better mimic the intact state when implant material stiffness was decreased. This cortical trend suggests that further reductions in implant material stiffness may lead to reconstructions that approach the intact bone. Accordingly, hypothesis 3 is accepted for cortical bone, and rejected for trabecular bone.

4.4 Strengths and Limitations

As with any *in-silico* study, this investigation contains several inherent assumptions, which led to various strengths and limitations. Firstly, a limitation of this work is the application of constant force magnitudes for all subject models. True joint reaction forces are subject specific percentages of body-weight, and accordingly would not be constant across a population. However for the purpose of this investigation, constant values were applied for each abduction angle to simplify the boundary conditions. The values chosen within this investigation were representative of a 50th-percentile male (body-weight = 85 kg), in order to provide realistic and non-conservative loads (McDowell *et al.*, 2008). Additionally, joint reaction forces were applied based on the location and magnitudes presented by Bergmann *et al.*'s 2007 *in-vivo* telemeterized shoulder implant data (Bergmann *et al.*, 2007). This method avoids the redundancy problems traditionally associated with the manual calculation of joint reaction forces.

While the geometry of the short stem implants used in this investigation was identical to the standard stems (asides from stem length), the diameter of each was set to create distal endosteal contact for the standard models. Accordingly, short stem diameters may have been undersized compared to clinical practice in order to isolate the effect of varying stem length and remove another potential confounding variable. Despite this, all implants were placed using repeatable mates, and implant position was approved by an orthopaedic surgeon for each subject.

While the application of anisotropic trabecular material properties was one of the strengths of this study, certain assumptions needed to be made to permit the application of a modulus-density relationship. In particular, the density-to-modulus equation used, developed by Morgan *et al* in 2003, was not specific to the humerus, but rather was an average pooled-value based on several sites throughout the body (*e.g.*, vertebrae, femur and tibia) (Morgan *et al.*, 2003). However this equation was chosen, due to several strengths, including a large sample size ($n = 142$), and that the values reported were specific to trabecular bone alone (*i.e.*, not a combination of trabecular and cortical bone). A related assumption of the present investigation was the application of a constant modulus of 20 GPa to the cortical bone. While the true modulus may fluctuate slightly, it is generally considered as transversely isotropic; also variations in cortical thickness and geometry are accounted for in this study. These variations allow for changes in the structural stiffness of cortical bone across specimens, creating an inhomogeneous structure similar to that of real bone. Moreover, the practice of applying a single value for the stiffness of cortical bone is well established in finite element analysis (Reimeringer *et al.*, 2013; Theodorou *et al.*, 2011). Furthermore, the repeated measures design of this investigation ensured that each implant condition and the intact model were subjected to identical parameters and meshes. This coupled with the normalization of most results to the intact state allowed the accurate identification of stress changes for each condition, and removed potential confounding variables (*e.g.*, reducing the effect of inter-specimen variability).

The use of pre-operative CT scans from a patient population who underwent total shoulder arthroplasty ensured that this work would better reflect a real-world population.

Unfortunately, since patients, unlike cadavers, cannot be exposed to excessive radiation, CT image quality was not optimal at times, which made bone model development challenging and less precise. Furthermore, no phantom of known density was present in the patient CT scans, which had implications for the density calibration of each image. To address this, additional scans of phantoms alone were taken in the same clinical CT scanner at the same settings used (*i.e.*, maximum, minimum and average mA settings) to develop post-hoc calibration curves.

Inter-specimen variation is a limitation of this study, and is quite evident when directly comparing the results of the each subject in this investigation. In particular, variation in trabecular bone quality led to differing lengths of trabecular bone progressing distally. This in turn caused a reduction in the number of specimens when comparing slice and single-element results. For instance, all five subjects presented with trabecular bone in the first two bone slices; however only two subjects' trabecular bone persisted to the third slice. Additionally, despite repeatable implant placement across specimens, changes in the distal endosteal contact patterns of the standard stem models were also evident between specimens due to geometry differences. These changes produced consistently higher scatter in the standard stem model stresses compared to both short and stemless implants. While higher standard deviations may have prevented the appearance of statistically significant differences in some slices, these geometry differences are more representative of the variation that would be seen in a population. Accordingly, these results support the inclusion of multiple specimens when conducting anything but specimen-specific (*i.e.*, single patient) implant analysis. Few studies to date have investigated the effect of inter-specimen variability on FE models (Taylor *et al.*, 2013). While the addition of multiple specimens substantially increases the computational time (*e.g.*, model development and run time) of an investigation, the above noted inter-specimen differences would not have been detected with a single specimen, and the results of such studies accordingly cannot be extrapolated to larger population sizes. While 5 specimens is an improvement over the traditional single-specimen finite element investigations, it is expected that this number must increase substantially in order to truly capture the variation present within real-world populations.

4.5 Future Directions

The use of patient specific CT scans demonstrated that methods could be developed for pre-operative planning. These methods require further development; however based on the processes described in this thesis, surgeons would be able to pick the plane for cutting the humerus head before the surgery using a computer generated 3D model of bone. Surgeons would then be able to alternate implant size and stiffness to more accurately match each subject to the correct implant. Moreover, these methods will allow surgeons to position the chosen implant prior to surgery, to balance contact between the stem and the cortical shell, and understand how this position will affect the surrounding bone. By these methods, estimates of bone stresses can be depicted visually using patient-specific trabecular bone stiffness's derived from CT scan data. To further increase the accuracy of proximal humerus stress analyses, a future study should develop a humerus specific density-Young's modulus relationship (for cortical and trabecular bone separately).

Using the methods that developed in this study, more variations in stem design can be investigated, including: changing the cross-sectional area of the stem, altering coating for the implant (*i.e.*, applying different friction coefficient between implant and bone), exploring cemented vs. press-fit implants, as well as the affect of implant placement.

Importantly, inter-subject variability seen in the present investigation highlights the need for all future arthroplasty finite element investigations to use multiple specimens if their results are to be extrapolated beyond a patient-specific model. While this investigation provides a strong foundation for future finite element investigations of proximal humeral implants, expansion of the variables under investigation would add to the understanding of the performance of humeral TSA components of reduced length and stiffness. In particular, in order to assess the stability of humeral reconstructions, stem micro-motion should be added to future investigations. Moreover, to account for failure modes beyond implant yielding, assessment of fatigue strengths should also be included.

4.6 Conclusion

The present work constitutes the first known attempt at using identical mesh finite element modeling techniques to quantify stress changes in the proximal humerus following reconstruction with stemless (25 mm), short (50 mm) and standard (100 mm) TSA implants of varying material stiffness (CoCr: $E = 210$ GPa, Ti: $E = 105$ GPa, PEEK: $E = 3.5$ GPa). With 150 models developed from the clinical CT scans of 5 patients, variation in stem length and material stiffness were quantified for 3 abduction angles (*i.e.*, 15° , 45° and 75°). Measures of interest were: single-element based stress paths along the medial, lateral, anterior and posterior endosteal bone surfaces, as well as the average stress in 9 pre-defined axial slices, and the overall average change in stress in the total cortical and trabecular bone segments. As hypothesized, reductions in stem length led to cortical stress states that better matched the intact bone; however shorter stems were found to raise trabecular bone stresses above intact levels. Similarly, reductions in material stiffness were found to return cortical bone stresses close to the intact state, but again led to elevated trabecular bone stresses. The results suggest that stress shielding in the proximal humerus may in-part be reduced through the use of shorter, less stiff humeral implants; however it is important to remember that other factors may influence the effect of implant design and use, such as implant stability, the ease of implant placement and the fatigue strength of the chosen material.

4.7 References

- Ackland, D. C., Pandy, M. G., 2011. Moment arms of the shoulder muscles during axial rotation. *Journal of Orthopaedic Research* 29, 658-667.
- Ambacher, T., 2013. Options and limits of stemless shoulder prostheses. *Der Orthopade* 42, 495-500.
- An, K., Browne, A., Korinek, S., Tanaka, S., Morrey, B., 1991. Three-dimensional kinematics of glenohumeral elevation. *Journal of Orthopaedic Research* 9, 143-149.
- Anglin, C., Wyss, U. P., Pichora, D. R., 2000. Glenohumeral contact forces. *Proceedings of the Institution of Mechanical Engineers. Part H, Journal of Engineering in Medicine* 214, 637-644.
- Arno, S., Fetto, J., Nguyen, N. Q., Kinariwala, N., Takemoto, R., Oh, C., Walker, P. S., 2012. Evaluation of femoral strains with cementless proximal-fill femoral implants of varied stem length. *Clinical Biomechanics* 27, 680-685.
- Au, A. G., James Raso, V., Liggins, A., Amirfazli, A., 2007. Contribution of loading conditions and material properties to stress shielding near the tibial component of total knee replacements. *Journal of Biomechanics* 40, 1410-1416.
- Austman, R. L., Beaton, B. J., Quenneville, C. E., King, G. J., Gordon, K. D., Dunning, C. E., 2007. The effect of distal ulnar implant stem material and length on bone strains. *The Journal of Hand Surgery* 32, 848-854.
- Austman, R. L., King, G. J., Dunning, C. E., 2011. Bone stresses before and after insertion of two commercially available distal ulnar implants using finite element analysis. *Journal of Orthopaedic Research* 29, 1418-1423.
- Austman, R. L., Milner, J. S., Holdsworth, D. W., Dunning, C. E., 2009. Development of a customized density-modulus relationship for use in subject-specific finite element models of the ulna. *Proceedings of the Institution of Mechanical Engineers. Part H, Journal of Engineering in Medicine* 223, 787-794.
- Ballas, R., Béguin, L., 2013. Results of a stemless reverse shoulder prosthesis at more than 58 months mean without loosening. *Journal of Shoulder and Elbow Surgery* 22, e1-e6.

Barrack, R. L., 2000. Early failure of modern cemented stems. *The Journal of Arthroplasty* 15, 1036-1050.

Bergmann, G., Graichen, F., Bender, A., Käb, M., Rohlmann, A., Westerhoff, P., 2007. In vivo glenohumeral contact forces—measurements in the first patient 7 months postoperatively. *Journal of Biomechanics* 40, 2139-2149.

Berth, A., Pap, G., 2013. Stemless shoulder prosthesis versus conventional anatomic shoulder prosthesis in patients with osteoarthritis. *Journal of Orthopaedics and Traumatology* 14, 31-37.

Bieger, R., Ignatius, A., Decking, R., Claes, L., Reichel, H., Dürselen, L., 2012. Primary stability and strain distribution of cementless hip stems as a function of implant design. *Clinical Biomechanics* 27, 158-164.

Bigliani, L. U., Kelkar, R., Flatow, E. L., Pollock, R. G., Mow, V. C., 1996. Glenohumeral stability: biomechanical properties of passive and active stabilizers. *Clinical Orthopaedics and Related Research* 330, 13-30.

Bolsterlee, B., Veeger, D. H., Chadwick, E. K., 2013. Clinical applications of musculoskeletal modelling for the shoulder and upper limb. *Medical & Biological Engineering & Computing* 51, 953-963.

Budynas R.G, N. K., 2011. *Shigley's Mechanical Engineering Design*. McGraw-Hill, New York, pp. 223.

Bureau, M. N., Legoux, J., Gritti, P., Yahia, L., 2006. Biomimetic polymer composites for orthopedic implants. In ANTEC 2006: Society of Plastics Engineers Annual Technical Conference 2006, Held may 7-11, 2006, Charlotte, North Carolina, USA, Conference Proceedings.

Burkart, A. C., Debski, R. E., 2002. Anatomy and function of the glenohumeral ligaments in anterior shoulder instability. *Clinical Orthopaedics and Related Research* 400, 32-39.

Carter, D., Orr, T., Fyhrie, D., 1989. Relationships between loading history and femoral cancellous bone architecture. *Journal of Biomechanics* 22, 231-244.

Carter, D. R., Hayes, W. C., 1977. The compressive behavior of bone as a two-phase porous structure. *The Journal of Bone and Joint Surgery*. American Volume 59, 954-962.

Cifuentes, A., Kalbag, A., 1992. A performance study of tetrahedral and hexahedral elements in 3-D finite element structural analysis. *Finite Elements in Analysis and Design* 12, 313-318.

Clark, J., Harryman, D. 2., 1992. Tendons, ligaments, and capsule of the rotator cuff. *Gross and microscopic anatomy. The Journal of Bone & Joint Surgery* 74, 713-725.

Conzen, A., Eckstein, F., 2000. Quantitative determination of articular pressure in the human shoulder joint. *Journal of Shoulder and Elbow Surgery* 9, 196-204.

Cook, S., Klawitter, J., Weinstein, A., 1980. The influence of design parameters on calcar stresses following femoral head arthroplasty. *Journal of Biomedical Materials Research* 14, 133-144.

Cowin, S., Hegedus, D., 1976. Bone remodeling I: theory of adaptive elasticity. *Journal of Elasticity* 6, 313-326.

Culham, E., Peat, M., 1993. Functional anatomy of the shoulder complex. *Journal of Orthopaedic & Sports Physical Therapy* 18, 342-350.

Curl, L. A., Warren, R. F., 1996. Glenohumeral joint stability: selective cutting studies on the static capsular restraints. *Clinical Orthopaedics and Related Research* 330, 54-65.

Engh, C. A., Bobyn, J. D., 1988. The influence of stem size and extent of porous coating on femoral bone resorption after primary cementless hip arthroplasty. *Clinical Orthopaedics and Related Research* 231, 7-28.

Grant, J., Bishop, N., Götzen, N., Sprecher, C., Honl, M., Morlock, M., 2007. Artificial composite bone as a model of human trabecular bone: The implant–bone interface. *Journal of Biomechanics* 40, 1158-1164.

Hadjidakis, D. J., Androulakis, I. I., 2006. Bone remodeling. *Annals of the New York Academy of Sciences* 1092, 385-396.

Halder, A., Halder, C., Zhao, K., O'Driscoll, S., Morrey, B., An, K., 2001. Dynamic inferior stabilizers of the shoulder joint. *Clinical Biomechanics* 16, 138-143.

Hess, S., 2000. Functional stability of the glenohumeral joint. *Manual Therapy* 5, 63-71.

Hopkins, A. R., Hansen, U. N., Amis, A. A., Taylor, M., Emery, R. J., 2007. Glenohumeral kinematics following total shoulder arthroplasty: a finite element investigation. *Journal of Orthopaedic Research* 25, 108-115.

Huguet, D., DeClercq, G., Rio, B., Teissier, J., Zipoli, B., TESS Group, 2010. Results of a new stemless shoulder prosthesis: radiologic proof of maintained fixation and stability after a minimum of three years' follow-up. *Journal of Shoulder and Elbow Surgery / American Shoulder and Elbow Surgeons ...[Et al.]* 19, 847-852.

Huiskes, R., Chao, E., 1983. A survey of finite element analysis in orthopedic biomechanics: the first decade. *Journal of Biomechanics* 16, 385-409.

Huiskes, R., Weinans, H., Van Rietbergen, B., 1992. The relationship between stress shielding and bone resorption around total hip stems and the effects of flexible materials. *Clinical Orthopaedics and Related Research* 274, 124-134.

Huiskes, R., Weinans, H., Grootenboer, H. J., Dalstra, M., Fudala, B., Slooff, T. J., 1987. Adaptive bone-remodeling theory applied to prosthetic-design analysis. *Journal of Biomechanics* 20, 1135-1150.

Inman, V. T., Abbott, L. C., 1944. Observations on the function of the shoulder joint. *The Journal of Bone & Joint Surgery* 26, 1-30.

Jain, N. B., Higgins, L. D., Guller, U., Pietrobon, R., Katz, J. N., 2006. Trends in the epidemiology of total shoulder arthroplasty in the United States from 1990–2000. *Arthritis Care & Research* 55, 591-597.

Jergesen, H. E., Karlen, J. W., 2002. Clinical outcome in total hip arthroplasty using a cemented titanium femoral prosthesis. *The Journal of Arthroplasty* 17, 592-599.

Jobe, C. M., Phipatanakul, W. P., Coen, M. J., 2009. *Gross anatomy of the shoulder*. Saunders Elsevier, Philadelphia, pp. 33-100.

Karduna, A. R., Williams, G. R., Iannotti, J. P., Williams, J. L., 1996. Kinematics of the glenohumeral joint: influences of muscle forces, ligamentous constraints, and articular geometry. *Journal of Orthopaedic Research* 14, 986-993.

Kask, K., Põldoja, E., Lont, T., Norit, R., Merila, M., Busch, L. C., Kolts, I., 2010. Anatomy of the superior glenohumeral ligament. *Journal of Shoulder and Elbow Surgery* 19, 908-916.

Kuiper, J. H., Huiskes, R., 1996. Friction and stem stiffness affect dynamic interface motion in total hip replacement. *Journal of Orthopaedic Research* 14, 36-43.

Kuroda, D., Niinomi, M., Morinaga, M., Kato, Y., Yashiro, T., 1998. Design and mechanical properties of new β type titanium alloys for implant materials. *Materials Science and Engineering: A* 243, 244-249.

Kurtz, S. M., Devine, J. N., 2007. PEEK biomaterials in trauma, orthopedic, and spinal implants. *Biomaterials* 28, 4845-4869.

Lee, Y., Welsch, G., 1990. Young's modulus and damping of Ti-6Al-4V alloy as a function of heat treatment and oxygen concentration. *Materials Science and Engineering: A* 128, 77-89.

Les, C., Keyak, J., Stover, S., Taylor, K., Kaneps, A., 1994. Estimation of material properties in the equine metacarpus with use of quantitative computed tomography. *Journal of Orthopaedic Research* 12, 822-833.

Leung, A. S., Gordon, L. M., Skrinkas, T., Szwedowski, T., Whyne, C. M., 2009. Effects of bone density alterations on strain patterns in the pelvis: application of a finite element model. *Proceedings of the Institution of Mechanical Engineers. Part H, Journal of Engineering in Medicine* 223, 965-979.

Lippitt, S. B., Masten, F., 1993. Mechanisms of glenohumeral joint stability. *Clinical Orthopaedics and Related Research* 291, 20-28.

Litchfield, R. B., McKee, M. D., Balyk, R., Mandel, S., Holtby, R., Hollinshead, R., Drosdowech, D., Wambolt, S. E., Griffin, S. H., McCormack, R., 2011. Cemented versus uncemented fixation of humeral components in total shoulder arthroplasty for osteoarthritis of the shoulder: a prospective, randomized, double-blind clinical trial-A JOINTs Canada Project. *Journal of Shoulder and Elbow Surgery / American Shoulder and Elbow Surgeons ...[Et al.]* 20, 529-536.

Manley, M., Stern, L., Gurtowski, J., 1983. Performance characteristics of total hip femoral components as a function of prosthesis modulus. *Bulletin of the Hospital for Joint Diseases Orthopaedic Institute* 43, 130-136.

- Mariotti, U., Motta, P., Stucchi, A., di Sant'Angelo, F. P., 2014. Stemmed versus stemless total shoulder arthroplasty: a preliminary report and short-term results. *Musculoskeletal Surgery*, 1-6.
- Massimini, D. F., Li, G., Warner, J. P., 2010. Glenohumeral contact kinematics in patients after total shoulder arthroplasty. *The Journal of Bone & Joint Surgery* 92, 916-926.
- Masten III, F. A., 1996. Early Effectiveness of Shoulder Arthroplasty for Patients Who Have Primary Glenohumeral Degenerative Joint Disease*†. *The Journal of Bone & Joint Surgery* 78, 260-264.
- McDowell, M. A., Fryar, C. D., Ogden, C. L., Flegal, K. M., 2008. Anthropometric reference data for children and adults: United States, 2003-2006. *National Health Statistics Reports* 10, 1-48.
- Morgan, E. F., Bayraktar, H. H., Keaveny, T. M., 2003. Trabecular bone modulus–density relationships depend on anatomic site. *Journal of Biomechanics* 36, 897-904.
- Mow, V. C., Huiskes, R., 2005. *Basic orthopaedic biomechanics & mechano-biology*. Lippincott Williams & Wilkins, Philadelphia, pp. 720.
- Munting, E., Smitz, P., Van Sante, N., Nagant de Deuxchaisnes, C., Vincent, A., Devogelaer, J. P., 1997. Effect of a stemless femoral implant for total hip arthroplasty on the bone mineral density of the proximal femur. A prospective longitudinal study. *The Journal of Arthroplasty* 12, 373-379.
- Nagels, J., Stokdijk, M., Rozing, P. M., 2003. Stress shielding and bone resorption in shoulder arthroplasty. *Journal of Shoulder and Elbow Surgery* 12, 35-39.
- NeerII, C. S., 1974. Replacement arthroplasty for glenohumeral osteoarthritis. *The Journal of Bone & Joint Surgery* 56, 1-13.
- NeerII, C. S., 1955. Articular replacement for the humeral head. *The Journal of Bone & Joint Surgery* 37, 215-228.
- Norris, T. R., Iannotti, J. P., 2002. Functional outcome after shoulder arthroplasty for primary osteoarthritis: A multicenter study. *Journal of Shoulder and Elbow Surgery* 11, 130-135.

O'Brien SJ, Allen AA, F. S., Rodeo SA, Arnoczky SP, 2009. Developmental anatomy of the shoulder and anatomy of the glenohumeral joint. In: Rockwood CA Jr, Matsen FA, editors. The shoulder. 4th edition. W.B. Saunders, Philadelphia, pp. 1-32.

Panagiotopoulou, O., Wilshin, S. D., Rayfield, E. J., Shefelbine, S. J., Hutchinson, J. R., 2012. What makes an accurate and reliable subject-specific finite element model? A case study of an elephant femur. *Journal of the Royal Society, Interface / the Royal Society* 9, 351-361.

Prendergast, P., 1997. Finite element models in tissue mechanics and orthopaedic implant design. *Clinical Biomechanics* 12, 343-366.

Ramos, A., Simoes, J., 2006. Tetrahedral versus hexahedral finite elements in numerical modelling of the proximal femur. *Medical Engineering & Physics* 28, 916-924.

Reimeringer, M., Nuño, N., Desmarais-Trépanier, C., Lavigne, M., Vendittoli, P., 2013. The influence of uncemented femoral stem length and design on its primary stability: a finite element analysis. *Computer Methods in Biomechanics and Biomedical Engineering* 16, 1221-1231.

Rho, J. Y., Ashman, R. B., Turner, C. H., 1993. Young's modulus of trabecular and cortical bone material: ultrasonic and microtensile measurements. *Journal of Biomechanics* 26, 111-119.

Rockwood Jr, C. A., Matsen III, F. A., Wirth, M. A., Lippitt, S. B., 2009. The shoulder. Elsevier Health Sciences, .

Rohlmann, A., Mössner, U., Bergmann, G., Hees, G., Kölbl, R., 1987. Effects of stem design and material properties on stresses in hip endoprostheses. *Journal of Biomedical Engineering* 9, 77-83.

Sakai, T., Sugano, N., Nishii, T., Haraguchi, K., Ochi, T., Ohzono, K., 1999. Stem length and canal filling in uncemented custom-made total hip arthroplasty. *International Orthopaedics* 23, 219-223.

Santori, N., Lucidi, M., Santori, F., 2006. Proximal load transfer with a stemless uncemented femoral implant. *Journal of Orthopaedics and Traumatology* 7, 154-160.

Schileo, E., Taddei, F., Malandrino, A., Cristofolini, L., Viceconti, M., 2007. Subject-specific finite element models can accurately predict strain levels in long bones. *Journal of Biomechanics* 40, 2982-2989.

Simon, U., Augat, P., Ignatius, A., Claes, L., 2003. Influence of the stiffness of bone defect implants on the mechanical conditions at the interface--a finite element analysis with contact. *Journal of Biomechanics* 36, 1079-1086.

Sluimer, J. C., Hoefnagels, N. H., Emans, P. J., Kuijjer, R., Geesink, R. G., 2006. Comparison of two hydroxyapatite-coated femoral stems: clinical, functional, and bone densitometry evaluation of patients randomized to a regular or modified hydroxyapatite-coated stem aimed at proximal fixation. *The Journal of Arthroplasty* 21, 344-352.

Staiger, M. P., Pietak, A. M., Huadmai, J., Dias, G., 2006. Magnesium and its alloys as orthopedic biomaterials: A review. *Biomaterials* 27, 1728-1734.

Stewart, M., Kelly, I., 1997. Total shoulder replacement in rheumatoid disease 7-to 13-year follow-up of 37 joints. *Journal of Bone & Joint Surgery, British Volume* 79, 68-72.

Sumner, D. R., Turner, T. M., Igloria, R., Urban, R. M., Galante, J. O., 1998. Functional adaptation and ingrowth of bone vary as a function of hip implant stiffness. *Journal of Biomechanics* 31, 909-917.

Taddei, F., Cristofolini, L., Martelli, S., Gill, H., Viceconti, M., 2006. Subject-specific finite element models of long bones: an in vitro evaluation of the overall accuracy. *Journal of Biomechanics* 39, 2457-2467.

Taylor, M., Bryan, R., Galloway, F., 2013. Accounting for patient variability in finite element analysis of the intact and implanted hip and knee: a review. *International Journal for Numerical Methods in Biomedical Engineering* 29, 273-292.

Terrier, A., Ramondetti, S., Merlini, F., Pioletti, D. D., Farron, A., 2010. Biomechanical consequences of humeral component malpositioning after anatomical total shoulder arthroplasty. *Journal of Shoulder and Elbow Surgery* 19, 1184-1190.

Theodorou, E. G., Provatidis, C. G., Babis, G. C., Georgiou, C. S., Megas, P. D., 2011. Large diameter femoral heads impose significant alterations on the strains developed on femoral component and bone: a finite element analysis. *The Open Orthopaedics Journal* 5, 229-238.

Torchia, M. E., Cofield, R. H., Settergren, C. R., 1997. Total shoulder arthroplasty with the Neer prosthesis: long-term results. *Journal of Shoulder and Elbow Surgery* 6, 495-505.

- van der Helm, F. C. T., 1994. A finite element musculoskeletal model of the shoulder mechanism. *Journal of Biomechanics* 27, 551-569.
- van Rietbergen, B., Huiskes, R., 2001. Load transfer and stress shielding of the hydroxyapatite-ABG hip: A study of stem length and proximal fixation. *The Journal of Arthroplasty* 16, 55-63.
- Walch, G., Boileau, P., Noël, E., 2010. Shoulder arthroplasty: evolving techniques and indications. *Joint Bone Spine* 77, 501-505.
- Wiater, J. M., Fabing, M. H., 2009. Shoulder arthroplasty: prosthetic options and indications. *The Journal of the American Academy of Orthopaedic Surgeons* 17, 415-425.
- Willing, R. T., Lalone, E. A., Shannon, H., Johnson, J. A., King, G. J., 2013. Validation of a finite element model of the human elbow for determining cartilage contact mechanics. *Journal of Biomechanics* 46, 1767-1771.
- Wolff, J., Maquet, P., Furlong, R., 1986. *The law of bone remodelling*. Springer Berlin, .
- Yan, W., Berthe, J., Wen, C., 2011. Numerical investigation of the effect of porous titanium femoral prosthesis on bone remodeling. *Materials & Design* 32, 1776-1782.
- Zannoni, C., Mantovani, R., Viceconti, M., 1999. Material properties assignment to finite element models of bone structures: a new method. *Medical Engineering & Physics* 20, 735-740.

Appendix A: Glossary of Medical Terminology

Abduction: Movement away from the midplane of the body, specifically, the humerus away from the rib cage.

ANOVA: Analysis of variance, a statistical test between groups.

Anterior: Near or closet to the front of the body.

Arthritis: Medical condition of joint leading to inflammation caused or metabolic causes or infectious.

Articular: Referring to adjacent moving components (*e.g.* joint).

Cadaver: Referring to the human body deceased, a dead body, corpse.

Cartilage: Firm flexible tissue that lines the articular surface of joints.

Clavicle: Typically known as the 'Collar Bone', horizontally placed linking the thorax to the scapula.

Diaphysis: The center region of a long bone typically slender.

Distal: Referring to the position further away from torso.

Finite element analysis (FEA): In-Silico method that discretizes a continuous geometry into a finite number of elements, each of which can be analyzed to determine the overall response of the system to an applied load.

Glenohumeral: The joint formed by the proximal head of the humerus and the glenoid of the scapula.

Humerus: Long bone of the upper arm which connects the shoulder to the elbow.

In-silico: Refers to studies performed on computer or using computer simulation.

In-vitro: Refers to studies accruing outside of normal biological environment.

In-vivo: In reference to events taking place within a living organism.

Lateral: Refers to the side that is further away from the median axis of the body.

Ligament: Tough fibrous band or tissue that link articulating bone.

Medial: Refers to the side that is closer to the median axis of the body.

Orthopaedics: Surgical discipline that deals with the restoration and preservation of the skeletal system (including articular structures).

Osteoporosis: Skeletal condition causing system-wide deterioration of bone on the microscopical scale and low bone mass.

Posterior: Near or closet to the back of the body.

Proximal: Referring to the position closes to the torso.

Scapula: Medial bone of the shoulder connecting the humerus to the torso.

Tendon: Fibrous tissue linking muscle to bone.

Torso: The center structure of the human body from which extend the limbs and neck.

Appendix B: Illustrations Permission

RE: Permission Request Form Canada

1 message

Fri, Jul 25, 2014 at 11:26 AM

To: [REDACTED]

Dear Najmeh:

Permission is hereby granted for the use requested subject to the usual acknowledgements (author, title of material, title of book/journal, ourselves as publisher). You shall also duplicate the copyright notice that appears in the Wiley publication in your use of the Material.

Any third party material is expressly excluded from this permission. If any of the material you wish to use appears within our work with credit to another source, authorization from that source must be obtained.

This permission does not include the right to grant others permission to photocopy or otherwise reproduce this material except for accessible versions made by non-profit organizations serving the blind, visually impaired and other persons with print disabilities (VIPs).

Sincerely,

Paulette Goldweber . Associate Manager, Permissions/Global Rights

John Wiley & Sons, Inc. . 111 River Street . Hoboken, NJ . 07030

----- Original Message -----

From: [REDACTED]
Sent: Monday, July 21, 2014 7:26 PM
To: Permissions - US
Subject: Permission Request Form Canada

A01_First_Name: Najmeh
A02_Last_Name: Razfar
A03_Company: The University of Western Ontario
A04_Address: 1151 Richmond Street
A05_City: London
A06_Province: ON
A07_Zip: N6A 3K7
A08_Country: Canada
A09_Phone: [REDACTED]
A10_Fax: [REDACTED]
A11_Email: [REDACTED]
A12_Reference_Number:
A13_Requestor_Name:
A14_Requestor_Phone:
A15_Requestor_Fax:
A16_Product_Title: Principles of Human Anatomy
A17_ISBN: 0-471-36686-2
A18_Author_Name: Gerard A. Tortora
A19_Page_Number: fig_06_02, fig_0602a, fig_06_02b, fig_08_01ab, fig_08_01cd, fig_08_04ab, fig_08_04cd, fig_09_03a, fig_09_07a, fig_09_12a, fig_09_12c, fig_11_19e, fig_11_19f, fig_11_19ab, fig_11_18fg, fig_11_18a
A20_Number_of_Copies: 5
A21_Semesters:
A22_Professor_Name: Dr. James Johnson
A23_Course_Name:
A24_Organization_Name: The University of Western Ontario
A25_Purpose_Reproduction: Master's Thesis
A26_Title_Your_Work:
A26A_Resale: No
A27_Print_Run:
A28_Publication_Date:
A29_World_Rights:
A30_Medium:
A31_Password:
32_Users:
A33_Duration_Posted_Web:
A34_CD_Print_Run: ,

Executive Editor: Daryl Fox
 Senior Project Editor: Kay Ueno
 Development Editor: Mark F. Wales
 Editorial Assistant: Nicki Richesin
 Managing Editor: Wendy Earl
 Production Supervisor: Sharon Montooth
 Text and Cover Designer: Andrew Ogus
 Copyeditor: Alan Titcher
 Art Coordinators: Claudia Durrell, Heena Pitchaikani
 Photo Editor: Mira Schachne
 Indexer: Katherine Pitcoff
 Market Development Manager: Mike Simpson

Credits appear following the Glossary.

About the cover: The image of the heart and great arteries reproduced within each of the cover's color panels is taken from Plate 64, number 4, of *De Humani Corporis Fabrica* (1543) by Andreas Vesalius. A milestone in the history of medicine, Vesalius' work marked the transition of the study of human anatomy from the realm of folklore to a modern observational science.

Copyright ©1999 by Addison Wesley Longman, Inc.
 This title published under the Benjamin/Cummings imprint.

All rights reserved. No part of this publication may be reproduced, stored in a retrieval system, or transmitted, in any form or by any means, electronic, mechanical, photocopying, recording or any other media or embodiments now known or hereafter to become known, without the prior written permission of the publisher. Manufactured in the United States of America. Published simultaneously in Canada.

Library of Congress Cataloging-in-Publication Data

Tortora, Gerard J.

Principles of human anatomy / Gerard J. Tortora. — 8th ed.

p. cm.

Includes index.

ISBN 0-321-00037-4

1. Human anatomy. 2. Human physiology. I. Title.

QM23.2.T87 1998

611—dc21

98-7560

CIP

ISBN: 0-321-00037-4

1 2 3 4 5 6 7 8 9 10-RNV-02 01 00 99 98



Benjamin/Cummings Science Publishing
 2725 Sand Hill Road
 Menlo Park, California 94025

Appendix C: Patient Demographic Information

Table C.1 demonstrates the information of the subjects that were used in this study.

Table C.1: Patient Demographic Information

Subject Number	Age	Sex
1	70	Male
2	79	Female
3	70	Female
4	65	Female
5	65	Male

Appendix D: Free Body Diagram Analysis of Muscle Wrapping

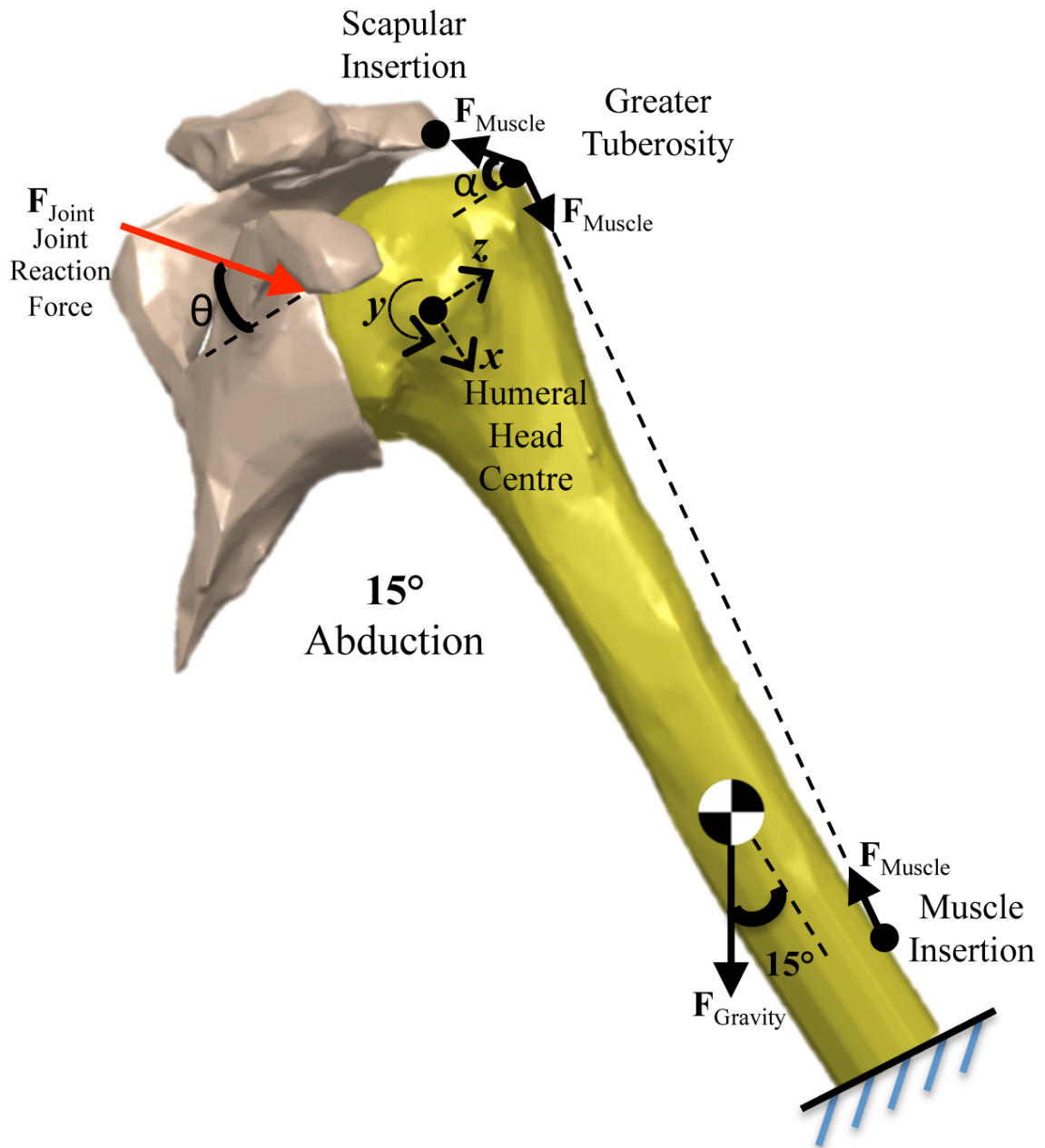


Figure D.1: Free body diagram of muscle force calculation

Humeral Head Centre = (0, 0, 0)

Scapula = (-22.87, 0, 15.61)

Greater Tuberosity = (-14.27, 0, 19.80)

Muscle Insertion (MI) = (88.45, 0, 9.10)

$F_{\text{Joint}} = 188.8 \text{ [N]}$ (Joint Reaction Force from Bergmann *et al* (2007))

$F_{\text{Gravity}} = (9.81) \times (88.3 \text{ kg [50-percentile male bodyweight]}) \times (0.05 \text{ [arm weight/bodyweight]})$

$F_{\text{Gravity}} = 43.3 \text{ [N]}$

Assumptions:

- Single point muscle origin and insertion on the scapula and humerus.
- 2D simplification of the force system.
- Consider F_{Muscle} at the greater tuberosity and Muscle Insertion to be internal forces that cancel each other out.

Solution:

$$\alpha = \tan^{-1} \left(\frac{-14.27 - (-22.87)}{19.80 - 15.61} \right) \Rightarrow \alpha = 64.03 \text{ degrees}$$

$$\theta = \tan^{-1} \left(\frac{19.93}{5.06} \right) \Rightarrow \theta = 75.74 \text{ degrees}$$

Summing the forces in the medial-lateral direction we find:

$$\sum F_z = 0: F_{\text{Joint}} \cos \theta = F_{\text{Muscle}} \cos \alpha + F_{\text{Gravity}} \sin(15 \text{ degrees}) \Rightarrow$$

$$F_{\text{Muscle}} = 80.6 \text{ [N]}$$

Accordingly, the muscle force applied is approximated by a magnitude of 80 [N].

Appendix E: Computational Parameters of FE Models

Table H.1: Computational Parameters of FE Models

Model*	Approximate Number of Elements	Approximate Computational Time
Intact	200,000	1.5 hours
Stemless	160,000	1.5 hours
Short	265,000	6 hours
Standard	280,000	7.5 hours

* All values are approximated based on a single specimen, using a computer with 16 GB of available ram.

Appendix F: Mimics and 3-Matics Procedures

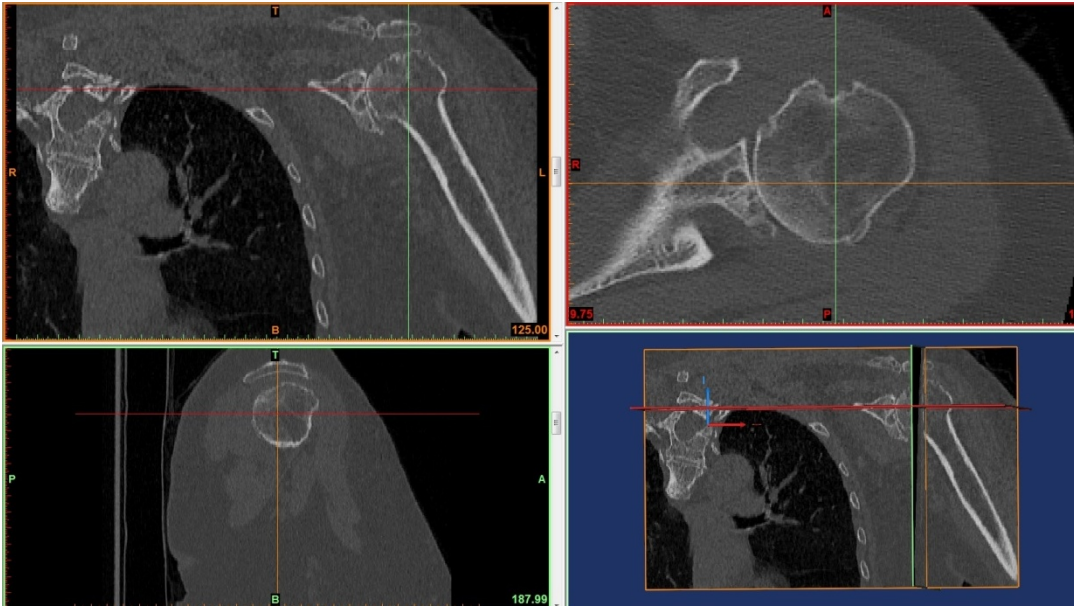


Figure F.1: DICOM files were imported into Mimics.

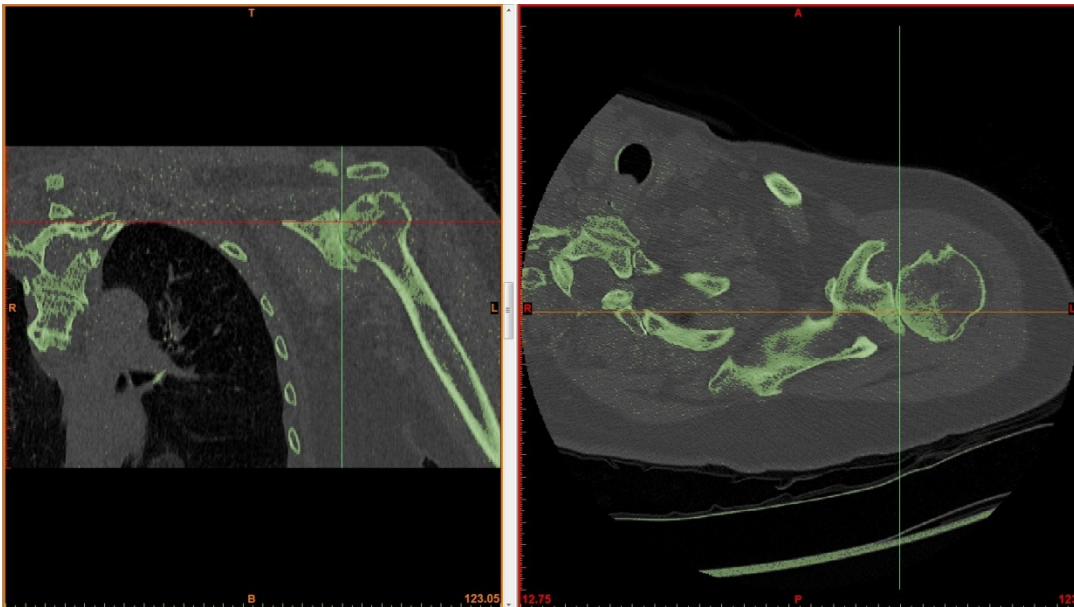


Figure F.2: The initial mask for cortical bone was created using thresholding function.

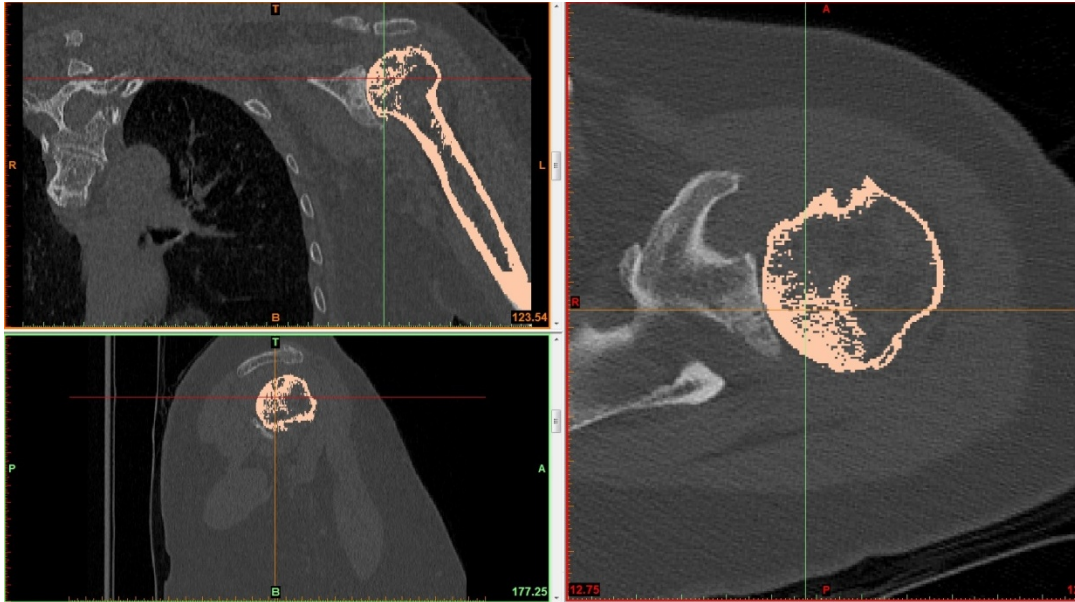


Figure F.3: Region Growing function in Mimics generated a mask (for cortical bone).

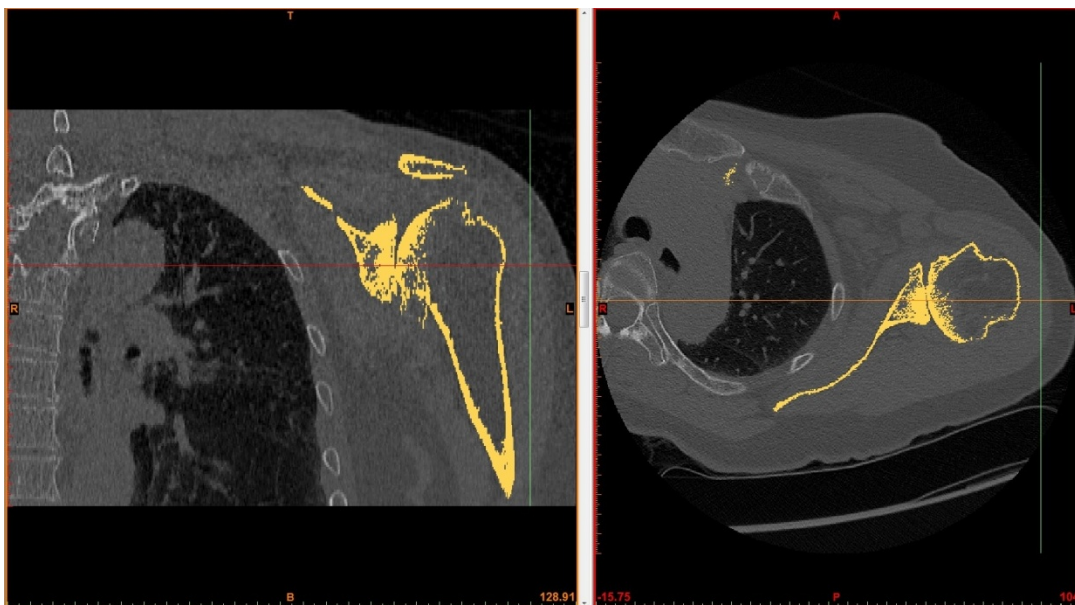


Figure F.4: In most of the cases, due to the connected pixels between humerus and scapula, after applying region growing, the humerus could not be separated from scapula.



Figure F.5: In this case, connected pixels were deleted in order to separate the scapula from humerus.

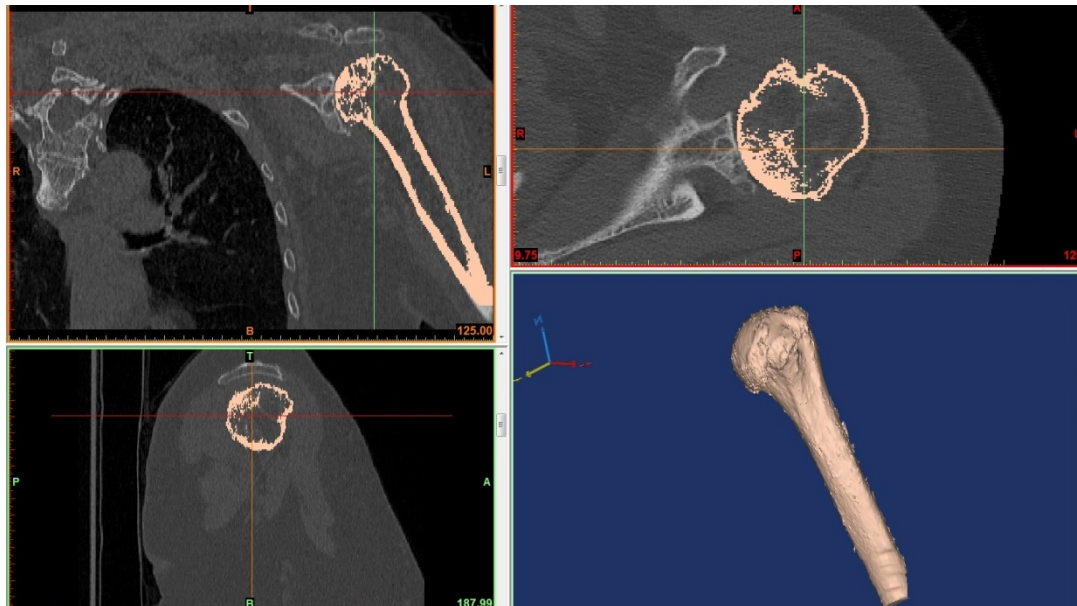


Figure F.6: The 3D model of the cortical bone was created.

Wrapping, Smoothing and Triangle Reduction features that are native to MIMICS were used to further refine the bone geometries. In the final stage, fine-smoothing was applied using 3-Matics software (Materialise, Leuven, Belgium).

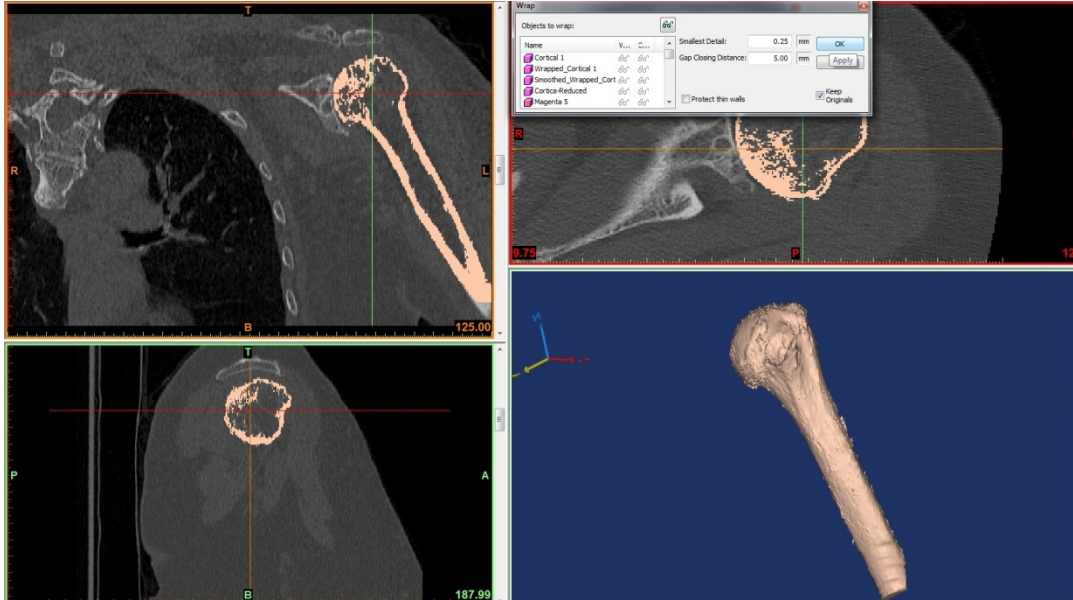


Figure F.7: The 3D model was wrapped.

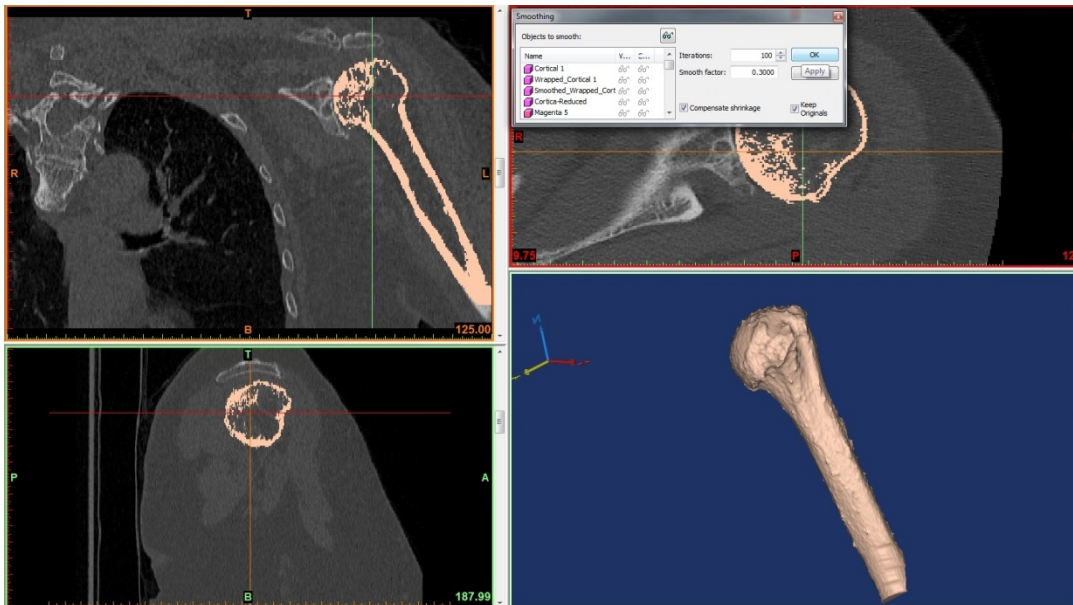


Figure F.8: The 3D model of cortical was smoothed.

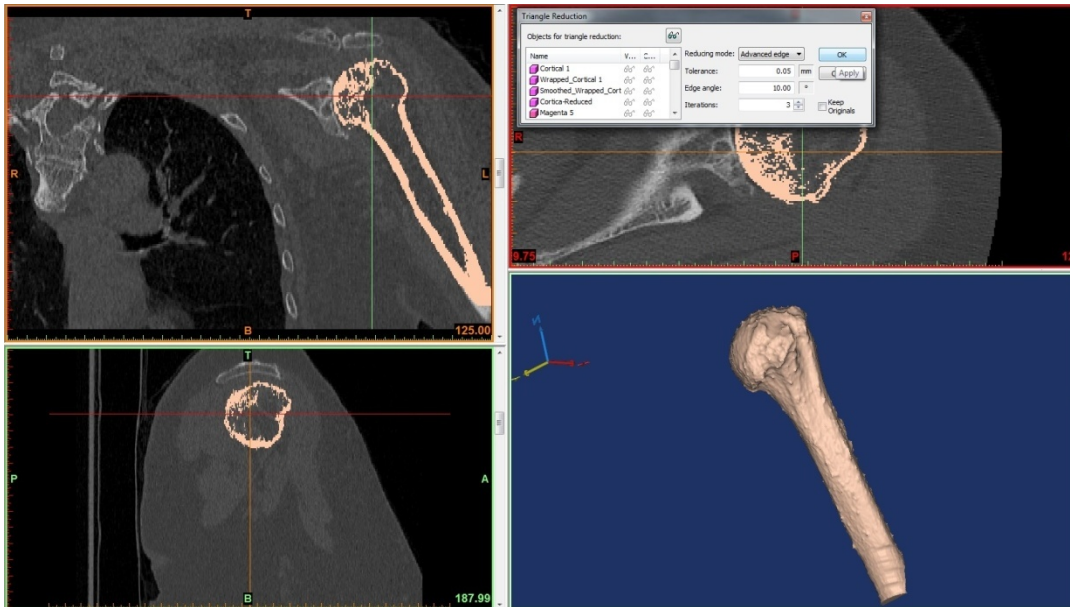


Figure F.9: Triangle reduction function was also applied for the cortical 3D model.

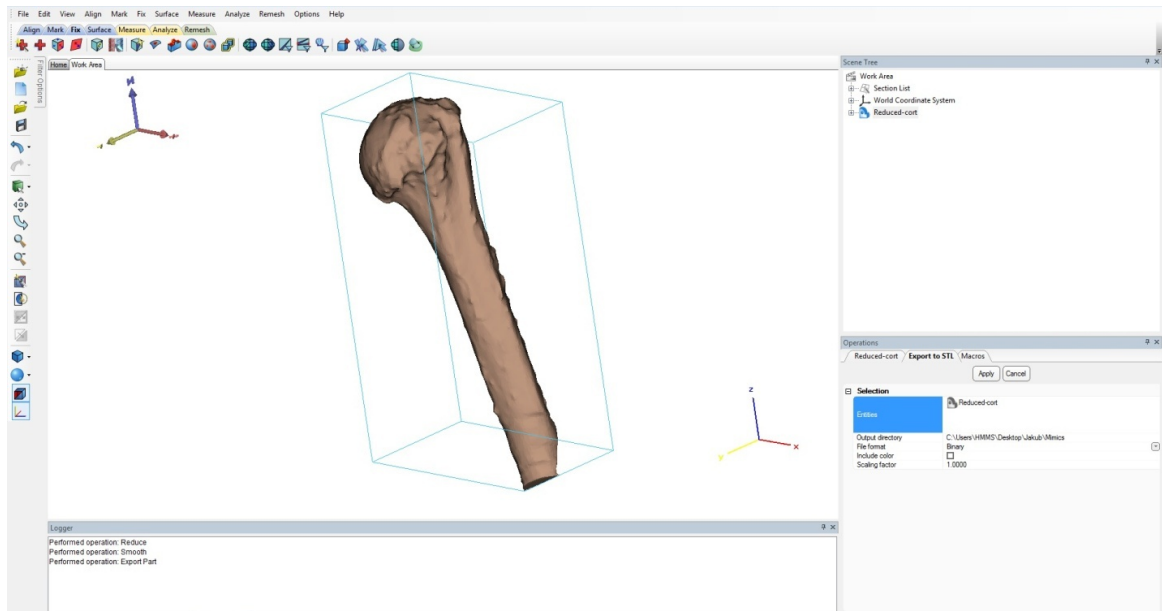


Figure F.10: 3D Bone in 3-Matics software export as an STL file, after applying triangle reduction and smooth features.

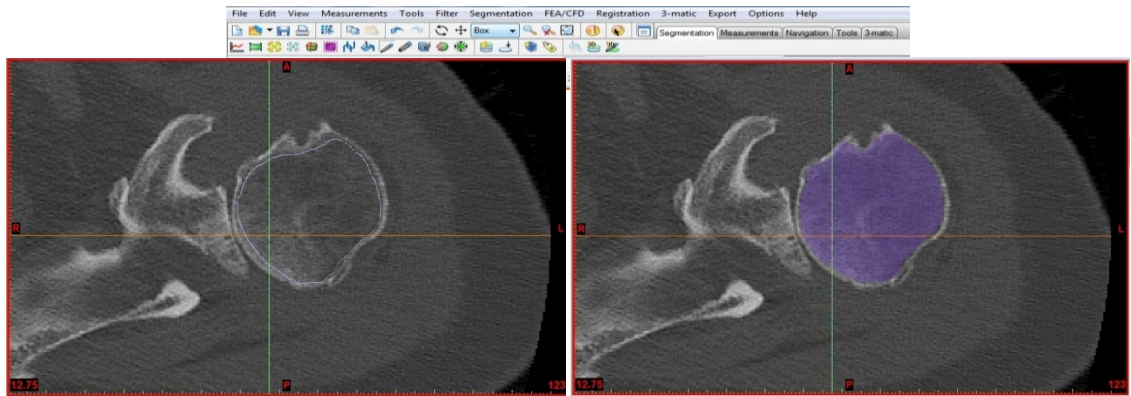


Figure F.11: Boundary of the trabecular bone was selected manually for each slice.

Cortical and trabecular geometries were then overlaid in MIMICS, and the cortical-trabecular boundary was inspected for overlapping regions. If overlapping occurred, the trabecular bone was re-masked to remove the conflicting regions. Once an appropriate cortical-trabecular boundary was obtained, surface geometries were exported in STL format to permit use with SolidWorks software (Dassault Systèmes, S. A. (Vélizy, France)).

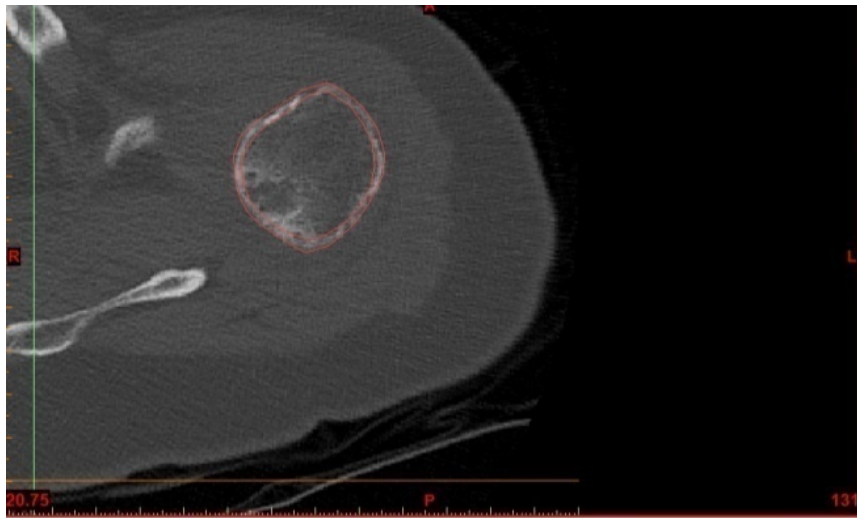


Figure F.12: Demonstrates the outer boundary of the cortical and trabecular bone.

Appendix G: All Single-Element Stress Path Results

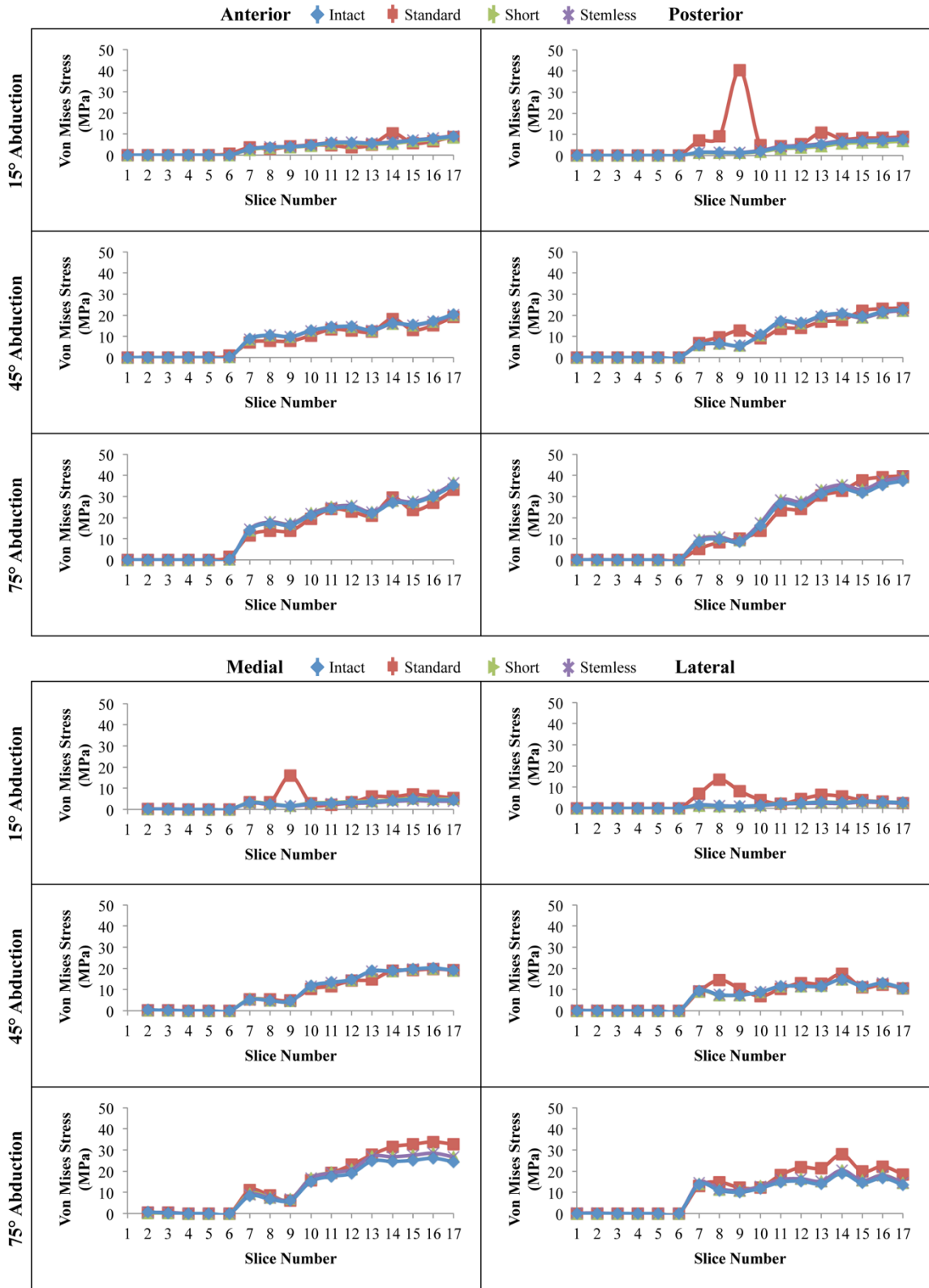


Figure G.1: Single-Element Stress Path Results of Subject 1 - CoCr

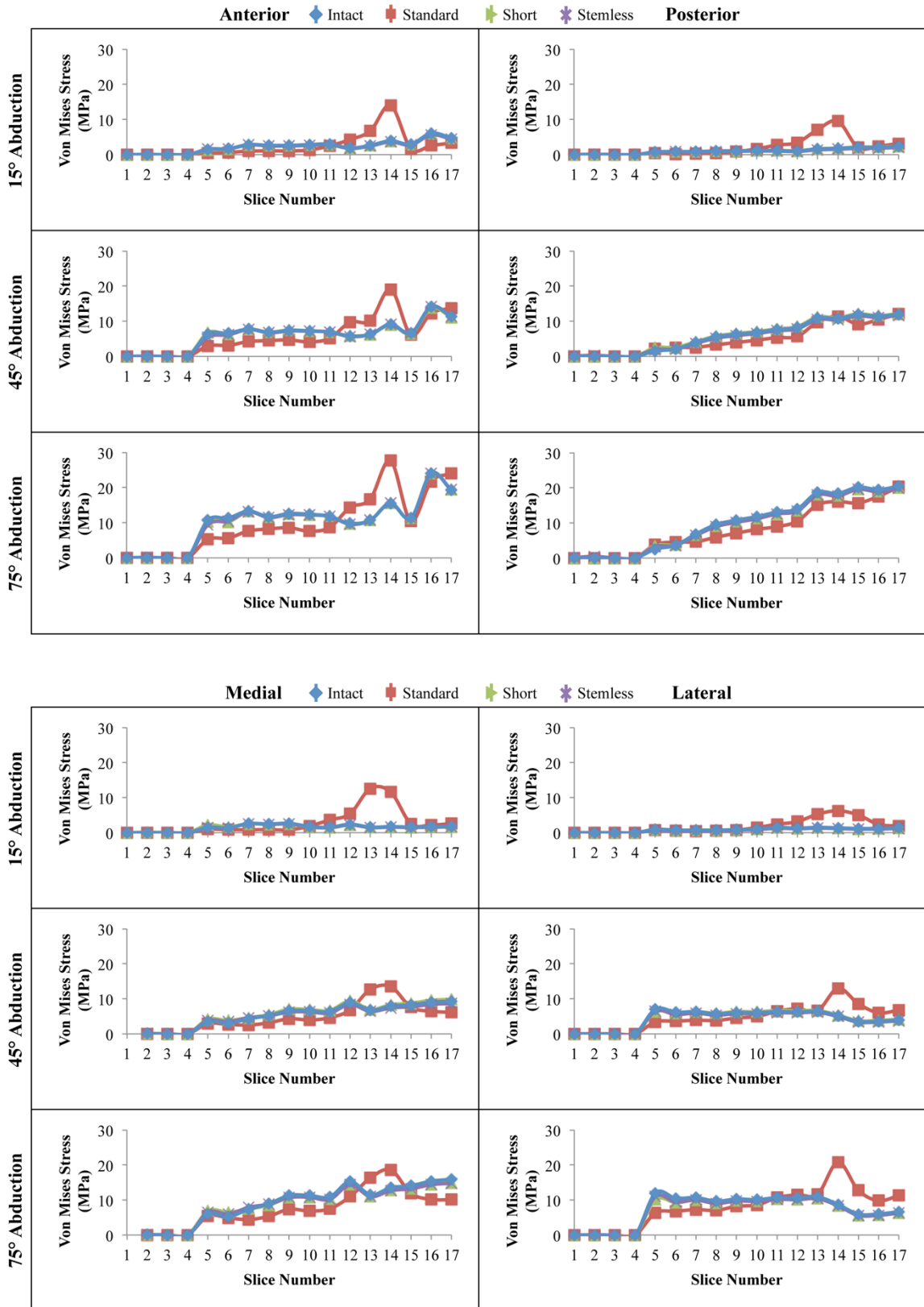


Figure G.2: Single-Element Stress Path Results of Subject 2 - CoCr

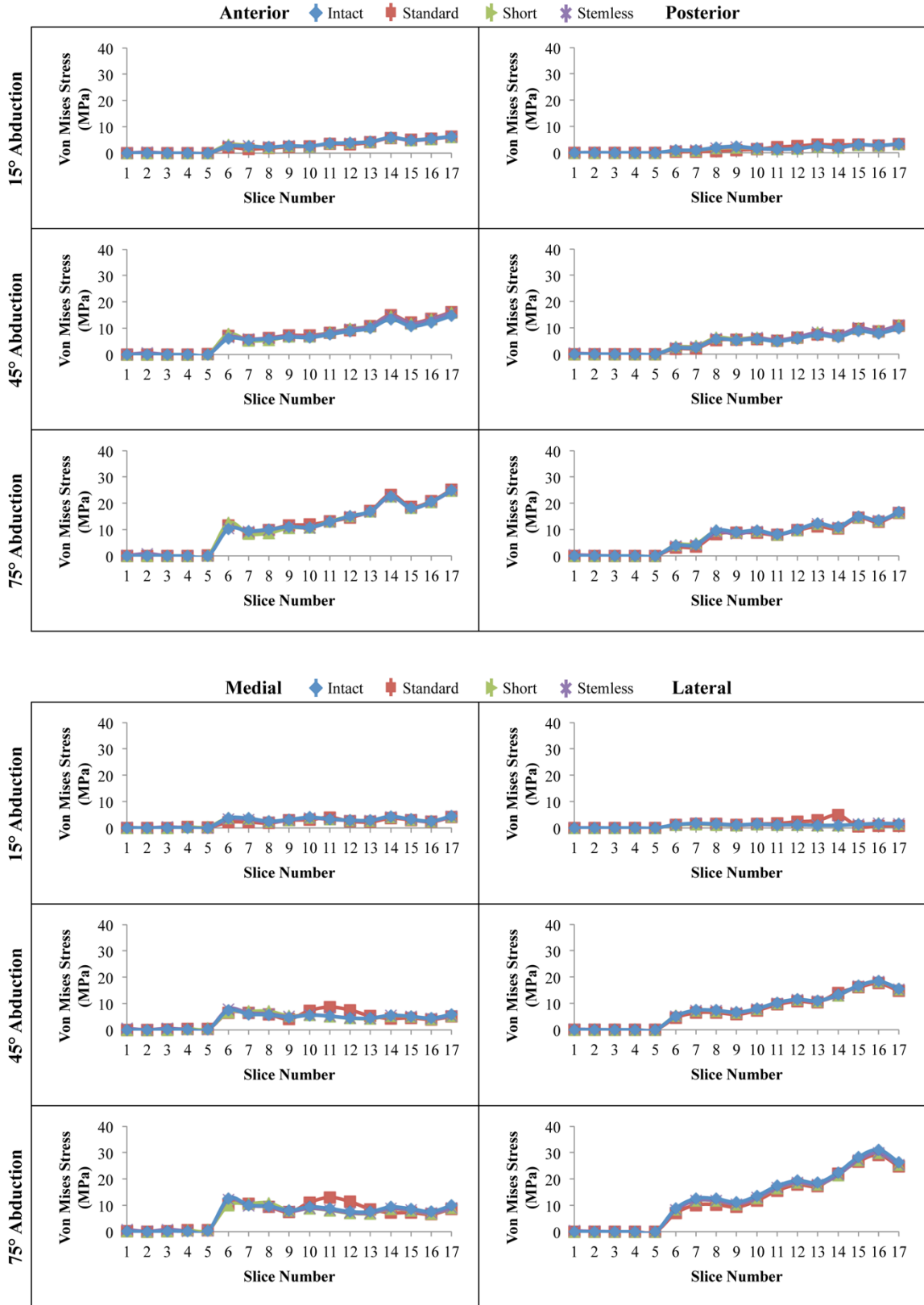


Figure G.3: Single-Element Stress Path Results of Subject 3 - CoCr

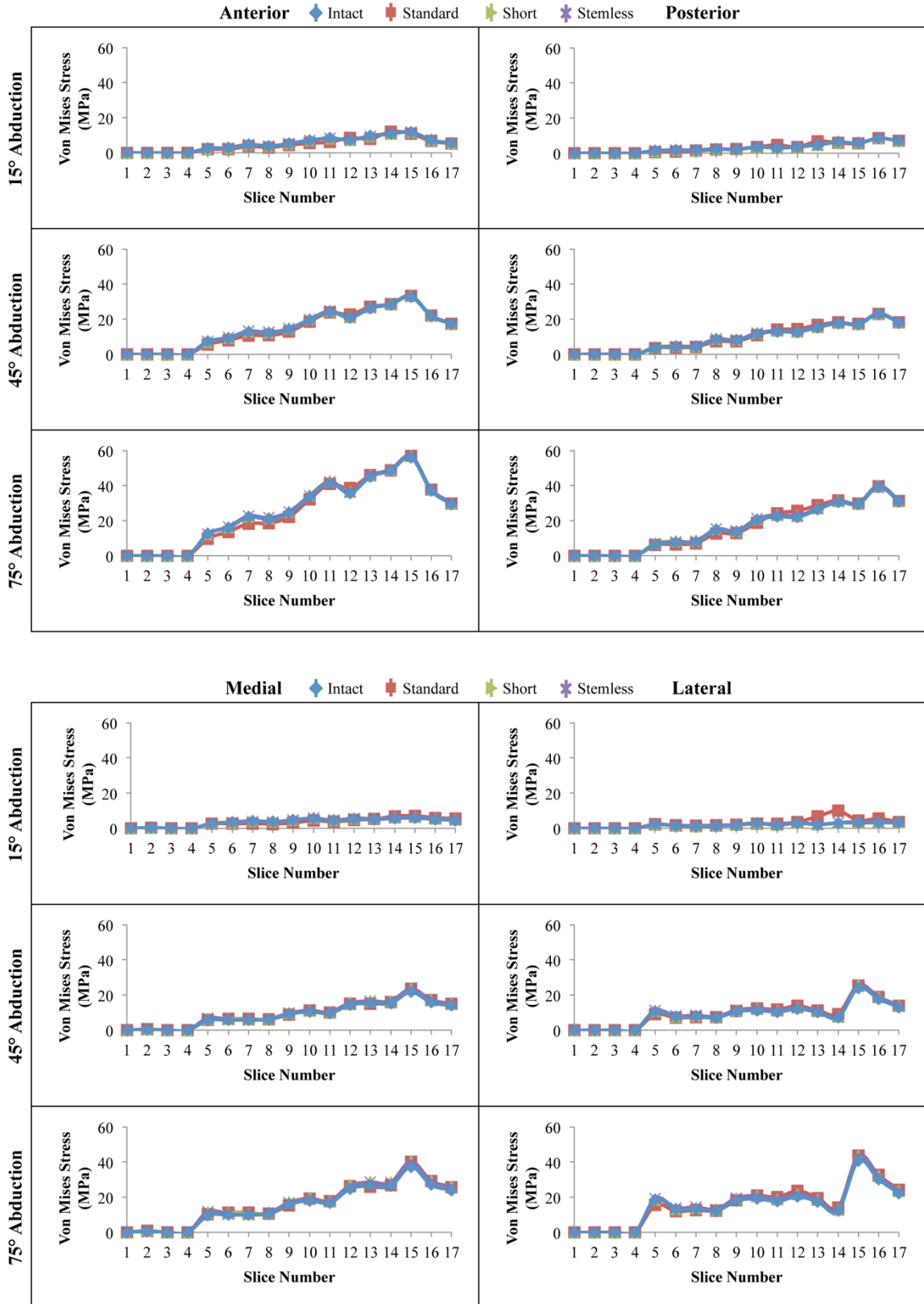


Figure G.4: Single-Element Stress Path Results of Subject 4 - CoCr

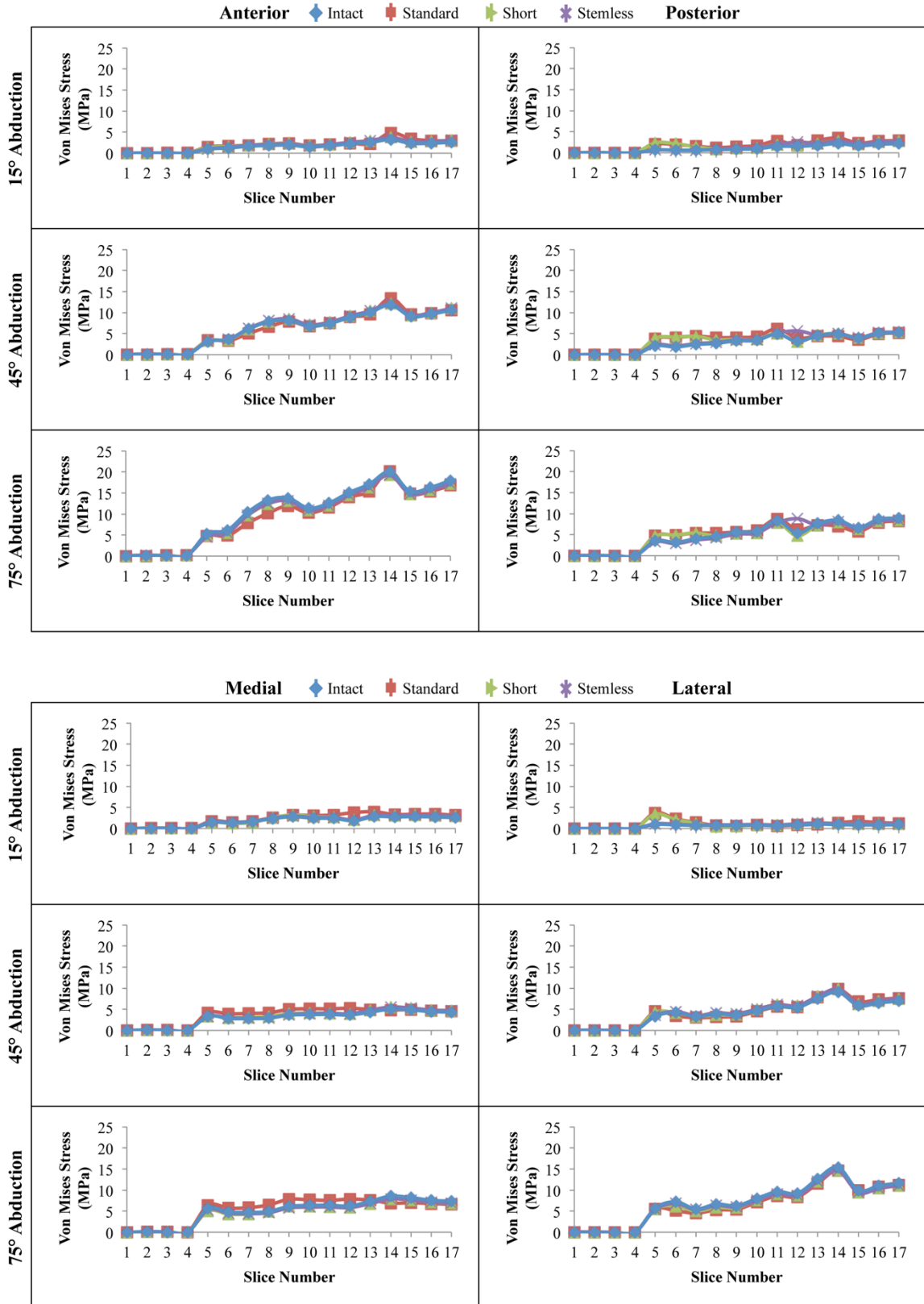


Figure G.5: Single-Element Stress Path Results of Subject 5 - CoCr

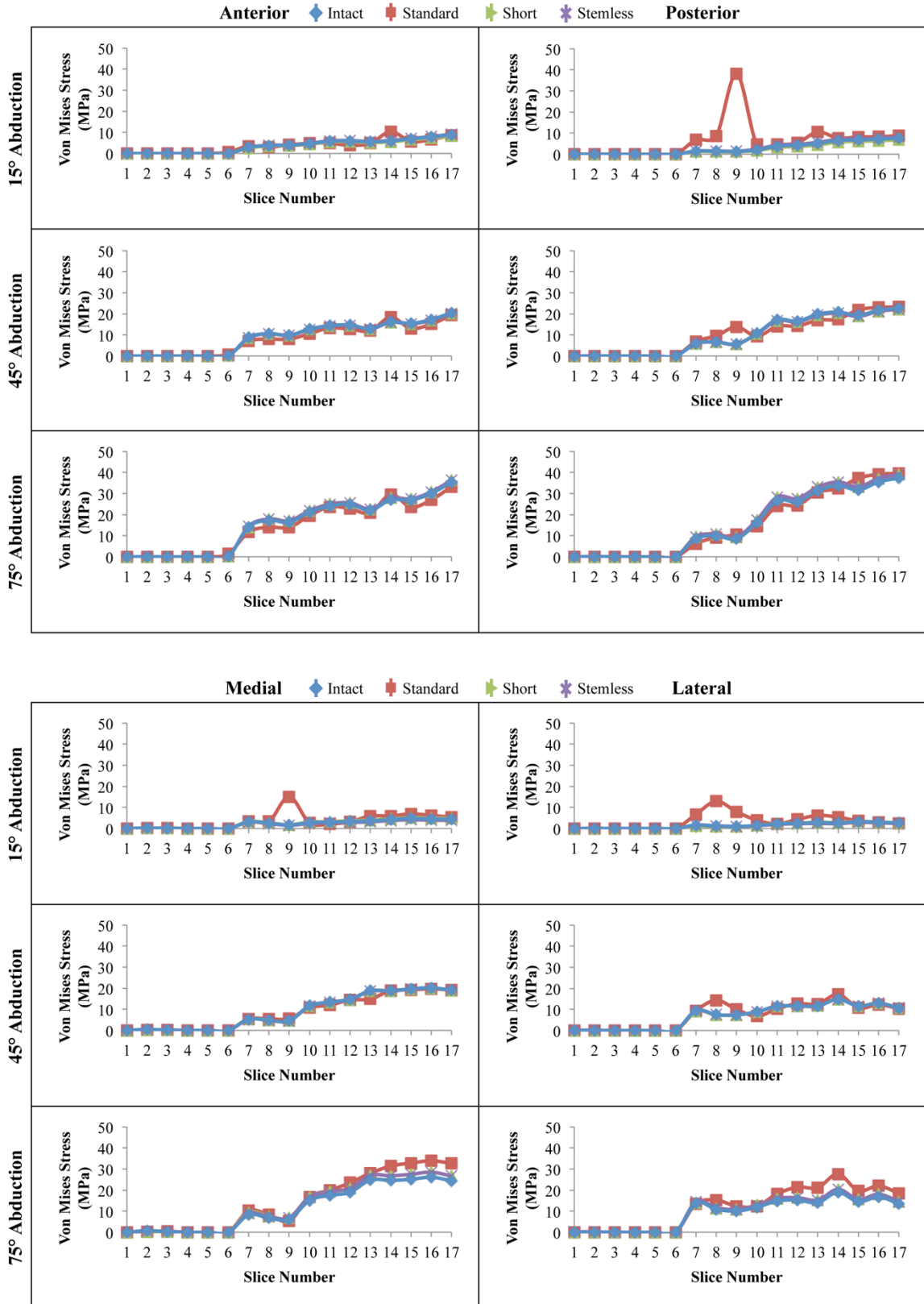


Figure G.6: Single-Element Stress Path Results of Subject 1 - Ti

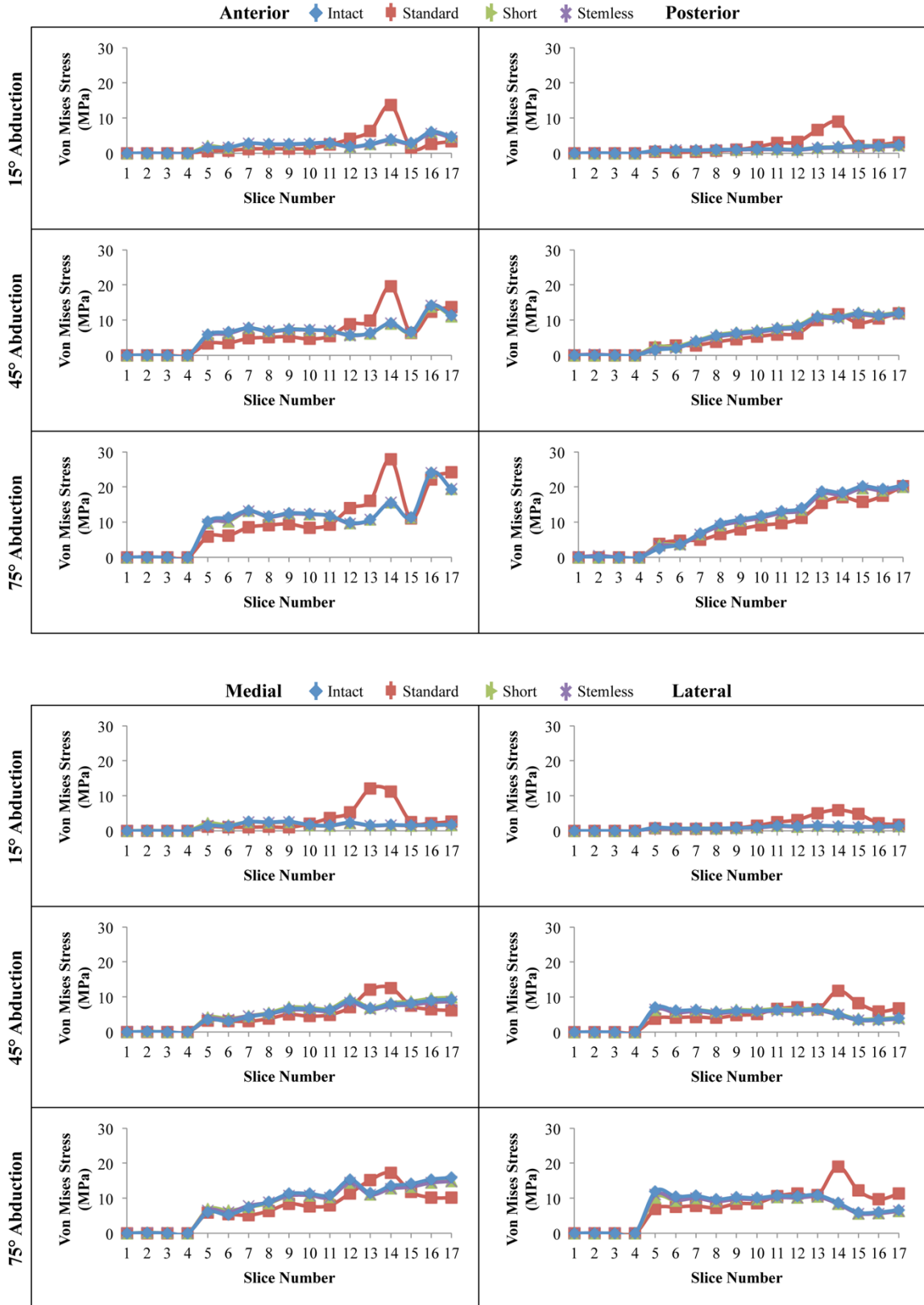


Figure G.7: Single-Element Stress Path Results of Subject 2 - Ti

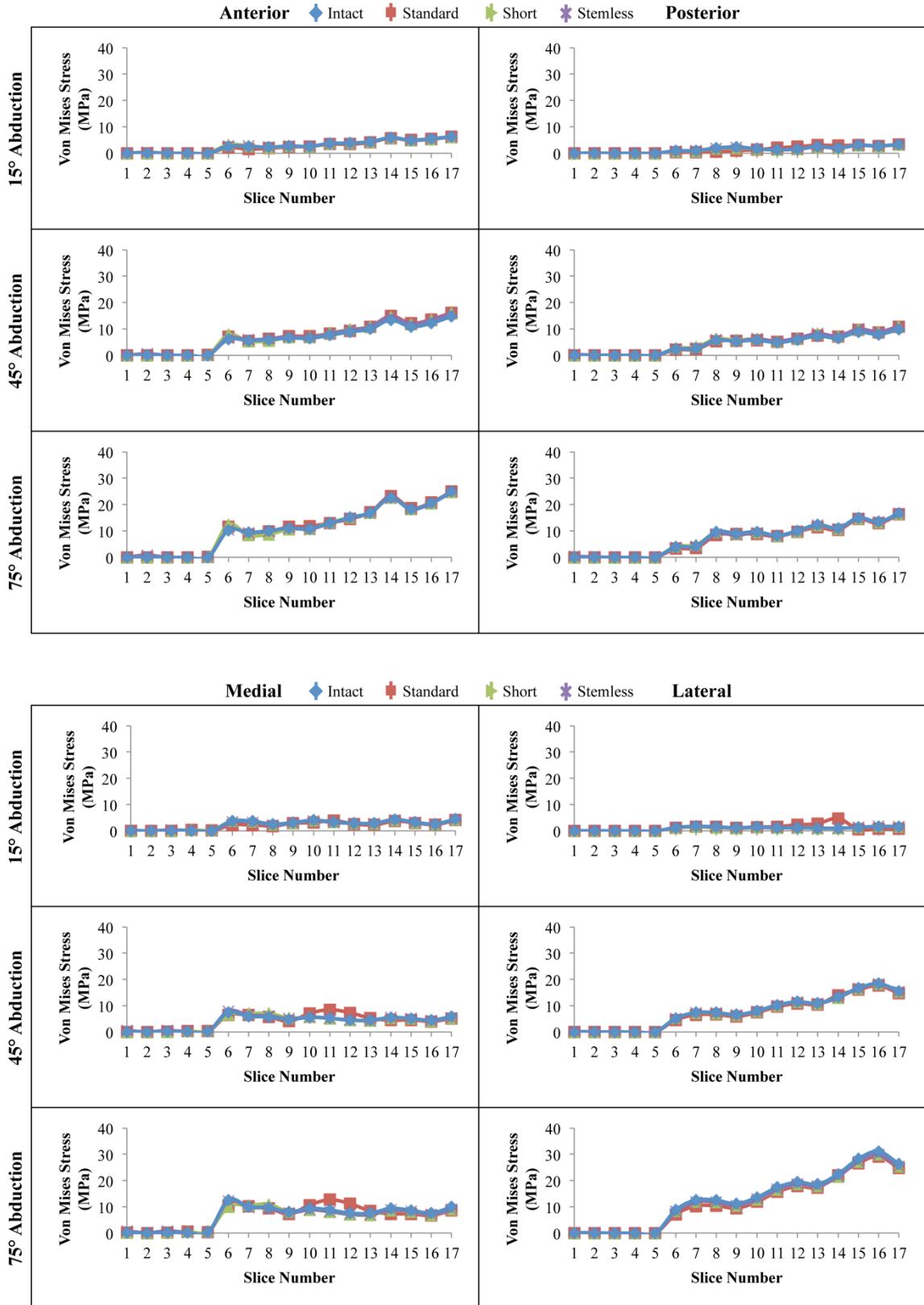


Figure G.8: Single-Element Stress Path Results of Subject 3 - Ti

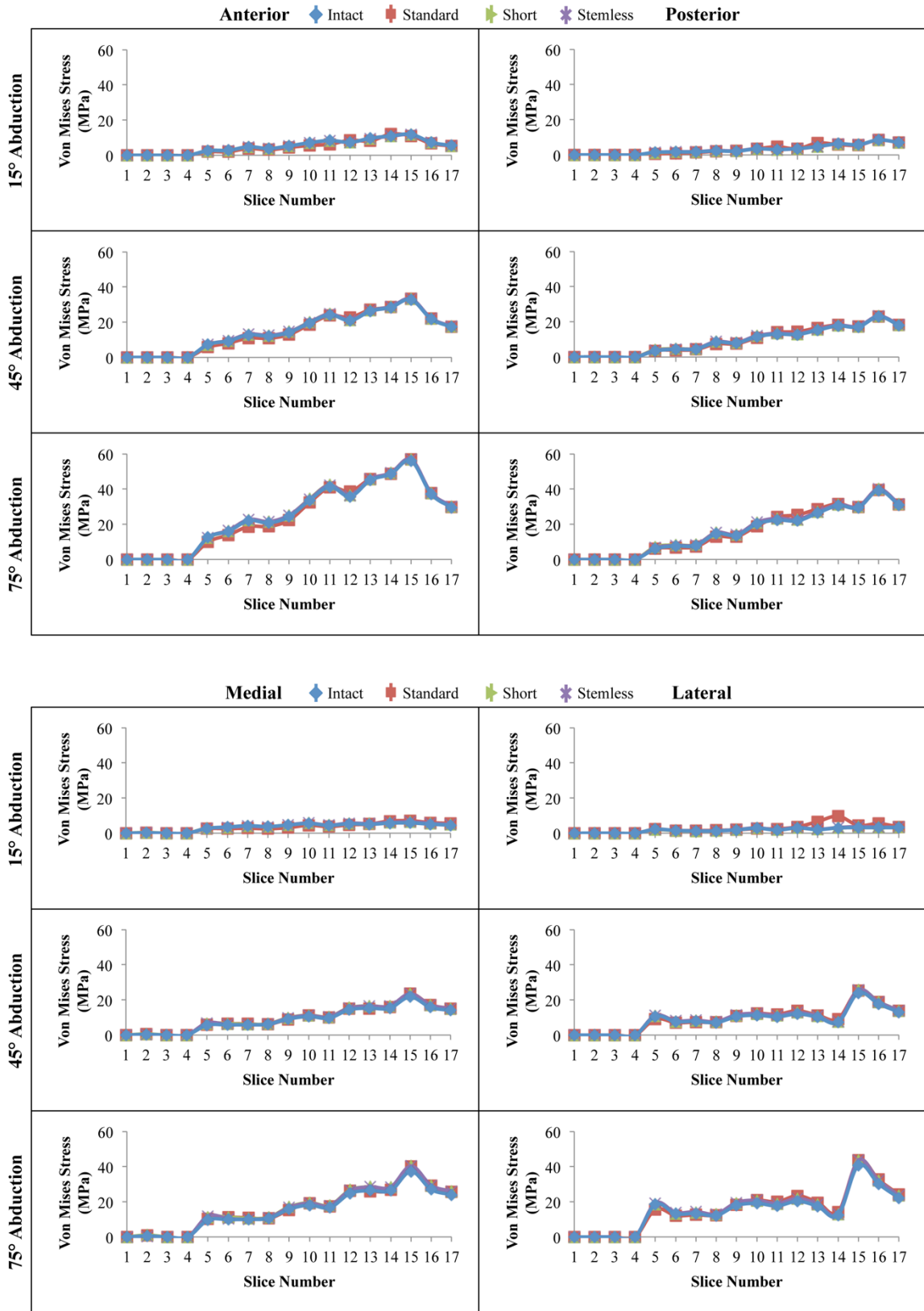


Figure G.9: Single-Element Stress Path Results of Subject 4 - Ti

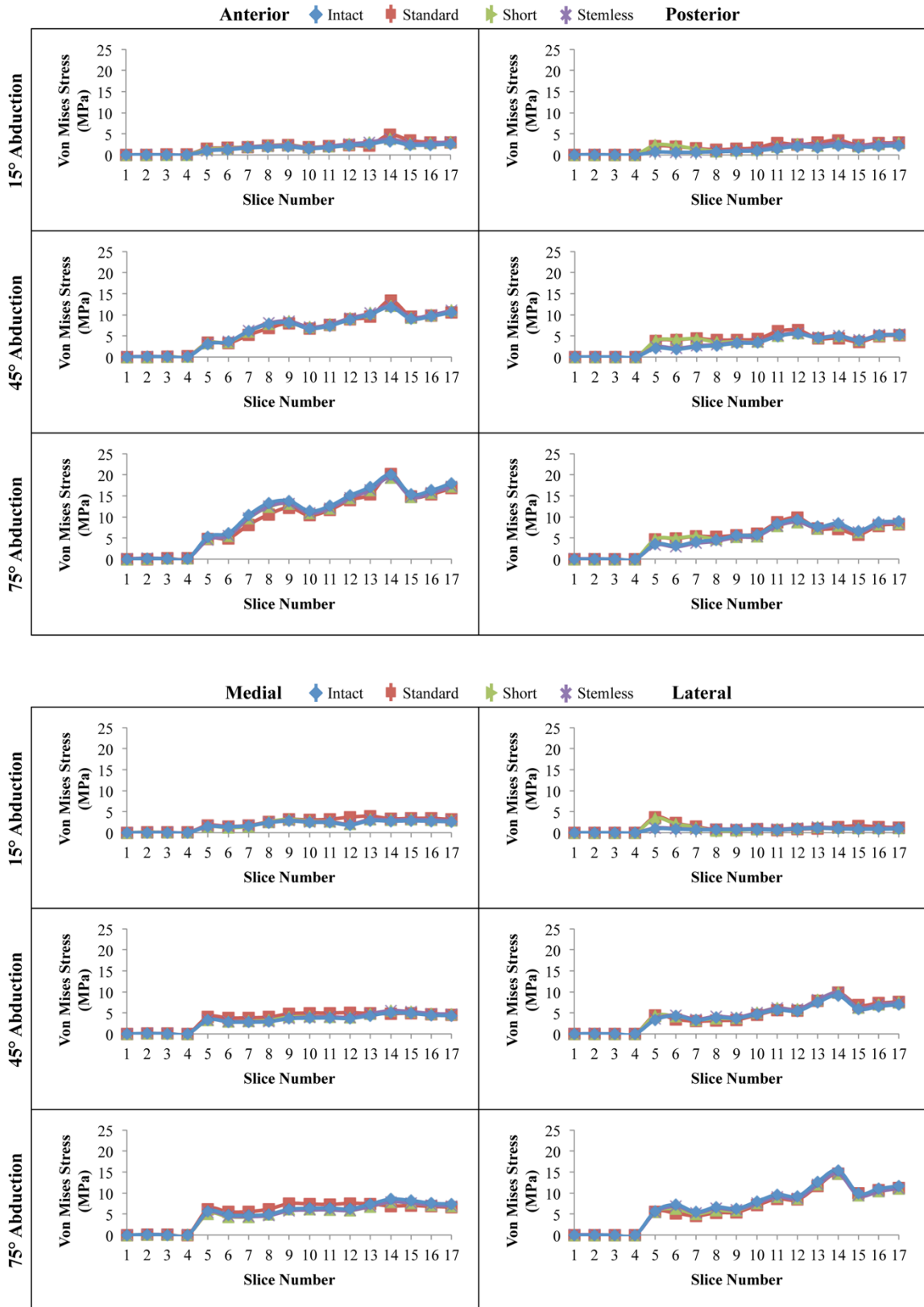


Figure G.10: Single-Element Stress Path Results of Subject 5 - Ti

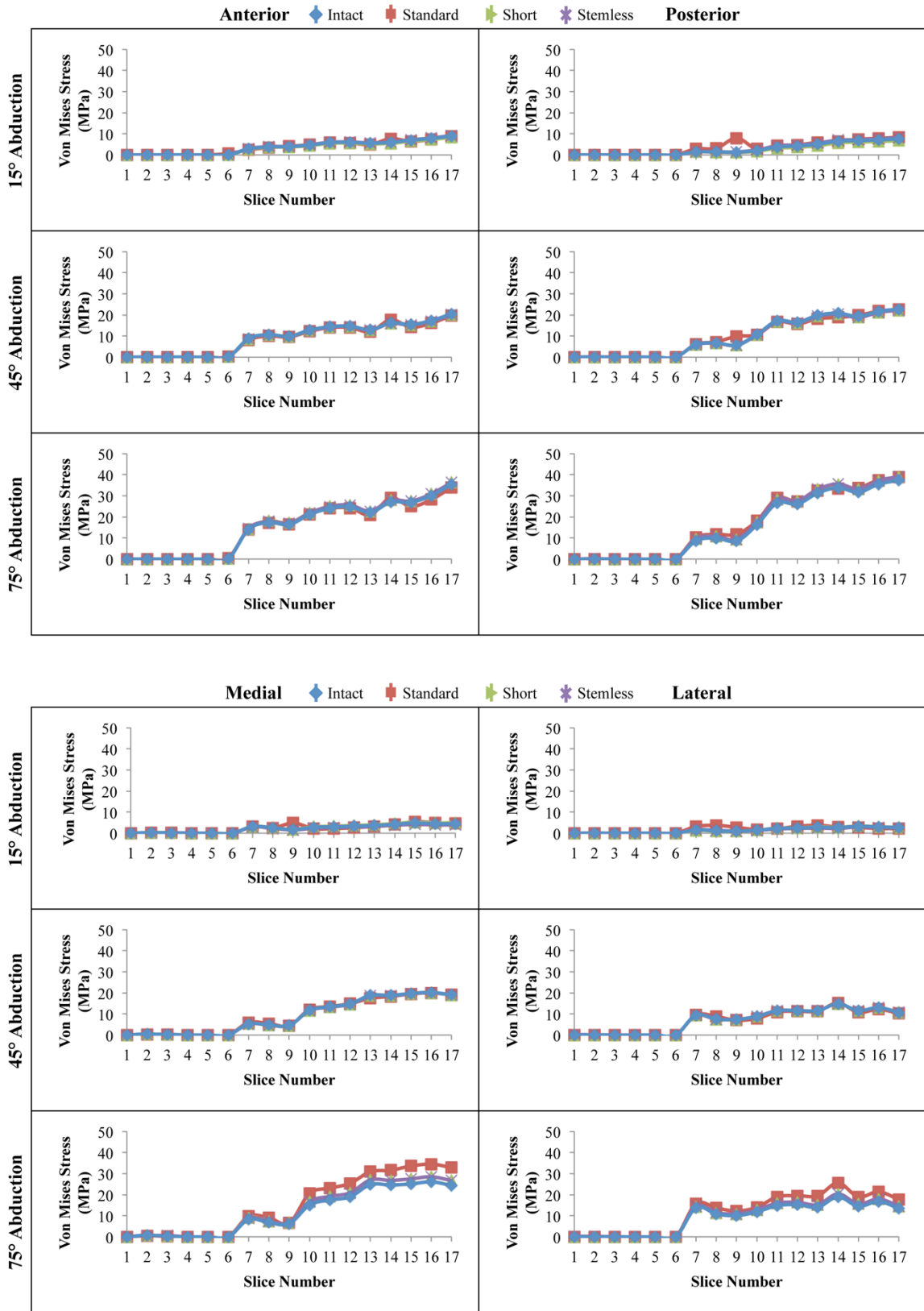


Figure G.11: Single-Element Stress Path Results of Subject 1 - PEEK

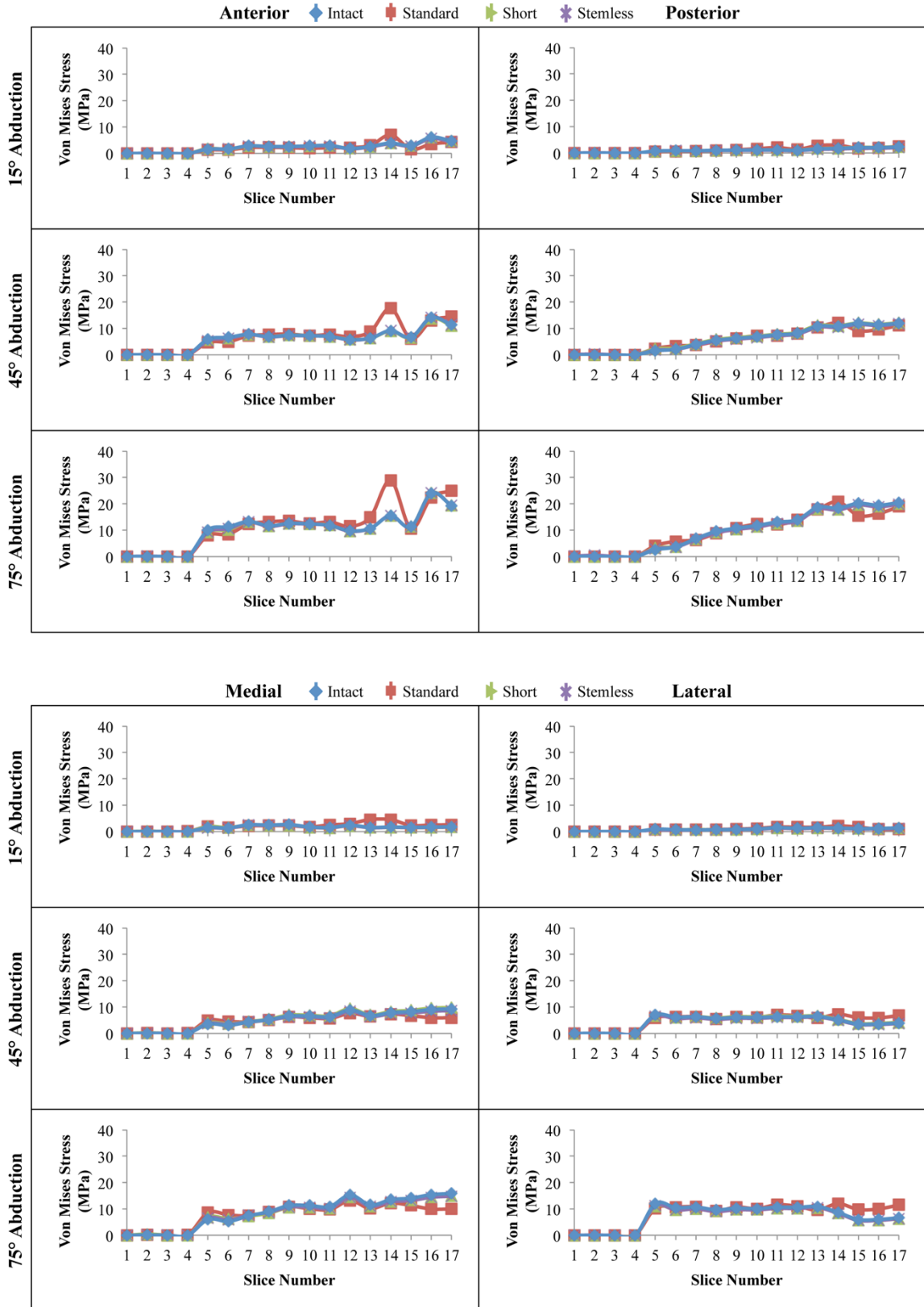


Figure G.12: Single-Element Stress Path Results of Subject 2 - PEEK

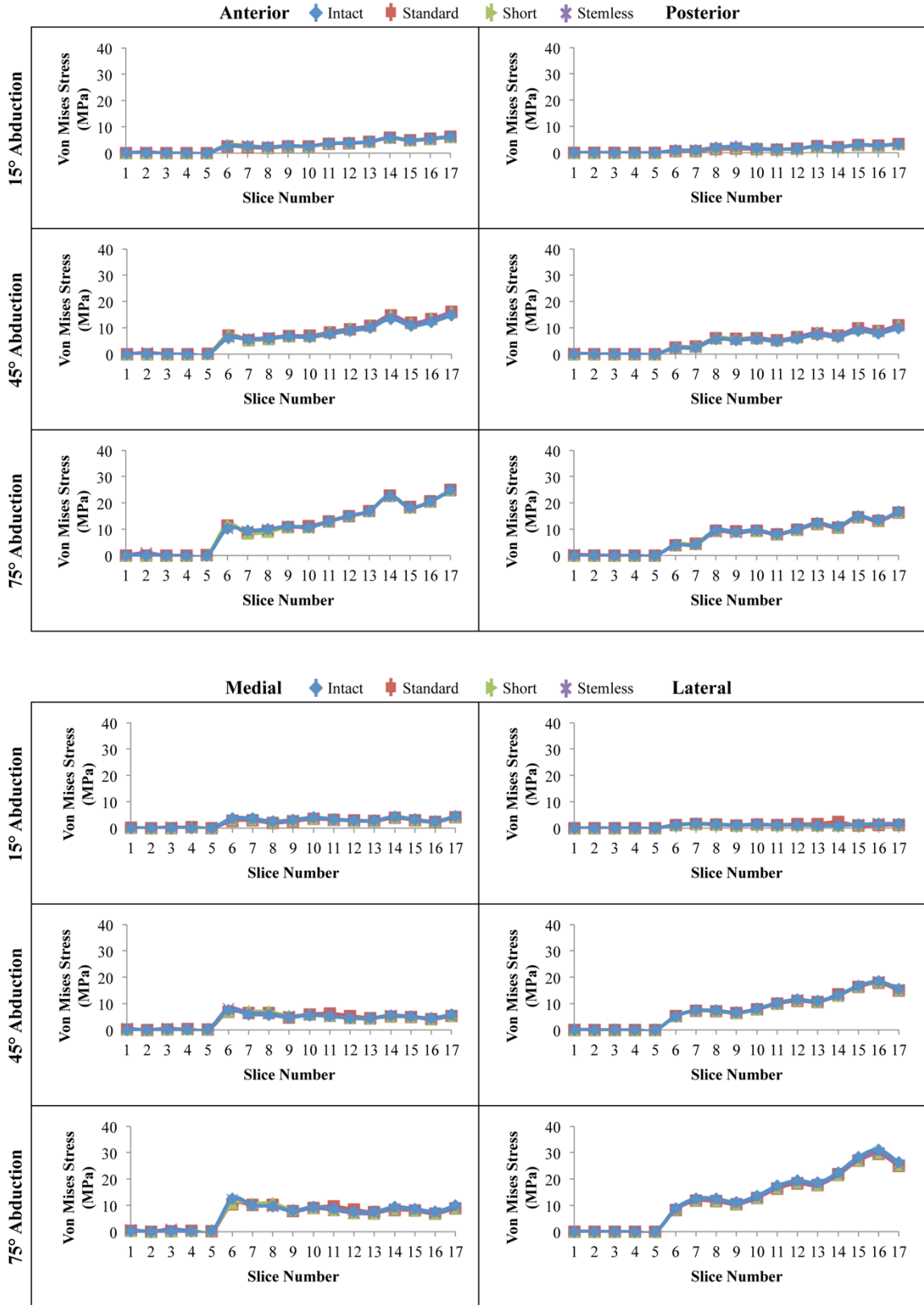


Figure G.13: Single-Element Stress Path Results of Subject 3 - PEEK

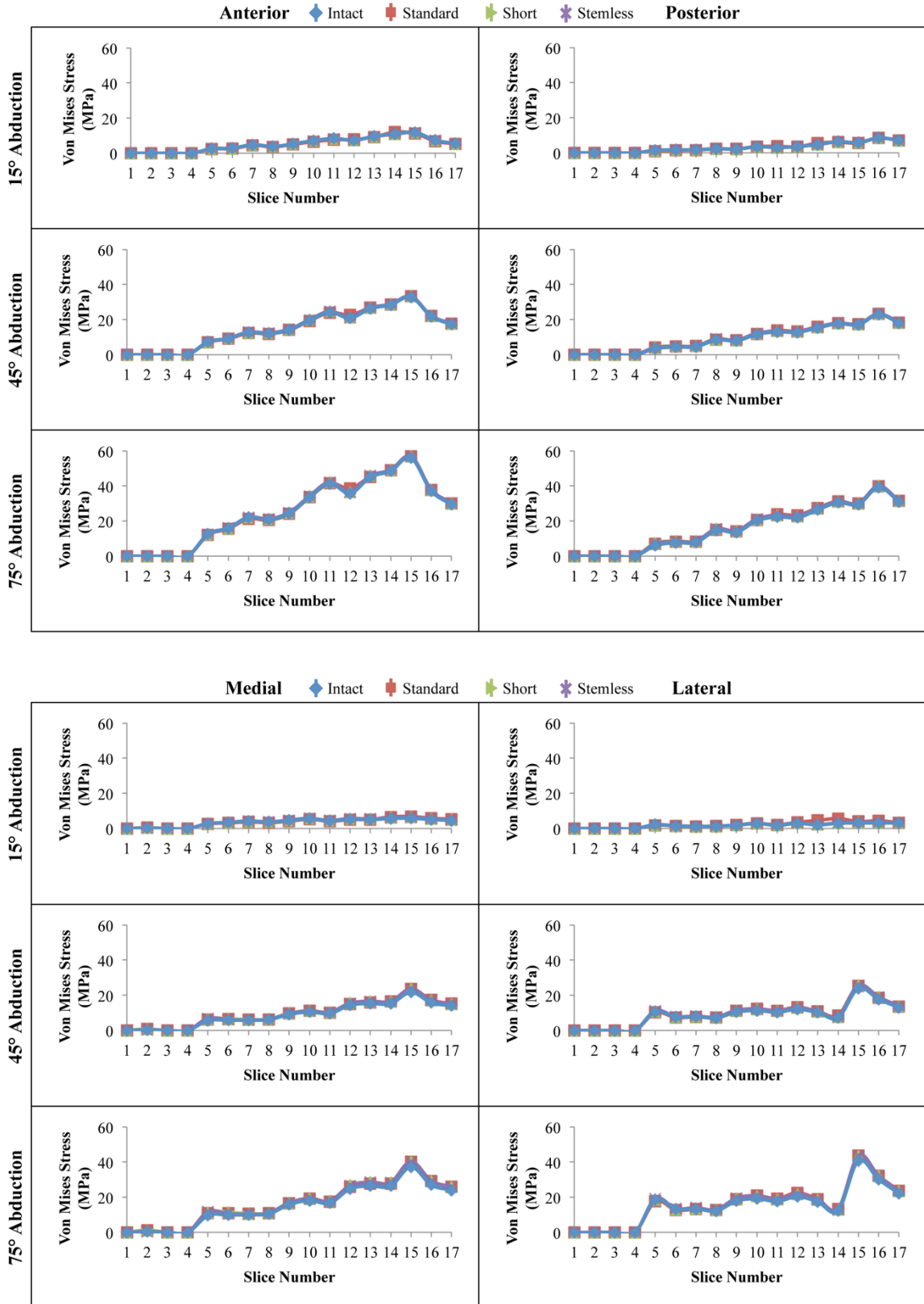


Figure G.14: Single-Element Stress Path Results of Subject 4 - PEEK

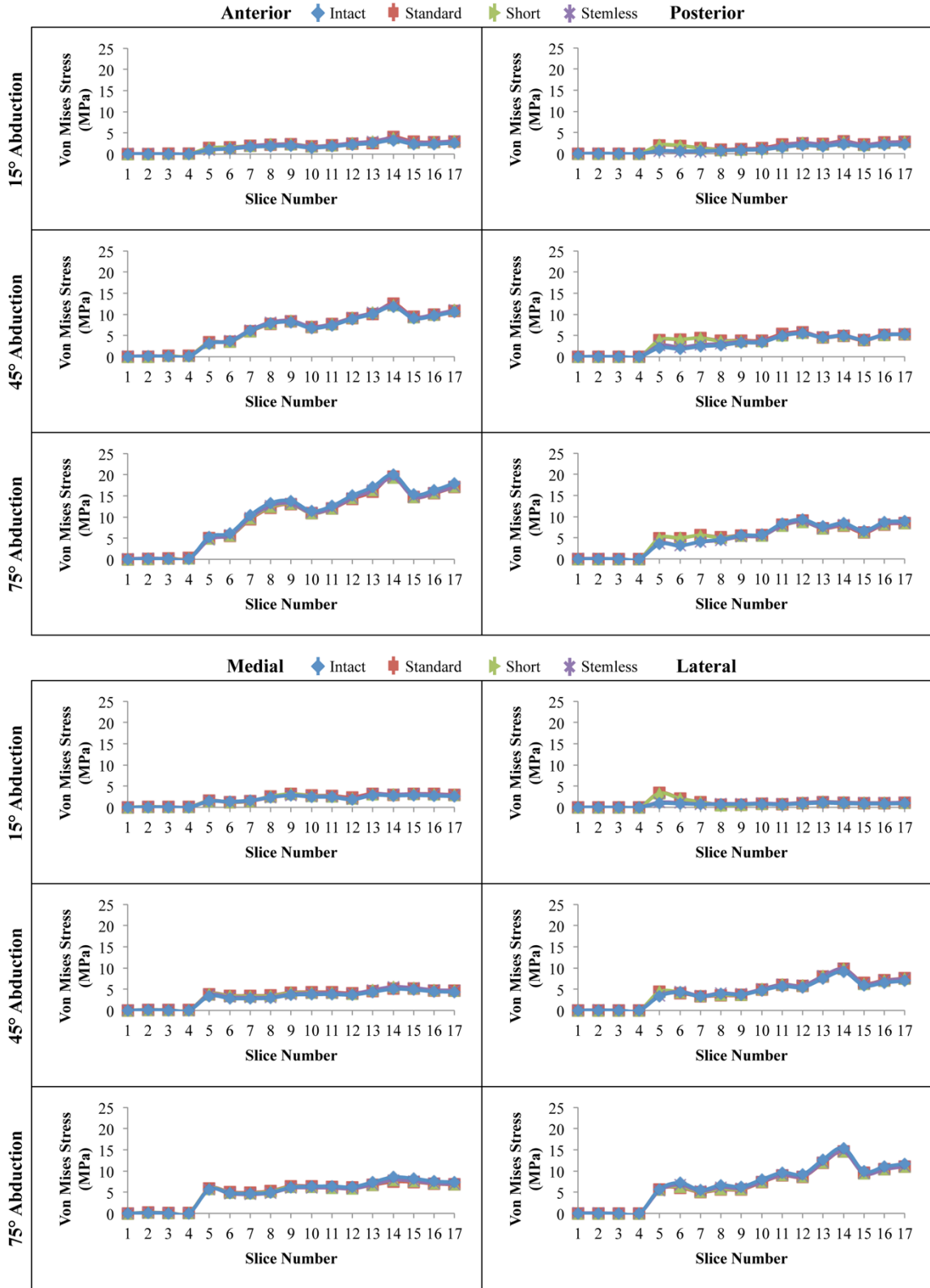


Figure G.15: Single-Element Stress Path Results of Subject 5 - PEEK

Appendix H: Peak Stem Stresses and Implant Yield Strengths

Table H.1: Implant Yield Assessment

Maximum Implant Stem Stresses [MPa]	Material	Stem Type	Specimen Number					Yield Strength *
			1	2	3	4	5	
	CoCr	Standard	125	190	38	39	46	450 - 1000
		Short	33	27	21	55	49	
		Stemless	8	11	9	9	8	
	Ti	Standard	124	164	36	39	46	758 - 1117
		Short	31	27	19	57	49	
		Stemless	8	10	9	9	7	
	PEEK	Standard	43	36	11	31	39	100 - 119
		Short	14	15	12	34	40	
		Stemless	6	6	4	7	4	

* (Kuroda *et al.*, 1998; Kurtz and Devine, 2007; Staiger *et al.*, 2006)

Curriculum Vitae

Name: Najmeh Razfar

**Post-secondary
Education and
Degrees:**

Ferdowsi University
Mashad, Iran
2004 – 2006, Cert. Applied Science

Ryerson University
Toronto, Ontario, Canada
2008 – 2012, BEng

The University of Western Ontario
London, Ontario, Canada
2012 – 2014, MEng

**Honours and
Awards:**

Dean's Honor List
2011 – 2012

**Related Work
Experience:**

Western Engineering Summer Academy Instructor
Introduction to Joint Replacement Design and Finite Element
Modeling
Western University Canada
2014

Graduate Teaching Assistant
C++ Programming
Department of Electrical Engineering
Western University Canada
2013 – 2014

Graduate Teaching Assistant
Tissue Engineering
Department of Chemical and Biomedical Engineering
Western University Canada
2012

Research Assistant, Summer Internship

‘Correlation between photo cross-linking of different concentration of PEG and resonance wavelength shift’

Harvard-MIT Division of Health Sciences and Technology (HST)
2012

Publications:

a. Peer Reviewed Oral Presentation:

N.Razfar, Reeves JM, G.Langohr DG, R.Willing, G.S.Athwal, J.Johnson. The Effect of Shoulder Humeral Component Length on Bone Stresses A Finite Element (FE) Analysis The 7th world Congress of Biomechanics Conference. (Poster, July 2014)

Reeves JM, **Razfar N**, G.Langohr DG, Athwal GS, King GJ, Johnson JA: The Effect of Material Selection of Partial Joint Replacement Prostheses on the Contact Mechanics of the Opposing Native Cartilage: A Finite Element Study. The 7th world Congress of Biomechanics Conference. (Poster, July 2014)

N.Razfar, Reeves JM, G.Langohr DG, R.Willing, G.S.Athwal, J.Johnson. The Effect of Shoulder Humeral Component Length on Bone Stresses A Finite Element (FE) Analysis The Pre-ORS (Orthopedic Research Society) Conference. (Presentation and Poster, March 2014)

N.Razfar, Reeves JM, G.Langohr DG, R.Willing, G.S.Athwal, J.Johnson. Comparison of Proximal Humeral Bone Stresses Resulting from Varying Shoulder Implant Stem Design. The Canadian Orthopedic Research Society (CORS) Conference, Montreal, Canada (Poster, June 2014)

Reeves JM, **Razfar N**, G.Langohr DG, Athwal GS, King GJ, Johnson JA: The Effect of Material Selection of Partial Joint Replacement Prostheses on the Contact Mechanics of the Opposing Native Cartilage: A Finite Element Study. The Canadian Orthopedic Research Society (CORS) Conference, Montreal, Canada (Poster, June 2014)

Razfar N, Reeves JM, G.Langohr DG, R.Willing, Athwal GS, Johnson JA. Comparison of Proximal Humeral Bone Stresses Resulting from Varying Shoulder Implant Stem Design. The Bone and Joint Injury and Repair Conference; London, Canada (Poster, January 2014)

Reeves JM, **Razfar N**, G.Langohr DG, Athwal GS, King GJ, Johnson JA: The Effect of Material Selection of Partial Joint Replacement Prostheses on the Contact Mechanics of the Opposing Native Cartilage: A Finite Element Study. The Bone and Joint Injury and Repair Conference; London, Canada (Presentation, January 2014)

N.Razfar, R.Willing, G.S.Athwal, J.Johnson. Finite element models of the humerus to compare short and long stem length for shoulder arthroplasty. London Health Research Day. (Presentation, February 2013)